University of Alberta

Effects of Microstructure and Abrasion Condition on Abrasive Wear of Composite Materials – A Computational Study

By

Jing Hu

A thesis submitted to the Faculty of Graduate Studies and Research in partial fulfillment of the
requirements for the degree of *Master of Science*

In

Materials Engineering

Department of *Chemical and Materials Engineering*

Edmonton, Alberta

Fall 2005

Library and Archives Canada

Published Heritage Branch

395 Wellington Street
Ottawa ON K1A 0N4
Canada

Bibliothèque et Archives Canada

Direction du Patrimoine de l'édition

395, rue Wellington
Ottawa ON K1A 0N4
Canada

0-494-09187-8

Your file *Votre référence*
ISBN:
Our file *Notre reference*
ISBN:

NOTICE:
The author has granted a non-exclusive license allowing Library and Archives Canada to reproduce, publish, archive, preserve, conserve, communicate to the public by telecommunication or on the Internet, loan, distribute and sell theses worldwide, for commercial or non-commercial purposes, in microform, paper, electronic and/or any other formats.

The author retains copyright ownership and moral rights in this thesis. Neither the thesis nor substantial extracts from it may be printed or otherwise reproduced without the author's permission.

AVIS:
L'auteur a accordé une licence non exclusive permettant à la Bibliothèque et Archives Canada de reproduire, publier, archiver, sauvegarder, conserver, transmettre au public par télécommunication ou par l'Internet, prêter, distribuer et vendre des thèses partout dans le monde, à des fins commerciales ou autres, sur support microforme, papier, électronique et/ou autres formats.

L'auteur conserve la propriété du droit d'auteur et des droits moraux qui protège cette thèse. Ni la thèse ni des extraits substantiels de celle-ci ne doivent être imprimés ou autrement reproduits sans son autorisation.

In compliance with the Canadian Privacy Act some supporting forms may have been removed from this thesis.

While these forms may be included in the document page count, their removal does not represent any loss of content from the thesis.

Conformément à la loi canadienne sur la protection de la vie privée, quelques formulaires secondaires ont été enlevés de cette thèse.

Bien que ces formulaires aient inclus dans la pagination, il n'y aura aucun contenu manquant.

Canada

University of Alberta

Dedication

Special thanks to my family and friends in China and Canada for their support and encouragement

Abstract

Keywords: Computer simulation, Abrasive wear, Microstructural effects, Composite materials

Composite materials are widely used in various industries to resist wear of machinery, equipment and facilities. The high wear resistance of composite materials benefits from a combination of hard reinforcing phase and ductile/tough matrix, which may effectively resist wear under various wear conditions. However, the performance of a composite could vary significantly in different wear situations, and the material may not be fully used with its maximum resistance to wear. For instance, a composite may possess extremely high resistance to sliding wear but perform less impressively when subject to impact wear. Wear is a complicated surface damage process, affected by many factors, such as microstructure, mechanical properties of the target material, and the wear condition. Microstructure may play a predominant role in resisting wear. However, the effect of microstructure on wear is difficult to investigate experimentally due to possible synergism between the microstructure and other factors. It is a challenging task to obtain the maximum wear resistance through microstructural optimization.

Computer simulation is an effective approach for such studies, since controllable "computational experiments" can be performed to investigate contributions from individual factors to wear and that from the synergetic interaction between these factors. In this work, a dynamic model, so-called Micro-Scale Dynamic Model (MSDM) based on the Newton's law of motion, was applied to simulate abrasive wear of hard particle reinforced metal-matrix composite materials. The microstructural effects of a composite, e.g. the size,

shape and volume fraction of reinforcement, and the interfacial bond strength on wear, were investigated. The synergism of the above parameters was also studied using the MSDM. Finally, effects of abrasive particle shape on the wearing stress and material loss were investigated. Mechanisms responsible for all the effects on abrasive wear of composite materials are analyzed and discussed.

Acknowledgments

I would first like to thank my supervisor, Dr. D. Y. Li for his constant guidance and advice throughout this endeavor. His useful suggestions and innovative ideas have been of great assistance to me in completing this project. I am also grateful for the timely help and beneficial discussion from my co-supervisor, Dr. Rees Llewellyn. His industrial expertise and practical advice have been of great help during the program.

I would also like to thank the Department of Chemical and Materials Engineering staff for their help and assistance, especially Bob Barton, Jack Gibeau, Lloyd White, Bob Scott, and Tina Barker for their technical support in using the computer facilities and conducting the experimental work.

My special thanks are given to my colleagues, Qiang Chen for his assistance in modeling, Xuanyi Wang and Walid Bouaeshi for their help in experiment, and all other members in the Surface and Tribology group for their encouragement.

Finally I am grateful for the financial support from the Natural Science and Engineering Research Council of Canada (NSERC), Syncrude Canada Ltd., and National Research Council (NRC).

TABLE OF CONTENTS

1 INTRODUCTION AND LITERATURE REVIEW 1

1.1 GENERAL INTRODUCTION TO WEAR 1

1.2 ABRASIVE WEAR 5

1.2.1 Abrasive wear and mechanism 6

1.2.2 Abrasive wear of composites 11

1.2.3 Experimental techniques for abrasive wear test 18

1.3 GENERAL INTRODUCTION TO COMPUTER SIMULATION IN MATERIALS SCIENCE 21

1.3.1 The Finite Element Method (FEM) 23

1.3.2 Molecular Dynamics (MD) Simulation 28

1.3.3 A new model for modeling wear processes—Micro-Scale Dynamic Model (MSDM) 32

1.4 OBJECTIVE OF THE WORK 34

2 MICRO-SCALE DYNAMIC MODEL DEVELOPMENT FOR ABRASIVE WEAR OF COMPOSITE MATERIALS 35

2.1 INTRODUCTION 35

2.2 MODEL DESCRIPTION 35

2.2.1 The properties of materials 35

2.2.2 External force influence 40

2.2.3 Calculation of the total force on each lattice site 42

2.2.4 The movement of lattice sites and deformation of the system 42

2.2.5 The strain distribution of the lattice system 44

2.2.5 The wear procedure 45

2.3 MODEL APPLICATION IN ABRASION FOR MULTIPHASE MATERIALS 46

2.3.1 Simulation of abrasion 46

2.3.2 Simulation of multi-phase materials 47

2.4 TIME INTERVAL Δt 52

2.5 ADVANTAGES OF MSDM AND FURTHER DEVELOPMENT 53

3 SIMULATION OF MICROSTRUCTURAL EFFECTS ON ABRASIVE WEAR OF COMPOSITES PART I: BASIC PARAMETERS 56

3.1 SIMULATION PROCEDURES 56

3.2 RESULTS AND DISCUSSION 57

3.2.1 Effects of reinforcement volume fraction on abrasive wear 57

3.2.2 Effects of interfacial bond strength on abrasive wear *60*
3.2.3 Effects of reinforcement size on abrasive wear *64*
3.2.4 Effects of the ratio of abrasive particle size to reinforcement size on abrasive wear *67*
3.3 CONCLUSION 71

4 SIMULATION OF MICROSTRUCTURAL EFFECTS ON ABRASIVE WEAR OF COMPOSITES PART II: COMBINED EFFECTS OF BASIC PARAMETERS 73

4.1 INTRODUCTION 73
4.2 RESULTS AND DISCUSSION 74
4.2.1 Effects of reinforcement size distribution on abrasive wear *74*
4.2.2 Combined effects of reinforcement size ratio and size distribution on abrasive wear *79*
4.2.3 Combined effects of size ratio and volume fraction on abrasive wear .. *84*
4.2.4 Combined effects of size ratio, volume fraction and interfacial bond strength on abrasive wear *89*
4.3 CONCLUSION 95

5 SHAPE EFFECTS OF THE REINFORCEMENT AND THE WEAR PARTICLE ON THE ABRASIVE WEAR OF COMPOSITE MATERIALS 96

5.1 INTRODUCTION 96
5.2 RESULTS AND DISCUSSION 97
5.2.1 Effects of reinforcement shape on abrasive wear of composite *97*
5.2.2 Effects of abrasive particle shape on abrasive wear of composites *100*
5.2.3 The combined shape effects on abrasive wear loss *103*
5.2.4 Strain analysis for reinforcement and abrasive particles having different shapes *105*
5.2.4.1 Abrasive shape and strain *107*
5.2.4.2 Reinforcement shape and strain *110*
5.3 CONCLUSION 115

6 OVERALL CONCLUSIONS AND FUTURE WORK 116

6.1 SUMMARY OF THE RESULTS IN DIFFERENT CHAPTERS 116
6.2 FUTURE WORK 118

REFERENCES 120

LIST OF TABLES

Table 1-1 Various situations in industries where different types of wear could occur [3]. 4
Table 1-2 Microstructure and property relationship for aluminum and its alloy [33].. 14
Table 1-3 Some micro/nano level computer simulation models and their applications [65]. 22
Table 1-4 Some macro level computer simulation models and their applications [65]. 22
Table 1-5 Applications of FEM in various fields [70] 25
Table 3-1 Mechanical properties of materials involved in the simulation study 57
Table 4-1 Size distributions of WC reinforcement used in the simulation 76
Table 4-2 The simulation wear loss results of different size distributions and size ratios 81
Table 5-1 The maximum tensile and compressive strains in a homogeneous material caused by different shapes of abrasive particles..... 107
Table 5-2 The maximum tensile and compressive strains caused by dissimilar shapes of reinforcements at different time steps 111

LIST OF FIGURES

Figure 1-1 Different wear modes [3, 9]. 3
Figure 1-2 Characteristic appearance of surfaces worn by (a) adhesion, (b) abrasion, (c) surface fatigue, and (d) corrosion [4]. 3
Figure 1-3 Tungsten carbide /Ni alloy binder composite hardfacing (arrowed) on new and used shovel teeth (photography courtesy of Syncrude Canada Ltd). 5
Figure 1-4 Geometry of contact between an idealized conical abrasive particle and a surface: (a) in elevation; (b) in plan view [9] 7
Figure 1-5 Slip line fields for the deformation caused by the sliding of a rigid two-dimensional wedge from right to left. Three modes can be identified as (a) cutting, (b) wedge forming, (c) ploughing [9]. 8
Figure 1-6 The geometry of a Hertzian cone crack formed by a sphere, which is pressed on to the surface of a brittle material [9]. 9
Figure 1-7 Diagram showing crack formation in a brittle material due to point indentation. The normal load increases from (a) to (c), and is then progressively reduced from (d) to (f) [9]. 10
Figure 1-8 Potential applications of titanium metal matrix composites and intermetallic matrix composites for a military aero-engine [24]. 12
Figure 1-9 Three different kinds of MMCs: (a) particulate-reinforced MMC, (b) whisker-reinforced MMC, (c) cross section view of long and oriented fiber-reinforced MMC [23]. 13
Figure 1-10 Schematic representation of the elements of a tribosystem [4]. 18
Figure 1-11 Typical rigs for evaluation of abrasive wear [3]. 19
Figure 1-12 The configuration of a rubber-wheel test system (ASTM G65) [3]. 20
Figure 1-13 Some characteristic space and time scale, (a) number of atoms in a cube, (b) characteristic times of typical simulation problems [65]. 21
Figure 1-14 FEM strain distribution for a Ni particle in an AHC (Anodic Hard Coating) +Ni composite layer (a) the initial state at the beginning of sliding, (b) the final state after sliding [93]. 27
Figure 1-15 Typical mixing of metallic glass at sliding interface [87]. 31
Figure 1-16 Sliding of a Cu (100) tip on a Cu (100) surface from the right-hand side [76]. 32
Figure 1-17 Cross section view of three asperities sliding on a silicon surface involving phase transformation [94]. 32
Figure 2-1 Schematic of a two-dimensional model for target composite material and an abrasive sand, different colors represent different phase components. 37
Figure 2-2 Schematic illustration of the definition of stress for a lattice site. (a) 3D view of an element with cross-sectional area of l_0^2 and a very large length of L (plain strain condition) (b) A corresponding 2D lattice having a unit thickness of l_0. 37
Figure 2-3 Schematic of stress-strain curve 38
Figure 2-4 Schematic representation of the work-hardening effect. 40

Figure 2-5 Illustration of the vectors used in equation (2-11) to calculate deformation. 43
Figure 2-6 The volumetric strain at site 0 may be calculated by considering the force equilibrium at the site. 45
Figure 2-7 The pressure distribution in the contact area between the rubber wheel and the specimen. 47
Figure 2-8 Schematic illustration of two types of bonds in a composite containing components with different mechanical properties. 48
Figure 2-9 Two presumptive interfacial strengths and a $\sigma \sim \varepsilon$ curve of the matrix. 51
Figure 2-10 The influence of time interval Δt on abrasive wear loss 53
Figure 2-11 Wear rate as a function of surface temperature during sliding for Ti-6Al-4V alloy [110]. 54
Figure 2-12 Modification of plastic modulus used in the simulation. 55
Figure 3-1 Wear loss vs. the volume fraction of reinforcement. 58
Figure 3-2 Cross-sectional morphologies of four composites with different volume fractions of reinforcement after abrasion by six abrasive particles. 59
Figure 3-3 (a)Two presumptive interfacial moduli and elastic modulus of the matrix. (b)Cross-sectional morphologies of composites with the two different interfacial bond strength after abraded by five sand particles. 62
Figure 3-4 The critical volume fraction of reinforcement changes as the interfacial bond strength changes. 63
Figure 3-5 (a) The effect of the reinforcement size on wear loss; (b) Experimental observation reported by S. Usmani et al. [49]; (c) Cross-sectional morphologies of four worn composites reinforced by hard particles with different sizes. 66
Figure 3-6 (a)The effect of the ratio of the abrasive particle size to the reinforcement particle size on abrasive wear of a composite; (b) Cross-sectional morphologies of the material abraded by abrasive particles of different sizes. 69
Figure 3-7 (a) Experimentally determined relative wear resistance vs. the abrasive penetration depth [59]. (b) The relative wear resistance vs. size ratio from the present simulation. 70
Figure 4-1 The wear loss of composite as a function of volume fraction of fine reinforcement when size ratio is 5:1 75
Figure 4-2 The effect of the reinforcement size distribution on wear. (a) Wear loss vs. the size distribution of reinforcement; (b) Cross-sectional view of four worn surfaces with different size distributions of reinforcement. 79
Figure 4-3 (a) Effects of the reinforcement size distribution and the ratio of abrasive size to the reinforcement size on wear loss, (b) typical morphologies of composite materials with various size distributions after abrasion by sand of different sizes. 82
Figure 4-4 Schematic illustration of the wear intensity as a function of abrasive size and the spacing between reinforcement particles. D-groove size, d-reinforcement size, λ - mean free path, $\lambda_{3\mu m}$ -mean free path of the composite reinforced by TiC with size of 3μm, $\lambda_{30\mu m}$ -mean free path of the composite reinforced by TiC with size of 30μm [57]. 83

Figure 4-5 Wear loss of composites with different volume fraction of fine particulates abraded by three sizes of abrasive grit. 85
Figure 4-6 Typical morphologies for composites containing by different volume fractions of fine reinforcements under small and large abrasive particles. 87
Figure 4-7 Wear loss as a function of volume fraction of reinforcement for three size ratio conditions. The critical volume fraction is shifted to a higher level when the size ratio decreases. 88
Figure 4-8 Wear losses of composites with weak bond and strong bond, respectively, under three size ratio conditions. 91
Figure 4-9 Typical morphologies of composites abraded by two different sizes of abrasive sand particles, under weak and strong bond conditions. 92
Figure 4-10 Wear losses as a function of volume fraction of reinforcement for three size ratio. Two bond strengths are considered. (a) strong bond. (b) weak bond. The critical volume fraction for each condition is different. Instead of resulting in a critical volume fraction, the weak bond likely results in continuous increase in wear loss as the volume fraction increases. 94
Figure 5-1 Effects of different reinforcement shapes on abrasive wear of composites under identical abrasion conditions. 98
Figure 5-2 The morphologies of three composites with different shapes of reinforcements abraded by diamond abrasive particles. 99
Figure 5-3 Effects of different abrasive particle shapes on abrasive wear of composites under identical abrasion conditions. 101
Figure 5-4 Morphologies of three composites abraded by particles of different shapes. 102
Figure 5-5 The contact between a abrasive particle and the target surface changes from an area contact to a point contact (a) an area contact (b) a point contact after the square abrasive is rotated by 45° 103
Figure 5-6 Effects of reinforcement shape and abrasive shape on wear. 104
Figure 5-7 The stress σ_x in particles and the equivalent strain ε_{eqv} in matrix when the displacement load $u_x = \varepsilon_x L_x$ ($\varepsilon_x = 2\%$) is applied at the right edge $x = L$ of each condition, where the plane strain condition is applied (P: the x-direction overall stress of each situation). (a) the stress and strain distribution around the angular particles; (b) the stress and strain distribution around spherical particles [120]. 105
Figure 5-8 During the ASTM G 65rubber wheel test, the velocity of the sand particle has two components, the vertical velocity V_n and the horizontal velocity V_h .The total velocity V_t is a function of time and the interaction between the abrasive particle and the target surface. 106
Figure 5-9 Strain distributions in a target material abraded by abrasive particles having different shapes, respectively: (a) diamond abrasive; (b) square abrasive; (c) half-sphere abrasive particles. The shown is the second abrasive particle sliding over the area which has been abraded by the first particle. 108
Figure 5-10 Contours of maximum principal stress caused by a combination of elliptical distribution of tangential and normal force [128] 110
Figure 5-11 Strain distributions from different approaches (a) from a commercial FEM package (ANSYS); (b) from the MSDM technique in previous study[129]..... 110

Figure 5-12 Strain distributions of composites with different reinforcement particle shapes under compression by a half-sphere abrasive particle at different simulation time steps (a) diamond reinforcement, (b) square reinforcement, (c) sphere reinforcement. 113

Chapter 1

Introduction and Literature Review

1 Introduction and Literature Review

1.1 General Introduction to Wear

Wear is recognized as one of the most important detrimental processes in mechanical devices, yet detailed scientific studies of this phenomenon have a relatively short history [1]. For a long time, it has even been difficult to give a precise definition of wear due to the common coexistence of several different modes during a specific process. In 1993, the American Society for Testing and Materials (ASTM) defined wear [2] as "the damage to a solid surface, generally involving the progressive loss of material, due to relative motion between two moving surfaces". This definition is now generally cited by researchers in the field.

There are two conventional approaches to classify wear. One is description of the results of wear, using the terms as pitting, fretting, scuffing and scoring, which are highly descriptive of the appearance of worn surfaces. The other is based upon the physical nature of wear processes, with focus on the mechanisms involved and is therefore more useful to scientific research. Generally, five categories [1] are used in the second approach: (1) adhesive wear, (2) abrasive wear (two-body and three-body abrasive wear, or sometimes high-stress and low-stress wear), (3) corrosive wear, (4) erosive wear by solid particles, fluid, cavitations and often exacerbated by synergistic corrosion attack, (5) fatigue wear. Figure 1-1 illustrates schematic view of the different wear modes. Figure 1-2 shows characteristic appearance of surface worn by (a) adhesion (b) abrasion (c) surface fatigue and (d) corrosion. Table 1-1 lists some common situations in various industries in which different types of wear occur.

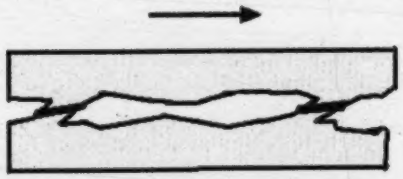

(a) Adhesive wear from the rubbing together of relatively smooth surfaces resulting in localized micro-welding, followed by tearing of the joined areas in subsequent movement.

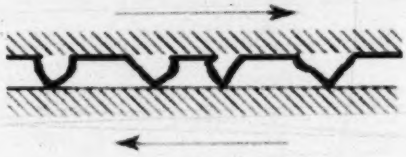

(b-1) Two-body abrasive wear from moving contact with hard protuberance at top surface.

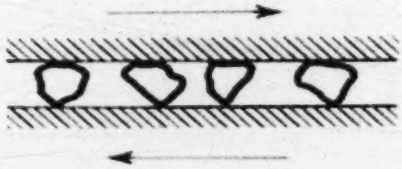

(b-2) Three-body abrasive wear from hard particles trapped between moving surfaces.

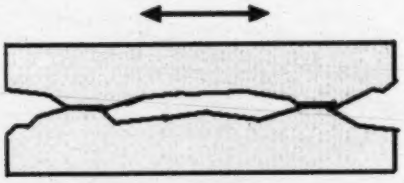

(c) Corrosive wear by fretting from small oscillatiory movements between relatively smooth surfaces.

(d-1) Erosive wear by cavitation from the collapse of vapor bubbles.

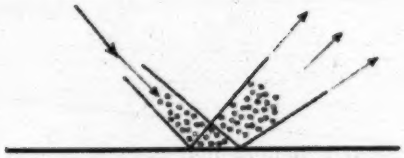

(d-2) Erosive wear by fine hard solids in a stream of fluid.

(e) Fatigue wear due to the release of particles from a surface.

Figure 1-1 Different wear modes [3, 9].

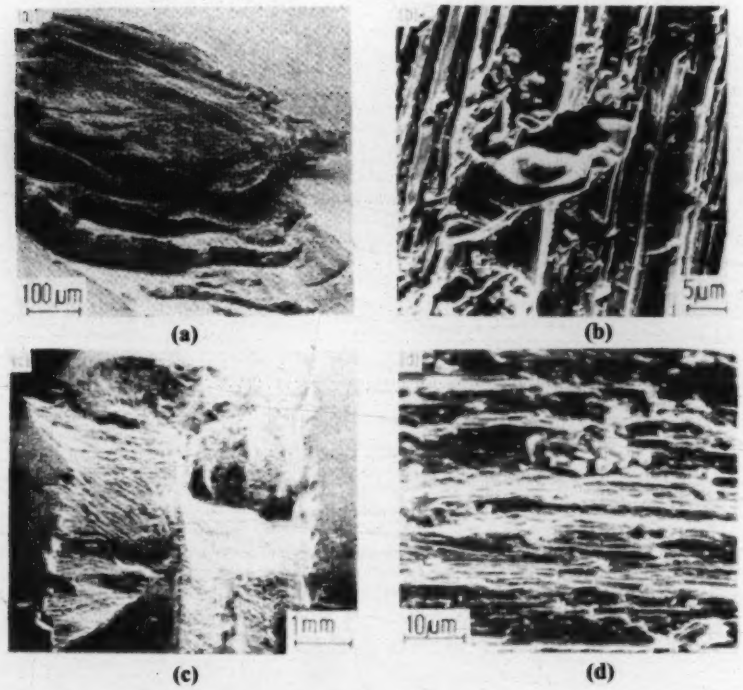

(a) (b) (c) (d)

Figure 1-2 Characteristic appearance of surfaces worn by (a) adhesion, (b) abrasion, (c) surface fatigue, and (d) corrosion [4].

Table 1-1 Various situations in industries where different types of wear could occur [3].

Type of wear	*Examples of industrial applications where this wear is likely to occur*	
1. Abrasive wear from contact with hard granular material	Earth-moving machines Material-handling chutes Rock crushers Mining conveyors	Rotors of powder mixers Extrusion dies for bricks and tiles
2. Abrasive wear from hard particles trapped between moving surfaces	Pivot pins in construction machinery Scraper blades in plaster-mixing machines	
3. Adhesive wear from the rubbing together of smooth surfaces	Rubbing bearings Clutches Press tools	Brakes Piston rings and cylinder liners
4. Fretting	Connecting rod joints in internal combustion engines Bearing-to-housing contact, with dynamic loads Spline and gear couplings with misalignment Wire ropes and overhead electrical conductor cables	
5. Cavitation erosion	Marine propellers Pump rotors Hydraulic control valves	
6. Particle erosion	Valves controlling the flow of sandy crude oil Pipelines carrying abrasive materials Helicopter rotors in desert operation	
7. Surface fatigue	Rolling bearing races and elements Heavily loaded high-speed plain bearings Clutches subject to excessive slip Surfaces in intermittent contact with molten metals	

The importance of wear has been ignored for a long time before people realized that wear is a very complicated surface damage process with time-dependent deformation, failure and removal of materials at contact moving surfaces. Wear is now recognized not only as a surface destructive process, but also as a major factor limiting the service life and performance of a mechanical component and even an entire system. According to Rabinowicz [5], surface deterioration is responsible for 70% of the loss of useful materials in the automobile industry while wear problem accounts for 55% of such material loss. As can be imagined, the total economical loss caused by repairing or replacing worn parts of the machinery and

facilities in all kinds of industries is huge. In North America, it has been conservatively estimated that wear and friction cost Canada in excess of $5 billion per year and in U.S.A. the cost is more than $100 billion annually [5, 6]. Therefore, scientific research on wear phenomenon and mechanism as well as material development must be conducted in order to make good use of currently available resources and reduce the significantly large capital loss due to wear.

1.2 Abrasive Wear

Figure 1-3 Tungsten carbide /Ni alloy binder composite hardfacing (arrowed) on new and used shovel teeth (photography courtesy of Syncrude Canada Ltd).

Among those five types of wear, abrasive wear is very common mode in industries such as construction, agriculture, mining, mineral processing industries, which involve earth moving, and handling of dirt, rock, mineral and sand [5]. Figure 1-3 illustrates the severity of abrasion wear in mining and mineral industries.

Abrasion may occur in association with other forms of wear, i.e. adhesion, corrosion and erosion [1, 5]. Studies show that abrasion takes more than 30% of total wear loss (some research shows as high as 60% of total wear loss) [5] and is about 1~ 4% of the gross national product of an industrialized nation [7]. Therefore studying abrasive wear phenomenon is of particular importance to industries.

1.2.1 Abrasive wear and mechanism

Abrasive wear can be simply described as the damage to surface by harder material. In ASTM G65-93 [2], it is defined as "wear due to hard particles or hard protuberances forced against and moving along a solid surface". Two-body abrasion and three-body abrasion are frequently used to describe two main modes of abrasive wear. As shown in Figure 1-1 (b-1) and (b-2), in the two-body abrasion case, a surface is abraded by a harder counterface; in the three-body abrasion case, a surface is abraded by a third body, generally small particles, caught between two moving surfaces. The particles are sufficiently harder than either one or both of the surfaces that are to be abraded [8]. The third body is free to roll and slide between two sliding surfaces [9]. Spending 90% of the contacting time rotating, the third particles would result in elastic deformation rather than removal of the materials. As a consequence, the three-body abrasion mode usually results in lower wear loss than the two-body abrasion [5]. In many other situations, high stress abrasion and low stress abrasion are used to describe the stress condition and the severity of damage to materials under abrasion attack [4, 9-11].

In order to understand how material properties affect abrasive wear, it is critical to understand the main mechanisms in abrasion processes. There are two extreme mechanisms for abrasion: plastic deformation and brittle fracture [9, 12]. Plastic flow can occur alone under some circumstances, but both often occur together, even in brittle materials [9]. During the abrasion process, the plastic flow occurs at the soft surface around the asperities of the harder counterface. Then microploughing, microcutting [8, 13-15], microcracking [8] and delamination [16]

will occur, causing removal of material from the softer surface, resulting in wear loss.

In plastic deformation mechanism, an abrasive particle is supposed to be a cone of semiangle α under an indentation pressure P (Figure 1-4). The normal load f carried by the particle results in plastic deformation beneath the abrasive particle. As the abrasive particle moves, a groove will be formed and the wear loss may occur by the removal of material from the groove. Assuming $P \approx H$ (H is the indentation hardness of the material); the total volume loss per unit sliding distance Q is given by equation (1-1) [9]:

$$Q = \frac{KF}{H} \tag{1-1}$$

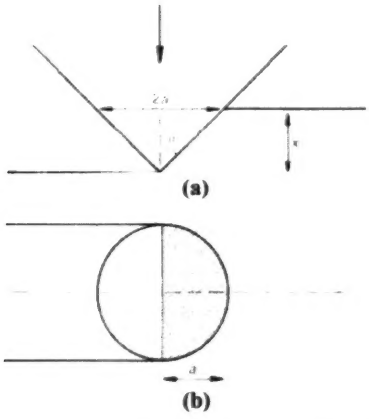

Figure 1-4 Geometry of contact between an idealized conical abrasive particle and a surface: (a) in elevation; (b) in plan view [9]

where F is the total applied normal load on all of the abrasive particles. The constant K is related to the average fraction of displaced material actually removed, and the geometry of the abrasive particles (i.e. on α). The experimentally determined values of K for two-body abrasion of metals are typically between 0.005 and 0.05. Equation (1-1) indicates that for a certain value of K, the wear loss increases with an increase in the total load on the material while decreases with an

increase in indentation hardness. Equation (1-1) has exactly the same form as the Archard equation for sliding wear and has been proved by confirmed experimental results [9]. However, as a possible result of work-hardening, the initial hardness of bulk material has little influence on wear loss while the hardness of the worn (i.e. work hardened) surface has closer correlation with the wear loss of a material [9].

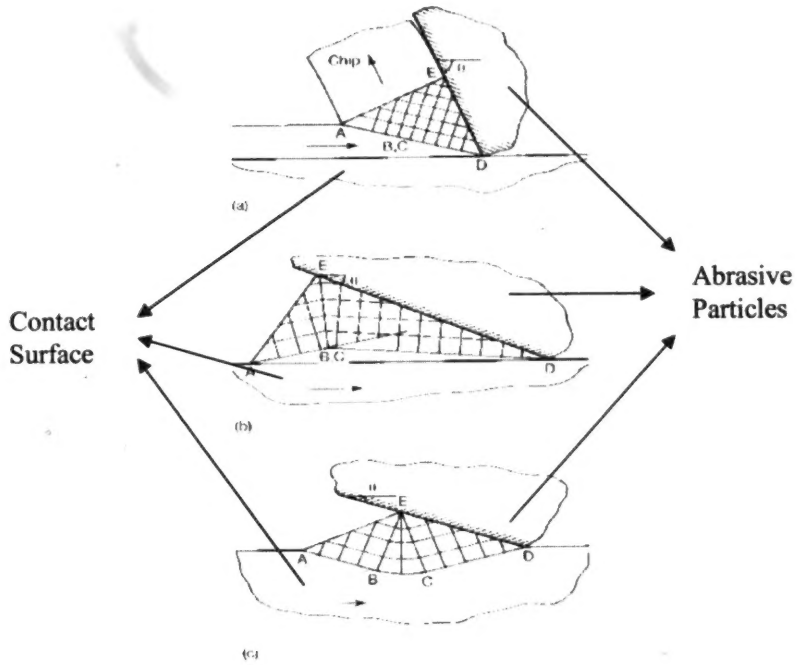

Figure 1-5 Slip line fields for the deformation caused by the sliding of a rigid two-dimensional wedge from right to left. Three modes can be identified as (a) cutting, (b) wedge forming, (c) ploughing [9].

By considering the particle angularity, the attack angle of abrasive particle and the shear force on the contact surfaces, the material removal mode can be described as cutting, wedge forming and plowing as shown in Figure 1-5 in which the slip-line field method is used to describe three different deformation modes. In the cutting mode, all the material displaced by the abrasive particle is removed in the form of chips. The displaced material is deflected through a shear zone and flows up the front surface of the abrasive particle. In this mode, the attack angle of the abrasive particle is high. While in the ploughing mode, a ridge of deformed material is

pushed along ahead of the abrasive particle. The material from the raised ridge flows beneath the particle and no material is removed from the surface. Wedge-forming is an intermediate mode in which some part of the deformed wedge material is removed from the surface. The attack angles of ploughing and wedge-forming modes are smaller than that of the cutting mode, which results in lower wear loss [9]. Both cutting mode and wedge forming mode lead to wear. However, experiments showed that the proper combination of shear force and attack angle can facilitate the transitions from ploughing to wedge formation and from wedge formation to cutting during abrasion [9].

There are some theories used to investigate brittle fracture in abrasion processes. The original theory is the Hertzian fracture theory [17], in which a brittle material is indented under a sufficiently high load by a spherical indenter and the contact stress remains elastic as shown in Figure 1-6. When the tensile stress component associated with the normal load reaches a critical value, it gives rise to fracture just at the edge of the circle of contact. The crack rapidly propagates underneath the contact area and forms the Hertizian cone cracks. If a tangential force is applied during the process, the critical load for crack nucleation and propagation will be reduced greatly, which often occurs in a sliding condition [9].

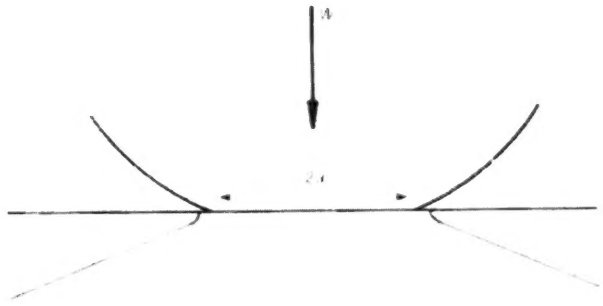

Figure 1-6 The geometry of a Hertzian cone crack formed by a sphere, which is pressed on to the surface of a brittle material [9].

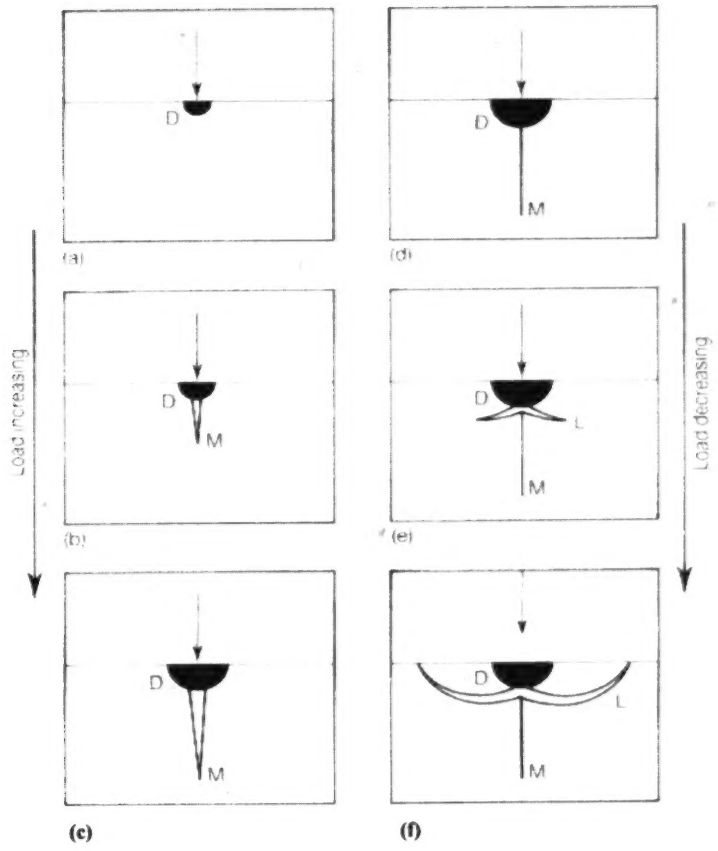

Figure 1-7 Diagram showing crack formation in a brittle material due to point indentation. The normal load increases from (a) to (c), and is then progressively reduced from (d) to (f) [9].

The situation of a brittle material under a point load differs from the spherical loading condition. Some researchers have investigated the crack behavior under a sharp indenter, shown in Figure 1-7 [9]. At the point of initial contact, very high stresses occur. Median cracks are generated right under the plastic deformation zone. Further increase in load is accompanied by progressive extension of the median cracks. The initiation and the propagation of the cracks release the large shear stresses and hydrostatic compression. As the stress magnitude decreases, the median cracks will be closed inside the material. However the residual stresses can initiate lateral cracks which could terminate at the free surface and result in volume loss of

the material. The studies show that the lateral cracks form only when the normal load on the indenter has exceeded a critical value, which depends on the fracture toughness and hardness of the material. Detailed study [9] show that wear loss resulted from brittle fracture is greater than that from plastic deformation. The relationships between load, particle size and wear loss in brittle fracture condition are different from those in plastic deformation. The transition on wear rate from plastic deformation to brittle fracture can be observed experimentally when normal load and particle size reach critical values [9].

1.2.2 Abrasive wear of composites

Although the concept of using two or more different materials to form the constituent phases of a composite has been employed ever since materials were first used thousands years ago [18], composite material has been a subject of intensive interest for only half of a century. Composite material is defined in ASTM D 3878-95c as "a substance consisting of two or more materials, insoluble in one another, which are combined to form a useful engineering material possessing certain properties not possessed by individual constituents" [19]. Nowadays, the composite materials are widely used in many industries, such as aerospace, automotive, electronic and biomedical engineering, as well as in some traditional ones like agriculture, mining and manufacturing [19-22]. New fibers, new matrices, novel composite architectures and innovative manufacturing processes continue to provide exciting opportunities for improvement in performance and reduction in cost [20].

Reinforcement and matrix are two essential components for composites. Composite materials are often classified based on materials used for the matrices, such as metal-matrix, ceramic-matrix, fiber-matrix, cement-matrix and carbon-matrix composites [19, 21]. Due to the combination of ductile metal matrix and hard reinforcement, metal matrix composites (MMCs) possess excellent mechanical properties for wide application as structure materials, substituting conventional steel and aluminum alloys. In addition, MMCs also have other improved properties, such

as wear resistance, high temperature stability, thermal and electronic conductivity and controllable thermal expansion [23]. This has largely attracted intensive interest from material researchers and motivated them to investigate such a group of materials during last few decades. Figure 1-8 demonstrates some application and potential uses of MMCs in the military field [24].

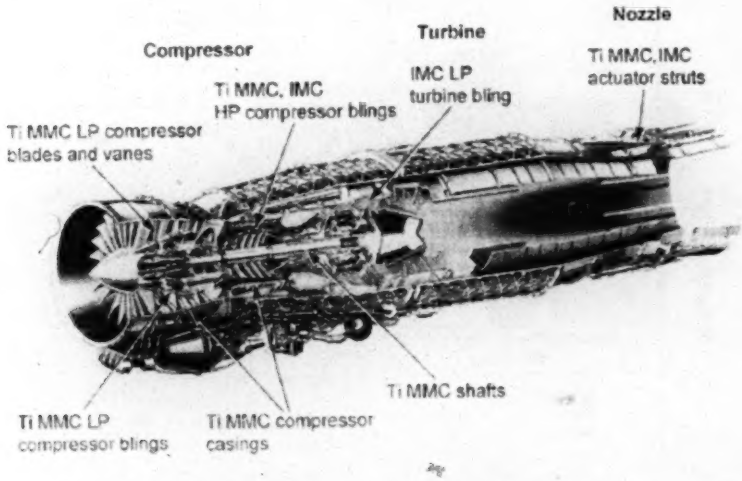

Figure 1-8 Potential applications of titanium metal matrix composites and intermetallic matrix composites for a military aero-engine [24].

The term metal matrix composite (MMC) actually covers various types of systems, and also a wide range of scales and microstructures [25]. MMCs are commonly subdivided into a few groups according to whether the reinforcement is in the form of (i) particles, which are approximately equiaxed, (ii) short fibers and/or whiskers (with or without a degree of alignment), or (iii) long aligned fibers. The former two classifications are often described as discontinuously reinforcement while the latter one is frequently referred as continuously reinforcement [19, 26]. These three kinds of composite materials are shown in Figure 1-9. Currently these MMCs are often focused on aluminum alloy matrices (beryllium, magnesium, titanium, iron, nickel, cobalt, copper, zinc, and silver based systems are also of interest). The particulate is most commonly SiC or Al_2O_3, but others (TiB_2, B_4C, SiO_2, TiC, WC, BN, ZrO_2, tungsten, graphite etc.) have also been investigated. The

majority of current MMCs are discontinuously reinforced with particulate or whisker forms of SiC or Al_2O_3 in aluminum, magnesium, and other matrix alloys [27]. Currently the MMCs are widely applied in aerospace, aircraft, automobile and construction industries. In the near future, MMCs will find their applications as superconductors, biomaterials and multi-functional materials.

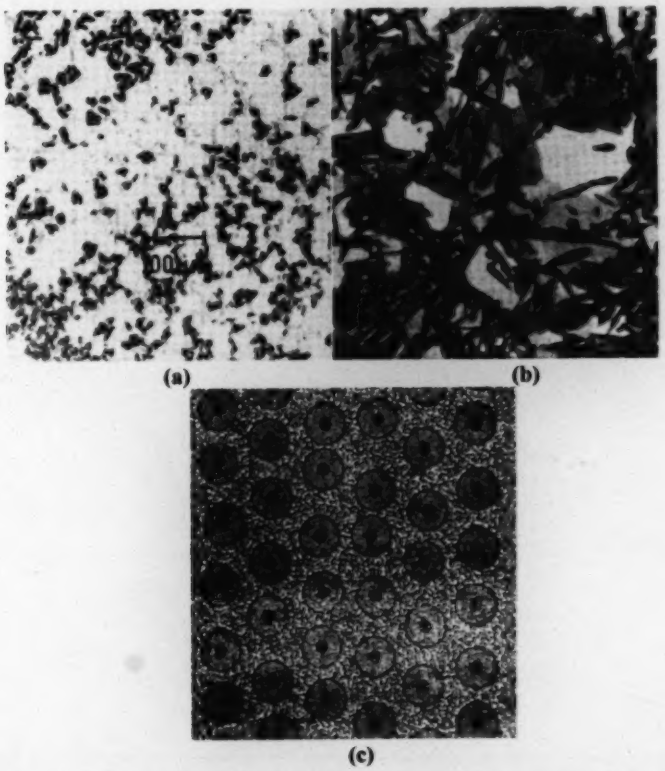

Figure 1-9 Three different kinds of MMCs: (a) particulate-reinforced MMC, (b) whisker-reinforced MMC, (c) cross section view of long and oriented fiber-reinforced MMC [23].

It is well known that the mechanical behavior of a material is determined by the processing and microstructure of the material. With the increase in the needs of advanced material, large-scale fabrication of commercial MMCs has been stimulated by the development of manufacturing and processing techniques [27]. The current techniques either involve solid [27-30] or liquid state [23, 25, 31, 32] fabrication of reinforcement and/or composites. Usually solid-state manufacturing of MMCs, such

as powder metallurgy [23, 31], diffusion bonding [23, 32] and vapor deposition [23] would result in compacted material with less porosity and improved interfacial bonding. However, liquid-state manufacturing, such as spray coating and dispersion process [23], is an easier and more economically feasible method, which has become the major approach for commercially viable application of MMCs.

The microstructure of a material plays the most important role in determining their physical properties. Table 1-2 lists various properties of aluminum and its alloys along with desirable microstructural features and their functions, which gives us a clear insight of the microstructural influences on properties of aluminum and its alloys [33]. For instance, hardness and toughness, which affect the wear performance of a material, have been known to relate directly to materials' microstructures [1]. Microstructures of MMCs are the functions of the processing methods, conditions and the chemical composition. The MMCs have a large variety of reinforcement and matrix combinations, which can be fabricated by different techniques. Therefore very different mechanical properties and wear performances can be expected for various MMCs.

Table 1-2 Microstructure and property relationship for aluminum and its alloy [33].

Property	*Microstructural Feature*	*Function of Feature(s)*
Yield Strength	uniform dispersion of fine, hard particles, fine grain size	inhibit dislocation motion
Toughness	no constituent particles, clean grain boundaries	encourage plasticity, inhibit void growth
Ductility	no constituent particles, clean grain boundaries, low dislocation density	encourage plasticity, inhibit void growth
Creep	thermally stable particles on grain boundaries, large grain size	inhibit grain boundary sliding
Fatigue Crack Initiation	no shearable particles, fine grain size	limit magnitude of slip steps at surface
Fatigue Crack Growth	shearable particles, no anodic phases or interconnected hydrogen traps, large grain size	encourage crack closure, branching, deflection and slip reversibility
Pitting	no anodic phases	prevent preferential dissolution of second phase particles
Stress Corrosion Cracking/HE	no anodic phases, or interconnected hydrogen traps	prevent crack propagation due to anodic dissolution or hydrogen embrittlement
Conductivity (electrical, thermal)	no particles with elastic strain fields, low solute concentration, low dislocation density	limit scattering sites for electron migration

For fiber-reinforced MMCs, it is widely accepted that the rule of mixtures (ROM) can be used to predict the elastic properties of such composites [19, 34]. For instance, when constant strain condition is considered, the longitudinal strength of the composite can be expressed as $\sigma_{cl} = \sigma_f V_f + \sigma_m V_m$, where σ_{cl} is the longitudinal strength of composite, σ_f and V_f are the longitudinal strength and the volume fraction of the fiber, respectively, σ_m and V_m are the strength and volume fraction of the matrix, respectively [19, 20]. While for the discontinuously reinforced MMCs, there are no quantitative relationships between composite's properties and its microstructures such as ROM. However, experimental data have shown certain microstructure-property correlations. For example, for SiC reinforced Al composites, the reinforcement content is the dominant factor in increasing the modulus of elasticity. The types of reinforcement and matrix microstructure have little influence on the composite's modulus [34]. Mechanical properties such as yield strength, ultimate tensile strength, ductility, hardness and fracture toughness, which would significantly affect the wear behavior of MMCs, are functions of reinforcement content, size, and distributions [34-37]. Usually, yield strength, ultimate tensile strength [34] and hardness [35] of composites increase as the volume fraction of reinforcement increases, while the ductility [36] and fracture toughness [36, 37] decrease. Small reinforcing particles (homogenously dispersed) could improve the hardness [4] of the composites. Therefore, it is very important to optimize the microstructure of the composite for improved mechanical properties and wear resistance. The relationships between abrasive wear and microstructural factors of particulate reinforced metal matrix composite are reviewed in details in the following paragraphs.

Wear involves two bodies in contact and it is a function of the microstructures of both materials. As wear is an irreversible process, the initial microstructure is altered substantially during wear to yield a completely different steady-state microstructure. In turn, the steady-state microstructure is a function of not only the initial microstructure but also the wear condition and the response of the material to wear. Thus one must follow the microstructural change from the time when the

material is brought into contact until a steady-state microstructure is reached. Furthermore, as wear is a surface process, a large difference in microstructure from the surface to the inner region of a material is possible. Such a gradient may affect its performance material during wear [4].

In recent years, considerable effort [4, 22, 38-64] has been made to understand the relationship between microstructural factors and the abrasive wear behavior of discontinuous MMCs.

From the previous discussion on the wear modes, we may conclude that for a ductile material, its hardness and the loading condition are important factors during abrasion, while for a brittle material the toughness and the attack angle of the abrasive seem to play a significant role. In fact, there are many influences on the abrasive wear behavior of a material. The main tribological parameters that control the abrasive wear performance of MMCs may be classified into two categories [22]. One includes mechanical properties of both the reinforcing phases and matrix [22, 38-44] as well as the microstructure of the composite, i.e. volume fraction [22, 38, 39, 45-47], size [22, 29, 45-51], size distribution, shape and shape distribution of the reinforcement. The other category involves external factors, including the effect of loading condition [22, 38, 52, 53], the size [22, 38, 45, 54-59] and shape [60-63] of the abrasive grit, surface finish, temperature and other environmental factors.

Among all those factors, mechanical properties, size and volume fraction of reinforcement, size of abrasive grit and the loading condition have been extensively studied. Hardness and fracture toughness of a composite as well as the interfacial strength are demonstrated to be the most important mechanical factors that determine the wear resistance of a composite. R. L. Deuis et al [38] have summarized studies conducted by Zum Gahr [41, 42], Hutching [43, 44] and some other researchers [45], and demonstrated that the hardness of a composite determined the indentation depth of abrasive particles and therefore an increase in hardness of the composite could reduce abrasive wear. The fracture toughness influenced the critical load for crack propagation, so that hard and tough materials were desired to reduce abrasion damage. Interfacial bonding strength can also be a

very important factor for composites. Higher interfacial bond strength could result in better resistance to abrasion as shown in the studies by S. Das, et al [40] and O. Yilmaz et al [45]. Most of the studies revealed that the wear resistance of MMC increased with volume fractions of the reinforcement [38] regardless of the types of the reinforcing phase and the matrix. However, this should not always be the case. Under different abrasion condition [38] or for different abrasive sizes [58], the volume fraction of the second phase influenced the wear behavior differently. Different loading conditions may correspond to different wear mechanisms, e.g., micro-cutting, micro-ploughing, brittle fracture [9], and thus lead to different wear rates of a composite [64]. Regarding the effect of the relative size of the reinforcement to that of the abrasive particle on wear, it was often observed that larger reinforcement enhanced the resistance to abrasion [38, 45-50], while the larger the abrasive particle resulted in more wear [52-58]. However, the situation may change, since wear of a composite is affected simultaneously by other factors, e.g. interfacial bonding, volume fraction of reinforcement, etc. As studied further, the abrasive shape effect on abrasive wear of composites attracts increasing interest [60-63]. Recent work [61-63] showed that the shape of an abrasive particle, especially its angularity, had a direct relation to microcutting behavior, which influenced the wear rate. However, the effect of shape can be affected by other factors such as abrasive size, loading conditions, etc.

In addition to the above mentioned factors, the size and shape distributions of reinforcement particles may also largely influence wear. However, research on this issue appears to have been very limited. It is logically expected that for instance, a distribution of reinforcing particles with various particle sizes could be more effective to resist wear. Large reinforcing particles usually bear most of the wearing force [40, 51] while uniformly dispersed small particles could strengthen the matrix [52]; therefore, if a composite consists of both large and small reinforcing particles, it could have higher resistance to wear than the one that is reinforced by either large particles or small particles only.

1.2.3 Experimental techniques for abrasive wear test

In order to study the wear mechanism under different service conditions and to select and design effective composites to resist abrasive wear in industry, the performance of materials under controllable abrasion condition needs to be evaluated. A tribological system usually consists of four elements: solid body, counter-body, interfacial element and environment as shown in Figure 1-10. The action on the elements or the interaction between them may vary considerably, depending on the wear condition [4]. There are a large variety of test techniques. However, attempts to standardize or correlate between different techniques have been unsatisfactory. Even when similar techniques are used, the test results obtained by different investigators could be different [4]. Therefore, when comparing the results obtained in different laboratories, one should pay attention to the configuration of testing systems used and the testing conditions under which the test results are valid. On the other hand, when selecting the most appropriate tester, one should recognize that it depends on the wear mechanism for a specific application [4].

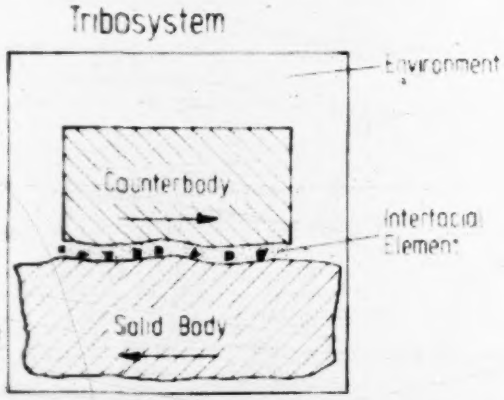

Figure 1-10 Schematic representation of the elements of a tribosystem [4].

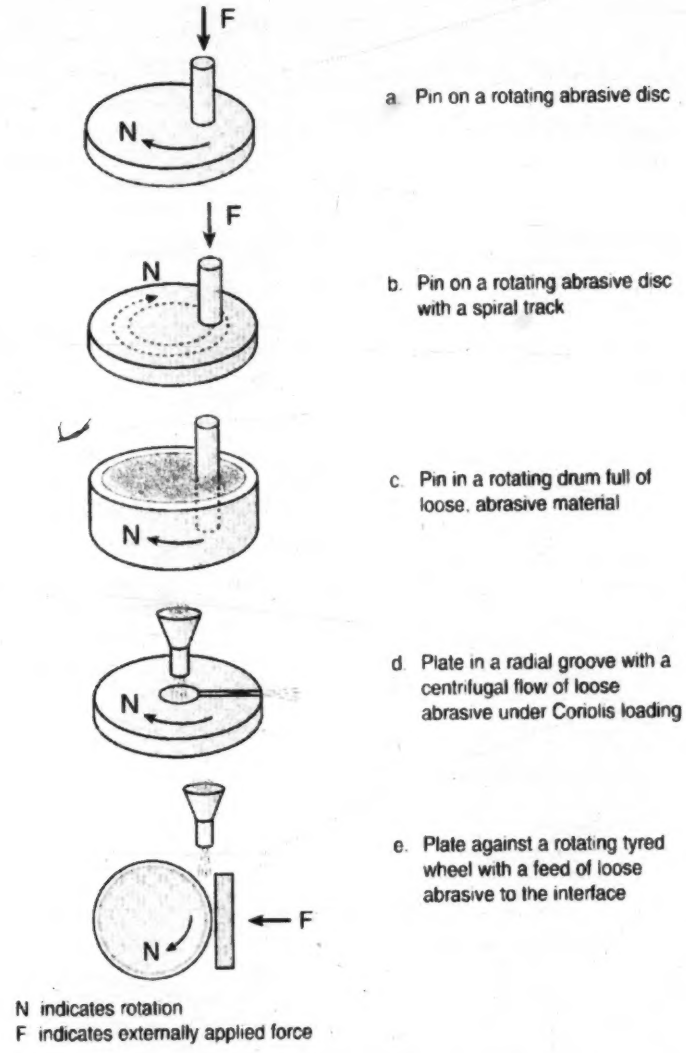
F
N
a. Pin on a rotating abrasive disc
F
N
b. Pin on a rotating abrasive disc with a spiral track
N
c. Pin in a rotating drum full of loose, abrasive material
N
d. Plate in a radial groove with a centrifugal flow of loose abrasive under Coriolis loading
F
N
e. Plate against a rotating tyred wheel with a feed of loose abrasive to the interface
N indicates rotation
F indicates externally applied force

Figure 1-11 Typical rigs for evaluation of abrasive wear [3].

For evaluation of abrasive wear, the test systems often used to investigate the mechanism and select materials are shown schematically in Figure 1-11. The pin-on-disc apparatus are shown in (a) and (b) in which the target material is always made in the form of pin and a steel disc is often used as the counter-body. During testing the pin will be pressed onto the rotating disc and abraded by the disc. This kind of tester is widely used to simulate two-body abrasion. Testers for three-body abrasion

are shown in (c), (d) and (e) in which abrasive sand is fed into the system at a certain flow rate by various methods, e.g. by a nozzle.

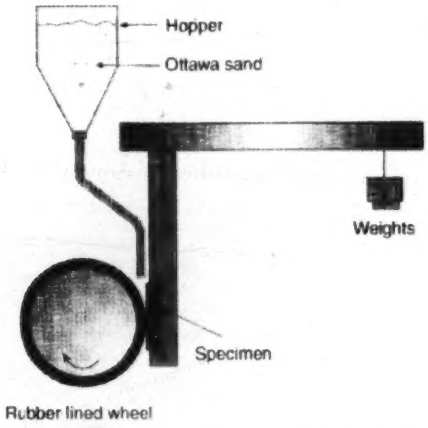

Figure 1-12 The configuration of a rubber-wheel test system (ASTM G65) [3].

The very commonly used dry sand rubber wheel test system (ASTM G65) is shown in Figure 1-12. A specimen is pressed into a rubber wheel by a dead-weight loaded lever. The abrasive sand is fed from a hopper by a nozzle between the sample and the wheel at a certain flow rate. The abrasive passes through the gap between the rubber wheel and the sample under a certain force. For a standard test, the rubber wheel of 228mm in diameter runs at 200rpm, fed with sand abrasives about 200 μm in size at a rate of 300-400 g/min. The test is run for a number of revolutions, typically in the range of 100-6000, under a load between 45 and 130 N. The wear resistance of a material is measured by its volume loss which is usually calculated from its weight loss and its known density. This low stress sliding abrasion test method is widely used to simulate the wear of machine or plant components from moving contact with hard granular abrasives which can result in fine scratching attack over its surface [3].

With these abrasive wear testers, researchers are able to select materials or to develop new materials with better performance and higher reliability for industrial applications.

1.3 General Introduction to computer simulation in materials science

The main task of materials science and engineering is to quantitatively relate properties of a material to its microstructure. Due to a large spatial and temporal spread of microstructural constituents and the complexity of possible interactions among lattice defects, quantitative prediction of microstructural evolution and microstructure-property relationship requires the employment of computer simulation. The use of computational approaches with predictive power is able to reduce the large number of experiments typically required to select materials, design new materials and related manufacturing processes. An effective model not only allows a material's behavior to be predicted with respect to microstructure in a specific environment but also provides an in-depth understanding of the mechanism responsible for a physical phenomenon. The controllable "experimental condition" can make it possible to explore mechanisms that may not be feasible by experimental investigation. There is very little doubt that computer modeling greatly facilitates and accelerates the development of high-performance materials [65].

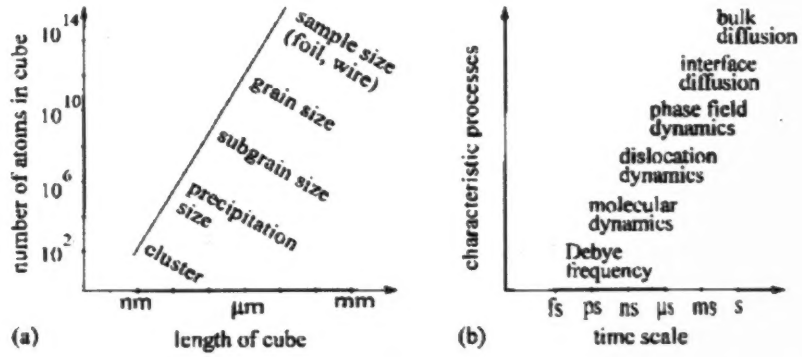

Figure 1-13 Some characteristic space and time scale, (a) number of atoms in a cube, (b) characteristic times of typical simulation problems [65].

Table 1-3 Some micro/nano level computer simulation models and their applications [65].

Scale [m]	Simulation method	Typical applications
$10^{-10} - 10^{-6}$	Metropolis Monte Carlo	thermodynamics, diffusion, ordering
$10^{-10} - 10^{-6}$	cluster variation method	thermodynamics
$10^{-10} - 10^{-6}$	Ising model	magnetism
$10^{-10} - 10^{-6}$	Bragg-Williams-Gorsky model	thermodynamics
$10^{-10} - 10^{-6}$	molecular field approximation	thermodynamics
$10^{-10} - 10^{-6}$	molecular dynamics (embedded atom, shell, empirical pair, bond order, effective medium, and second moment potentials)	structure and dynamics of lattice defects
$10^{-12} - 10^{-8}$	ab-initio molecular dynamics (tight-binding potentials, local density functional theory)	materials constants, structure and dynamics of simple lattice defects

Table 1-4 Some macro level computer simulation models and their applications [65].

Scale [m]	Simulation method	Typical applications
$10^{-5} - 10^{0}$	large-scale finite element, finite difference, linear iteration, and boundary element methods	averaged solution of differential equations at the macroscopic scale (mechanics, electromagnetic fields, hydrodynamics, temperature fields)
$10^{-6} - 10^{0}$	crystal plasticity finite element models, finite elements with advanced constitutive laws considering microstructure	microstructure mechanics of complex alloys, fracture mechanics, textures, crystal slip, solidification
$10^{-6} - 10^{0}$	Taylor–Bishop–Hill, relaxed constraints, Sachs, Voigt, and Reuss models, Hashin–Shtrikman model, Eshelby and Kröner-type self-consistent models	polyphase and polycrystal elasticity and plasticity, microstructure homogenization, crystallographic textures, Taylor factors, crystal slip
$10^{-8} - 10^{0}$	cluster models	polycrystal elasticity
$10^{-10} - 10^{0}$	percolation models	nucleation, fracture mechanics, phase transformation, current transport, plasticity, superconductivity

With the rapid development in computer techniques in recent years, a number of computer models have been proposed to simulate many processes, especially mechanical processes, for different materials [65-98]. For example, the Finite Element Method (FEM) is used to determine stress and strain distributions in polycrystalline materials [68], a topological network model describes grain growth during heat treatment [72], the Monte Carlo method has been successfully used to demonstrate the formation of texture during thin film deposition [80], and the Molecular Dynamics (MD) can vividly illustrate the microcrack propagation in NiAl

alloys [77, 79]. Those simulation methods fall into two groups respectively at macro and micro/nano- scales [65] according to the spatial and the temporal scales. Figure 1-13 illustrates the characteristic scales associated with various lattice defects that establish a certain hierarchy of microstructure. Tables 1-3 and 1-4 show the corresponding methods developed to simulate the microstructural evolution and resultant properties from atomistic level to macro-scale level [65]. The representative method of macroscopic level is the FEM, while for atomistic simulation, the MD method has been widely used in many fields. However, due to the limitation of current computer facility, it is difficult to apply MD technique for macro- and micro- level simulations. The attempt to use MD approach to simulate a system containing 10^{14} atoms which might be enough to investigate processes with thin films will fail because of unreasonably long simulation time. The FEM is also not suitable for nano- and micro- scale simulation. If a small scale is involved in FEM, the properties of bulk materials used as basic parameters in FEM are no longer valid for simulation at atomistic or microscopic level. The gap between macroscopic simulation and atomistic simulation therefore needs to be filled by developing suitable simulation methods and models [65]. Considerable efforts are being made currently to develop models which may have the capability for integrated modeling at different scales.

In the following sections, the two most widely used methods, FEM and MD, are briefly introduced. In addition a Micro Scale Dynamic Model (MSDM) is described for the purpose of studying abrasive wear for discontinuous MMCs which is the topic of this research.

1.3.1 The Finite Element Method (FEM)

The Finite Element Method is a well-developed technique which has been applied in many fields of engineering. It is a versatile numerical means for obtaining approximate solutions with known boundary and initial-value conditions by using polynomial interpolation functions [65]. Steady, transient, linear, or nonlinear

problems in stress analysis, heat transfer, fluid flow, and electromagnetism problems may be analyzed by this method [85]. The method was first developed in 1956 to analyze aircraft structural problems [68, 70]. Thereafter, within a decade, the power of this method for solving different types of problems in applied science and engineering was recognized. Table 1-5 shows some of the applications of finite element method in many fields [70]. The popularity of this method is based on the fact that once a general computer code is written, it can be used to solve many related problems by simply changing the input data and boundary conditions [70]. With the development of high speed digital computers, the finite element method has increasingly spread into many fields as such computers provide a rapid means for performing many large-scale calculations and thus make the method particularly functional and valuable.

In the finite element method, the material of interest is represented as an assembly of subdivisions called finite elements. Those finite elements have relatively simple shape and connected at specified joints which are called nodes or nodal points. As a matter of fact, field variables (e.g. displacement, stress, temperature, pressure or velocity) inside the continuum are unknown. One can determine variations of the field variable at nodal points by using some approximating functions (also called interpolation models). By solving the field equations (i.e. equilibrium equations), which are generally assembled in the form of matrix equations for the whole system, the nodal values of the field variable will be determined. Once these nodal values are known, the entire system is then determined [65].

The solution of a general continuum problem given by the finite element method always follows an orderly step-by-step procedure, which may be simply stated as follows [69]:

1. Formulate governing equations and boundary conditions

An engineering problem can usually be described by a set of governing differential equations with boundary conditions. Once these are known, the appropriate finite element solution algorithm can be obtained.

Table 1-5 Applications of FEM in various fields [70]

Area of study	Equilibrium problems	Eigenvalue problems	Propagation problems
1. Civil engineering structures	Static analysis of trusses, frames, folded plates, shell roofs, shear walls, bridges and pre-stressed concrete structures.	Natural frequencies and modes of structures. Stability of structures.	Propagation of stress waves. Response of structures to aperiodic loads.
2. Aircraft structures	Static analysis of aircraft wings, fuselages, fins, rockets, spacecraft and missile structures.	Natural frequencies, flutter, and stability of aircraft, rocket, spacecraft and missile structures.	Response of aircraft structures to random loads, dynamic response of aircraft and spacecraft to aperiodic loads.
3. Heat conduction	Stead state temperature distribution in solids and fluids	—	Transient heat flow in rocket nozzles, internal combustion engines, turbine blades, fins and building structures.
4. Geomechanics	Analysis of excavations, retaining walls, underground openings, rock joints and soil-structure interaction problems. Stress analysis in soils, dams, layered piles and machine foundations.	Natural frequencies and modes of dam-reservoir systems and soil-structure interaction problems.	Time-dependent soil-structure interaction problems. Transient seepage in soils and rocks. Stress wave propagation in soils and rocks.
5. Hydraulic and water resources engineering. Hydrodynamics.	Analysis of potential flows, free surface flows, boundary layer flows, viscous flows, transonic aerodynamic problems. Analysis of hydraulic structures and dams.	Natural periods and modes of shallow basins, lakes and harbours. Sloshing of liquids in rigid and flexible containers.	Analysis of unsteady fluid flow and wave propagation problems. Transient seepage in aquifers and porous media. Rarefied gas dynamics. Magnetohydrodynamic flows.
6. Nuclear engineering	Analysis of nuclear pressure vessels and containment structures. Steady state temperature distribution in reactor components.	Natural frequencies and stability of containment structures. Neutron flux distribution.	Response of reactor containment structures to dynamic loads. Unsteady temperature distribution in reactor components. Thermal and viscoelastic analysis of reactor structures.
7. Biomedical engineering	Stress analysis of eyeballs, bones and teeth. Load bearing capacity of implant and prosthetic systems. Mechanics of heart valves.	—	Impact analysis of skull. Dynamics of anatomical structures.
8. Mechanical design	Stress concentration problems. Stress analysis of pressure vessels, pistons, composite materials, linkages, and gears.	Natural frequencies and stability of linkages, gears, and machine tools.	Crack and fracture problems under dynamic loads.

2. Divide analysis region into elements

Dividing a system into appropriately shaped elements is the second step. For a typical one-dimensional problem, a rod with the axial displacement may be divided up into sections of desired length. For two-dimensional areas, triangles and rectangles are the usual element shapes. Three-dimensional regions can be divided up to tetrahedrons, rectangular prisms or some more complicated shapes.

3. Select interpolation functions

Within an element, a physical variable such as displacement, temperature, pressure, or stress is approximated by a simple function called interpolation function. Linear polynomial is often used as interpolation function because it is easy to be differentiated and integrated. Specific points within the elements are designated as nodal points. The value of those physical variables at the nodal point can be known from boundary conditions. The degree of the polynomial is related to the number of nodes in element. The physical variables for the whole system can be determined by knowing the values at the nodal points and the interpolation function on each element in the system.

4. Determine element properties

Each element makes a contribution to the overall region that is a function of element geometry, material properties (e.g. thermal conductivity or Young's modulus), number of nodal points, and the degree of the interpolation function. It is generally easy to determine the element properties due to the relatively simple assumed state of stress, displacement, temperature or other variables in the element.

5. Assemble global equations

All of the element properties must be assembled to form a set of algebraic equations for the nodal values of the physical variables. In a typical case of a linear system described by linear differential equations, the resulting algebraic equations will be linear in form and can be assembled using matrix techniques. Generally, the global equations for the entire system have forms similar to those for individual elements but contain more terms.

6. Solution of global equations

Many standard techniques are available to solve linear global equations. For nonlinear algebraic equations, the techniques are more complicated. The solution of the global equation will provide the information of the physical variables of each element.

7. Verification of solution

The accuracy of the numerical solution of differential equations must be verified. Generally, if the value of the physical variable at the nodal points is not significantly changed with the change of the sizes of elements, the solution is considered to be accurate. Sometimes resubstitution into the original differential equation can be used.

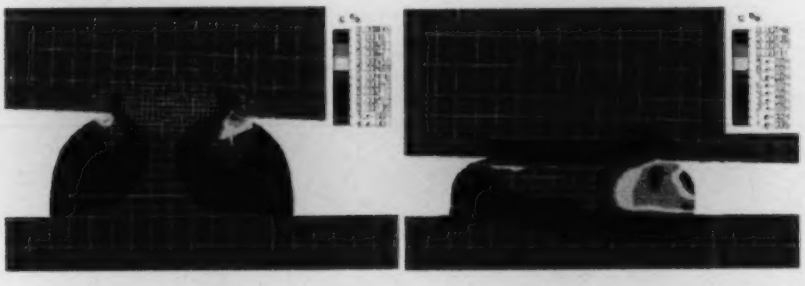

(a) (b)

Figure 1-14 FEM strain distribution for a Ni particle in an AHC (Anodic Hard Coating) +Ni composite layer (a) the initial state at the beginning of sliding, (b) the final state after sliding [93].

This approach has been applied to investigate adhesive [71], abrasive [78], erosive wear [91] for various materials such as metal alloys [90], diamond coatings [74], composite materials [81 and 93] and biomedical polymers [98] etc. For a wear process, the contact mechanics can be studied under some assumptions. The final morphology and stress and/or strain distributions can be obtained from a FEM simulation. For instance, Andrzej Posmyk [93] simulated a wear process of a composite surface layer with the Huber's hypothesis for the maximal shear fracturing stress. The strain distributions for the initial and final states are shown in Figure 1-14. It illustrates the plastic deformation of a Ni particle during the sliding

process. This approach can give us in-depth understanding of how the deformation takes place during the whole process. This information is useful for mechanical design and investigation. However, the microstructural influences of the composite layer on wear, such as volume fraction and size distribution of the reinforcement, were not taken into account. The target material was treated homogeneously, which simplified the wear process and some important detail factors might be missing.

1.3.2 Molecular Dynamics (MD) simulation

Since Alder and Wainwright [66] proposed the Molecular Dynamics (MD) method in 1959, this approach has become one of the main simulation techniques for the investigation of many-body interaction phenomena at the atomistic level [65]. With the development of nanotechnology, more and more researchers make efforts to improve the MD method to investigate a wide variety of systems and processes, such as chemical reactions, medical delivery processes, gene chips, and phase transformations. MD simulation enables us to explore the fundamental rules behind phenomenological behavior of materials at the nano scale which is difficult to be investigated using present experimental techniques. MD simulation also allows us to examine our current understanding of micro/nano scale phenomena. Depending on the number of particles and potentials employed, optimized computer codes for molecular dynamics simulation could be used on personal computers and workstations dealing with as many as 10^8 to 10^9 particles [65]. The rapid development of computer techniques will significantly benefit the MD simulation for larger systems of interest in the future.

The molecular dynamics method is a deterministic technique, which can track the motion of individual particles. An exact treatment of a many-body problem requires the formulation and solution of a Schrödinger wave equation for all atoms under study. This requires one to consider the interactions among charged nuclei and electrons as well as their kinetic energies. However, the quasi-classical MD method substitutes the atomic interactions and dynamics by potentials and classical

equations of motion. This treatment makes the solution given by MD simulation consistent with the solution given by Schrödinger wave equation [65]. This justifies the molecular dynamics method to some extent.

There are four major factors that need to be considered in the MD simulation. The first one is the typical potential functions which are related to the properties of the materials. The second is the motion equations which govern the movement of atoms. The third is the finite difference method which solves the equations in the manner of approximation. The last is the boundary conditions which offer the parameters in the initial state and defines the spatial and temporal ranges of the simulation.

The potentials used in the MD simulation reflect the interaction among the atoms. They may include a number of parameters such as the electronic charges, the polarizabilities of the ions, and the local atomic density etc. In simple pair potentials (e.g. Morse [67, 83], Lennard-Jones [89]) only the direct interaction between two particles is considered. However, in modern many-body potentials, the influence of neighboring particles is also taken into account [65]. Currently, a large variety of interatomic potentials are used to simulate different materials with different emphases on predominant factors.

The most fundamental form to describe atomic motion in a conservative system is given by the Lagrangian formulation in conjunction with Hamilton's principle of least action. In order to compare the atomic scale simulation with experimental observation, the environmental constraints, such as constant pressure, constant temperature or constant bond length, are realized by using Lagrangian transformation [65].

To integrate all the equations of motion with a given potential, the finite difference algorithm should be employed. The time-reversible Verlet algorithms [99] are relatively easy to be applied in MD simulations, which allow one to calculate the actual position and velocity of an atom at any time after the initial state. The acceleration is calculated from the conservative force, mass and a thermodynamic friction coefficient. The force is obtained as a derivative of the respective potential,

and the velocity and the position of each atom or molecule can be determined by applying conventional kinematics.

The reason for considering boundary conditions is twofold. On one hand, in order to reduce the effort for computation (e.g. computation time, coding convenience, required random access memory), the system should be as small as possible. On the other hand, the system should be large enough to provide reliable statistics. A physically realistic coupling should be considered, which accounts for volume expansion, strain compatibility, and stress equilibrium between the environment and the simulation system. The simplest boundary condition applied in many simulations is periodic boundary condition. In this case, a small volume of bulk material is considered as a primary cell and the bulk material is treated to be composed of the primary cell surrounded by exact replicas of itself. All these cells are connected by translation vectors, which allow one to describe the positions and velocities of all atoms inside and outside the primary cell.

The last important factor is the scale of time. The MD method involves the calculation of the present position and velocity of each atom, and its position and velocity after a small time interval. The typical time step used in MD simulation is in the range of 10^{-14} to 10^{-15}s. Typical scalling parameters of MD simulations are nanometers for the atomic spacing. Usually the number of involved particles is from 10^3 to 10^9. It is worth noting that most MD simulations only cover a real time period less than 1 nanosecond [65].

MD simulation plays an important role in understanding tribological processes. Unlike laboratory experiments, the MD simulation enables the full dynamics of all atoms to be followed and analyzed. Moreover, the MD simulation helps to obtain detailed information about many complex systems [92]. Although it is not yet possible to apply the MD method to large systems involved in wear processes of engineering materials, MD simulations have revealed a great deal of information about the microscopic origins of static and kinetic friction, the behavior of boundary lubricants, and the interplay between molecular geometry and tribological properties

[86]. These results provide valuable input for many traditional macroscopic calculations.

MD simulations have been applied to investigate different material systems and various processes [75, 76, 82, 83, 86, 87, 89, 92, 94]. Figure 1-15 illustrates the mixing at the sliding interface of metallic glass which may indicate large strain rate during sliding [87]. The most common case of the application of MD simulation is to investigate single or multi- asperity interaction. Figure 1-16 illustrates a single asperity sliding on a surface, which mimics the motion of an Atomic Force Microscope (AFM) tip. The adhesion of the material is demonstrated to have a great influence on wear performance of small-scale instruments. Such study has offered a deep insight into the surface/interface contact. The multi-asperity contact (as shown in Figure 1-17) simulated by W. C. D. Cheong and L. C. Zhang [94] illustrates the mechanism of nano-wear, the phase transformation of silicon and resultant plastic deformation beneath the surface. The MD simulations also have been extended to in many other aspects of tribology, such as grinding and abrading [82, 83], lubricant and material interactions [75]. MD simulation is becoming more popular for investigation of nanoscale tribological phenomena and the mechanisms involved. In the future, with the improvement of computing capability, this promising technique could eventually become a very effective industrial tool for material design and prediction of a material's behavior.

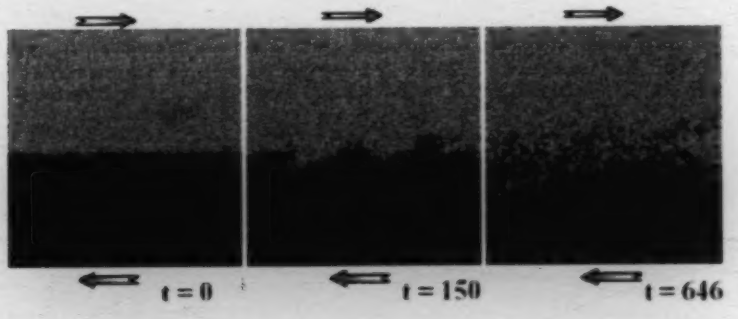

Figure 1-15 Typical mixing of metallic glass at sliding interface [87].

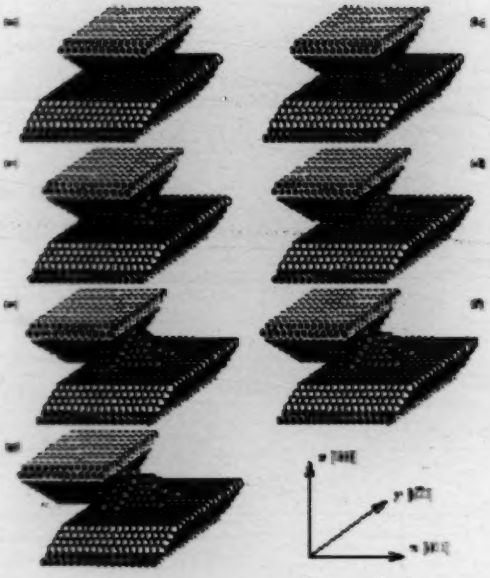

Figure 1-16 Sliding of a Cu (100) tip on a Cu (100) surface from the right-hand side [76].

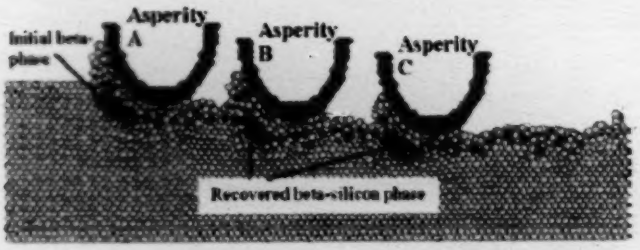

Figure 1-17 Cross section view of three asperities sliding on a silicon surface involving phase transformation [94].

1.3.3 A new model for modeling wear processes---Micro-Scale Dynamic Model (MSDM)

Although the FEM and MD methods are effective for modeling and increasing our understanding of wear processes, they have some disadvantages which retard their application in industry. Currently most FEM applications are focused on two-dimensional and three-dimensional elastic/plastic contact problems and fracture

phenomena in the contact region. However, the FEM is limited when used to analyze dynamic wear processes. Firstly, a realistic engineering surface has many asperities which change with time during wear. Therefore, treating a large number of mesh elements to map continuously changing asperities would take an unacceptably long computing time [78]. Secondly, wear of composite materials always involves dynamic failure of phases and interfaces which make the FEM treatment complicated. Thirdly, it is also difficult to investigate the effects of composite microstructure on wear, since it is not practically suitable to use FEM to deal with an inhomogeneous system that contains a large number of irregular domains. All these make the FEM approach less feasible to solve actual wear problems. While for MD simulations, although it is developed based on fundamental physical laws and can be used to investigate crystal defects i.e. vacancies, dislocations, grain boundaries, and second phases etc. This method is obviously limited to very small systems both in temporal and spatial scales due to the current limits of computing capability. It can be used to simulate a process involving $10^3 \sim 10^4$ atoms and in the simulation time of $10^{-12} \sim 10^{-11}$ s. To simulate a bulk material as small as $1\ \mu m^3$, the system will contain $10^9 \sim 10^{10}$ atoms. If micro/macroscopic elements are considered, the model should involve more atoms. Another drawback of MD simulation is the availability of suitable interatomic potentials. For most of the engineering material pairs, the potentials are not available or are only approximate semi-empirical/empirical such as Lennard-Jones potential and Morse potential.

Besides the FEM and MD approaches, there are some other approaches to model the wear problems, but these were proposed with assumptions, or macroscopic tribological rules or empirical equations, so that they may be suitable only for predicting wear loss in specific situations but not for investigating general cases and the mechanisms involved [100-103]. Lacking of generality, flexibility and feasibility limits the application of these models. It is necessary to bring new models based on simple physical rules to fulfill such tasks with satisfactory accuracy, efficiency and generality. Recently, a simple micro-scale dynamic model (MSDM) combined the advantages of both FEM and MD methods was proposed for wear

simulation, which has been successfully applied to investigations of abrasion [84, 88, 104], erosion [95, 96], and erosion-corrosion [97] of single-phase and composite materials with meaningful predictions consistent with experimental observations. In this model, a material is meshed with small elements. Mechanical properties of each component are the inputs. The motion of such a system is not determined by the assembled stiffness matrix but Newton's law of motion. Thus MSDM simulation is based on the basic physical law with the input of basic mechanical properties to simulate relatively large scale of materials. This could be its most beneficial feature. In the following chapters, MSDM is described and the results of its application to studies of microstructure - abrasive wear relationships for composite materials are presented.

1.4 Objective of the work

As stated before, there are so many factors which can influence a material's wear behavior. Experimental investigation of all the influences systematically is expensive and time consuming. However, the application of computer simulation has demonstrated that it is a promising approach to study wear processes. Since many existing simulations have difficulty for modeling damage processes, the present work applies MSDM to simulate the abrasion process of composites with emphasis on microstructural effects on wear attack. These microstructural factors includes the size, size distribution and volume fraction of reinforcement, interfacial bonding strength between matrix and reinforcing particles. Effects of abrasive particle size and shape on wear are also investigated. This research has established some general guidelines for microstructural optimization against wear of composite materials.

2 Micro-Scale Dynamic Model Development for Abrasive Wear of Composite Materials

2.1 Introduction

To model wear of materials, a micro-scale dynamical model for abrasive wear has been developed in this study. It is based on the molecular dynamics technique by applying the fundamental physical principle, i.e. Newton's Law of motion:

$$\bar{F} = m \times \frac{d^2 \bar{r}}{dt^2} \tag{2-1}$$

Instead of using atomic potentials as in traditional MD methods to determine the interaction between two adjacent sites, the new model introduces the same mechanical properties of a material as those used in Finite Element method in order to decrease the simulation time and increase the system dimensions. With such a model, simulating the microstructural effects on abrasion of composites using a PC becomes possible.

2.2 Model description

2.2.1 The properties of materials

In the present work, the simulation is performed in a two-dimensional space. The given target material and abrasive particle are both discretized into lattice sites (as shown in Figure 2-1). Each lattice site represents a small volume of the material and is connected to its neighbor sites by spring-like bonds. The force coefficient of such a bond, k, is expressed as,

$$k = E \cdot l_0 \tag{2-2}$$

where E is the modulus of the material which can be elastic modulus or plastic modulus, depending on the magnitude of deformation; l_0 is the initial stress-free

length of the bond between two adjacent lattice sites. Such a relation between the force coefficient and the modulus is derived in the following way:

$$\because \sigma = E \cdot \varepsilon,$$

$$\because \sigma = \frac{f}{l_0^2},$$

$$\text{and } \varepsilon = \frac{\Delta l}{l_0},$$

$$\therefore E \cdot \varepsilon = \frac{f}{l_0^2},$$

$$f = E \cdot \varepsilon \cdot l_0^2 = E \cdot \frac{\Delta l}{l_0} \cdot l_0^2 = E \cdot l_0 \cdot \Delta l;$$

$$\because f = k \cdot \Delta l;$$

$$\therefore k = E \cdot l_0.$$

where f is the force on a bond and σ is the corresponding stress; ε is the engineering strain of the bond. Although the true strain $\varepsilon_T = \ln\frac{l}{l_0}$ should be used when large strain is involved, it is easier to apply the directly measured mechanical properties of materials based on the engineering strain. This dose not affect the simulation result, since the input mechanical properties of relevant materials such as fracture strain and yield strain are engineering ones. In figure 2-2 (a), F is the total force exerted on a bulk material in a plane strain condition. When a slice of bulk material with thickness of l_0 is studied, the unit force over a distance of l_0 is equal to $f = F/(L/l_0)$. The lattice sites represent certain volumes of material with mass center connected by bonds as demonstrated in Figure 2-2 (b). The normal stress resulted from the force on a bond is $\sigma = \frac{f}{l_0^2}$. Since in 2D the xz and yz surfaces shrink to be lines, the stress may also be expressed as $\sigma = \frac{(\frac{f}{l_0})}{l_0}$, where $\frac{f}{l_0}$ is the force per unit length. In such a way, the deformation on xy surface is influenced by

the stresses in x or y direction of a bond. Δl is the change in bond length as the force is exerted, which is considered as the deformation of the bond.

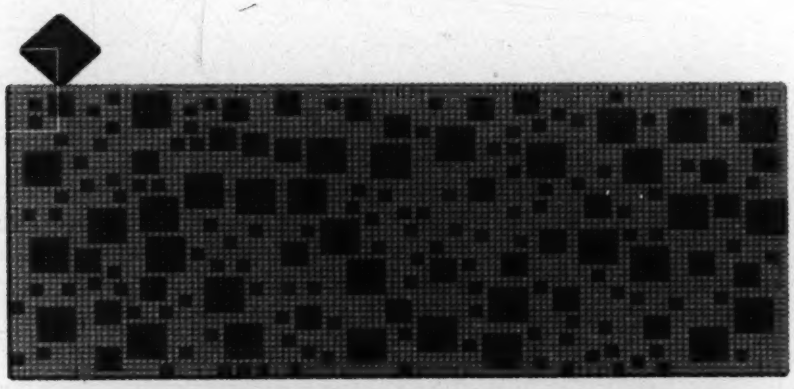

Figure 2-1 Schematic of a two-dimensional model for target composite material and an abrasive sand, different colors represent different phase components.

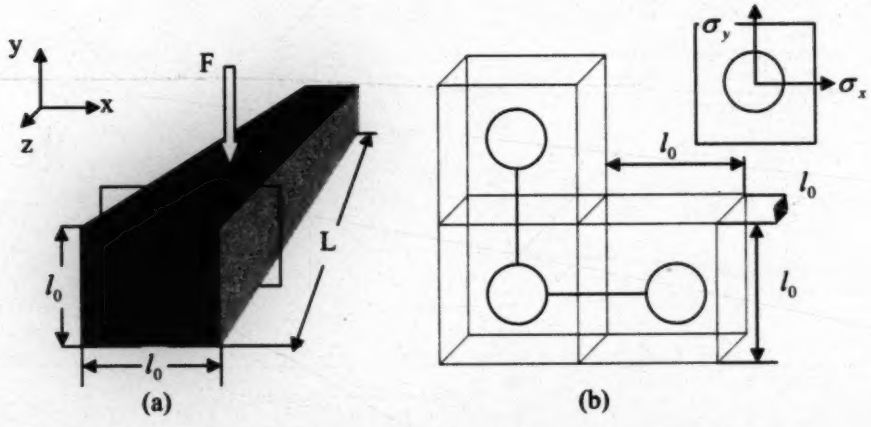

Figure 2-2 Schematic illustration of the definition of stress for a lattice site. (a) 3D view of an element with cross-sectional area of l_0^2 and a very large length of L (plain strain condition) (b) A corresponding 2D lattice having a unit thickness of l_0.

The deformation of the bond Δl is actually a vector and can be calculated as: $\Delta\vec{l} = \vec{l} - \vec{l}_0$, where $\vec{l}$ and $\vec{l}_0$ represent the deformed and the initial bond length vectors, respectively. When the value is negative, the bond is compressed; when the value is positive, the bond is stretched.

The modulus E of the material can be obtained from the stress-strain curve of the material. As shown in Figure 2-3, within the elastic region, the relationship between stress and strain is linear. The slope is $\frac{\sigma_y}{\varepsilon_y}$, corresponding to the elastic modulus E_e. In plastic region, the modulus varies with strain. An average plastic modulus E_p is applied to simplify the model by taking the slope of the curve between the yield point and the ultimate tensile stress point. E_e is defined as $E_e = \sigma_y / \varepsilon_y$ and E_p is defined as $E_p = (\sigma_T - \sigma_y) / (\varepsilon_T - \varepsilon_y)$, where σ_y and σ_T are yield strength and ultimate tensile strength of the material, respectively; ε_y and ε_T are yield strain and ultimate tensile strain, respectively. If the deformation of the bond, Δl, is in the elastic limit, the modulus E, which is used in the simulation corresponds to the elastic modulus of E_e; if the deformation Δl exceeds the elastic region, E is equal to the plastic modulus E_p.

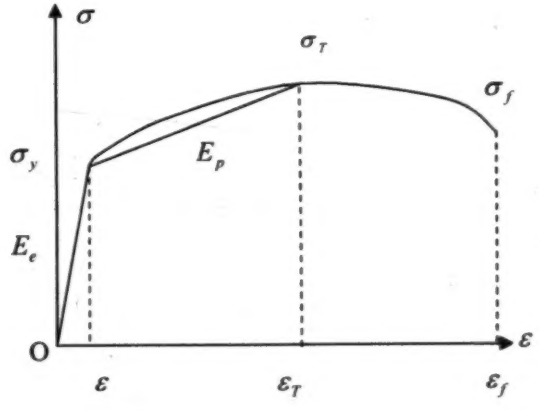

Figure 2-3 Schematic of stress-strain curve

The above description for determining E is valid when the bond is under a tensile condition i.e. the deformation of the bond, Δl, is larger than zero. However, if it is under compression which means Δl is negative, it is assumed that E is equal

to the elastic modulus and no damage occurs to the bond. The site-site bond will not be broken when the sites approach each other under the compressive stress. This also indicates that the bond will only break when it is elongated and the accumulated plastic strain is larger than the fracture strain. There will be no further interaction between two lattice sites with broken bond under tensile stress.

For a metal, the work-hardening is often very important, which strengthens the material after plastic deformation occurs. In this model, the work-hardening effect has been taken into account. For example, as shown in Figure 2-4, in the elastic strain region OM, the deformation will be recovered upon unloading, i.e. the bond length returns to the initial length after load is withdrawn. However, when the strain exceeds the yield strength, σ_y, plastic deformation occurs. In this situation, the strain of the bond ε consists of two parts. One is the recoverable elastic strain ε_y' or a new yield strain, which is larger than the original yield strain ε_y because of work-hardening. The other is the permanent plastic strain ε_p. It means that after unloading, the bond length can not return to the initial length. The residual strain is ON as shown in Figure 2-4. In the simulation, the new elastic strain ε_y', can be calculated according to the stress strain curve of the material using the following relationship:

$$\varepsilon_y' = \frac{E_p}{E_e - E_p}\varepsilon_p + \varepsilon_y \tag{2-3}$$

It is obvious that in this model the interaction between two adjacent lattice sites is a function of the mechanical properties of the bulk material which includes the Young's modulus, yield strength, tensile strength, ductility and work-hardening behavior of the material.

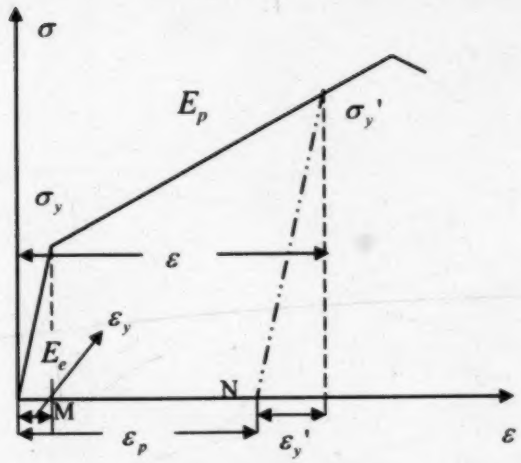

Figure 2-4 Schematic representation of the work-hardening effect.

2.2.2 External force influence

An external force can be exerted on a target material either by point contact or surface contact. In most situations the latter one will apply. The external force is transferred from another surface through contact with the target surface. This interaction will result in the motion of each lattice site in the target surface layer and finally cause fracture and failure if the external force is large enough. In order to determine how much external force is transferred to each lattice site on the target material, the surface contacting the target surface must also be descritized. In other words, the contact is analyzed by using basic element, i.e. lattice sites, on both surfaces. One thing should be noted is that there is no real bond connecting the lattice sites of two bodies in contact. An imaginary bond is used to transfer the external compressive wearing force when the distance between a target material lattice site and a abrasive surface lattice size is smaller than half of the initial length of a real bond l_0. However, when the distance is larger than half of the initial bond

length, there will be no interaction between the target material and the abrasive particles. As mentioned earlier, when compressed, the deformation on a site-site bond is assumed to be elastic. Assuming that the force coefficient of the target material is k_m and that of the moving surface (e.g. a abrasive particle) is k_s, the compressive force between a contacting pair of the target material surface and sand sites may be expressed as:

$$f = k_m \Delta l_m = -k_s \Delta l_s \tag{2-4}$$

where Δl_m and Δl_s are the target-portion compressive deformation and sand-portion compressive deformation of an imaginary bond, respectively. The minus sign indicates the force on a sand lattice site is opposite in direction to that on a target material lattice site. The total deformation on the imaginary bond between these two sites is:

$$\Delta l = \Delta l_m + \Delta l_s \tag{2-5}$$

Suppose the average force coefficient of such a "bond" under compression is $\bar{k}$, the force on this bond is calculated as:

$$f = \bar{k}\Delta l = \bar{k}(\Delta l_m + \Delta l_s) \tag{2-6}$$

From equation (2-4) and (2-5), the average force coefficient $\bar{k}$ can be determined as:

$$f = \bar{k}(\Delta l_s + \frac{k_s}{k_m}\Delta l_s) = k_s \Delta l_s$$

$$\bar{k} = \frac{k_s k_m}{(k_s + k_m)} \tag{2-7}$$

To calculate the total external force on the surface, all the bonds in contact should be counted and expressed as:

$$f = \sum_i \bar{k}\Delta l_i \tag{2-8}$$

where i is the number of bonds "connecting" target material surface and sand surface.

2.2.3 Calculation of the total force on each lattice site

The total force on a lattice site consists of two components, the external force and the interaction between this lattice site and all its nearest neighbors. The total force can be represented as:

$$\vec{F}_p = \vec{f}_p + \sum_q^n k\Delta\vec{l}\,(p,q) \tag{2-9}$$

where $\vec{F}_p$ is the total force on lattice site p, $\vec{f}_p$ is the external force on lattice site p, resulted from abrasive particles, and the second term on the right hand side is the interaction between lattice site p and all its adjacent lattice sites. n is the number of nearest neighbors of site p, k is the force coefficient for the bond between two lattice sites as derived in the previous section, and $\Delta l(p,q)$ is the deformation of the bond connecting lattice sites p and q. If the lattice site is not at the surface of the target material which interacts with the sand particle, the term of external force $\vec{f}_p$ is equal to zero. In this case the interaction between sites p and its neighbors is responsible for the motion of site p.

2.2.4 The movement of lattice sites and deformation of the system

As long as the force on each lattice site is known, the motion of each lattice site can be determined; the trajectory of each lattice site is calculated using Newton's Law of Motion:

$$\vec{F} = m \times \frac{d^2\vec{r}}{dt^2} \tag{2-10}$$

where $\vec{F}$ is the total force on a lattice site, m is the mass of the lattice site, $\vec{r}$ is the position of the site, t is the time.

One thing should be noticed in the simulation is that since the experimental mechanical properties are used as input, which involves plastic deformation, a non-

reversible process is simulated. In other words, during a wear process, an internal friction component is introduced in the equation (2-10), which can be modified as $F - f_{inter-friction} = ma$. This results in non-conservative force. However, the total energy in the entire system, including rubber wheel, abrasive particles and target materials, should be conservative.

In simulation, the deformation of bonds is determined by the position change of each lattice site. As shown in Figure 2-5, the deformation of the bond connecting lattice site p and q, after shearing, can be expressed in the following equation:

$$\Delta\vec{l}(p,q) = \vec{l}(p,q) - \vec{l}_0(p,q) = [\vec{r}(q) - \vec{r}(p)] - [\vec{r}_0(q) - \vec{r}_0(p)] \qquad (2\text{-}11)$$

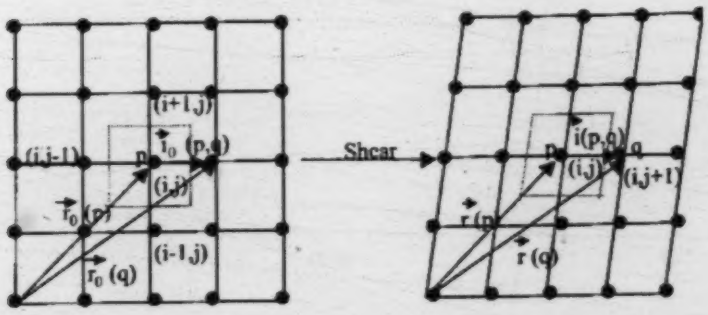

Figure 2-5 Illustration of the vectors used in equation (2-11) to calculate deformation.

where $|\vec{l}(p,q)|$ is the length of bond after deformation; $\vec{r}(p)$ and $\vec{r}(q)$ are the positions of lattices p and q after shearing, respectively; $|\vec{l}_0(p,q)|$ is the original length of the bond before shearing, and $\vec{r}_0(p), \vec{r}_0(q)$ are the original positions of lattices p and q before shearing, respectively.

The force can be calculated for each lattice site at any time if its position is known. Once the force is calculated, the movement of each lattice site can be predicted using Newton's Law of Motion. At the initial condition, there is no external force exerted on the system, all the bonds are in the stress-free state and all the lattice sites are at rest. After loading, the external force would result in changes

in velocity and position of the lattice sites after a time interval Δt. The new velocity and position of each lattice site after Δt are:

$$\vec{V}_{t+\Delta t}(p)=\vec{V}_t(p)+\frac{1}{m}\vec{F}_t(p)\Delta t \tag{2-12}$$

$$\vec{r}_{t+\Delta t}(p)=\vec{r}_t(p)+\frac{1}{2}\left[\vec{V}_t(p)+\vec{V}_{t+\Delta t}(p)\right]\Delta t \tag{2-13}$$

where, $\vec{V}_t(p)$ and $\vec{V}_{t+\Delta t}(p)$ are velocities of site p at time t and $t+\Delta t$, respectively; $\vec{r}_t(p)$ and $\vec{r}_{t+\Delta t}(p)$ are positions of site p at time t and $t+\Delta t$, respectively. m is the mass of the lattice site. $\vec{F}_t(p)$ is the total force on lattice site p at time t. Here, it is assumed that the acceleration of each lattice site is constant during the small time interval Δt. By repeating the above procedure, the trajectory of any lattice site at time t can be predicted. In other words, the movement of the whole system during a mechanical process can be predicted according to the above basic rules.

2.2.5 The strain distribution of the lattice system

In order to study effects of different shapes of reinforcement and abrasive particle on abrasive wear resistance of a material, the strain distribution of the entire lattice system was studied. In the simulation, the strain of the system is referred to the volumetric strain, i.e. $e=\Delta V/V=\varepsilon_x+\varepsilon_y$ in a 2D simulation and $e=\frac{\Delta V}{V}=\varepsilon_x+\varepsilon_y+\varepsilon_z$ in a 3D simulation, where $\varepsilon_x,\varepsilon_y,\varepsilon_z$ are the strain components in x, y and z directions, respectively. It should be indicated that the above equations are only suitable for small deformation. Since the focus of the study is put on how the strain distribution varies with shapes of reinforcements and abrasive particles rather than its absolute values, the above equations are used for qualitative information. In the simulation, the local volume strain on each lattice site is calculated as follows. An arbitrary state of a lattice site is considered as shown in

Figure 2-6. The lattice site 0 is connected to lattice site 1, 2, 3, 4 with the strains on each bond as ε_1, ε_2, ε_3, ε_4, respectively. The angles between the bonds and the horizontal direction are α_1, α_2, α_3, α_4, respectively. When the forces on site 0 are in equilibrium and the deformations are small, the total strains in x and y directions at lattice site 0 in the descritized system may be approximately expressed as:

$$\varepsilon_x = \frac{1}{2}(\varepsilon_1 \cos\alpha_1 + \varepsilon_2 \cos\alpha_2 + \varepsilon_3 \cos\alpha_3 + \varepsilon_4 \cos\alpha_4)$$

$$\varepsilon_y = \frac{1}{2}(\varepsilon_1 \sin\alpha_1 + \varepsilon_2 \sin\alpha_2 + \varepsilon_3 \sin\alpha_3 + \varepsilon_4 \sin\alpha_4)$$

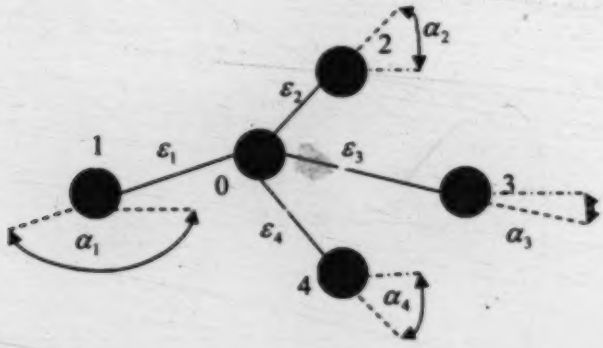

Figure 2-6 The volumetric strain at site 0 may be calculated by considering the force equilibrium at the site.

2.2.6 The wear procedure

As described earlier, if the strain of a bond, ε, is larger than the yielding strain ε_y, plastic deformation occurs. This results in irreversible strain when the force on the bond is removed. The residual strain is $\varepsilon_p = \varepsilon - \varepsilon_y'$. Consequently, the length of the bond is stretched to $l = l_0(1+\varepsilon_p)$. If the bond experience a series of plastic deformation events, the irreversible deformation can be accumulated and when it exceeds the fracture strain of the material, ε_f, the bond is broken. There is no

further interaction between two lattice sites under tensile condition if the bond connecting these two sites is broken. If all the bonds connecting a site or a cluster of sites and its neighbors are broken, the site or the cluster of sites will be worn away from the bulk material. Totaling such worn lattice sites could establish how much material is removed. The wear resistance of a material can thus be predicted.

2.3 Model application in abrasion for multiphase materials

2.3.1 Simulation of abrasion

The loading condition for abrasive wear in this study was similar to the rubber-wheel abrasion sliding test condition (ASTM G65) [84] as shown in Figure 1-12. According to Hertzian theory [105], the vertical pressure on the abrasive sand in the contact area between the rubber wheel and the specimen may have an elliptical distribution as illustrated in Figure 2-7 and as expressed by equation (2-14):

$$P(x) = P_{max}\sqrt{1-\frac{x^2}{a^2}} \tag{2-14}$$

where P_{max} is the maximum pressure and a is the radius of the contact area between the rubber wheel and the specimen. The radius of the contact region a is given by equation (2-23):

$$a = \sqrt[3]{\frac{3}{4}\frac{(1-\nu^2)FR}{E}} \tag{2-15}$$

where ν, R and E are the Poisson's ratio, radius and elastic modulus of the rubber wheel, respectively; F is the applied load on the rubber wheel, so that P_{max} can be calculated as:

$$P_{max} = \frac{3F}{2\pi a^2} \tag{2-16}$$

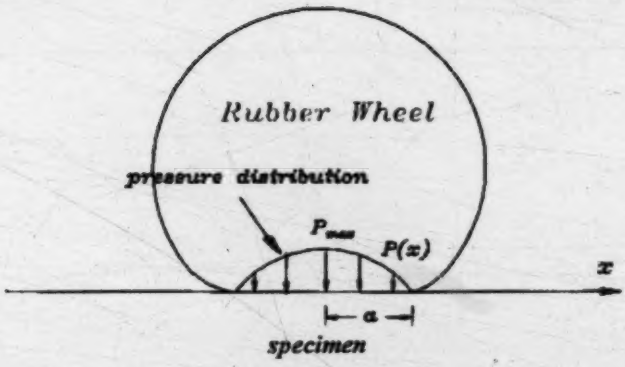

Figure 2-7 The pressure distribution in the contact area between the rubber wheel and the specimen.

During each test, abrasive sand particles are fed into the gap between the rubber wheel and test samples and are gripped and transported across the sample surface by the rubber wheel, scratching the surface and resulting in wear. In order to simplify modeling, the abrasive particles are assumed to have an initial velocity of $v_{inital} = \omega R$ that is parallel to the sample surface. ω is the angular speed of the wheel and R is its radius. The velocity of a sand particle changes when its movement is obstructed. It may be expressed as $\vec{v} = \vec{v}_{inital} + \vec{v}_{change}$, where $\vec{v}_{change}$ is the variation in velocity of an abrasive lattice site when it is in contact with the specimen surface. In the present simulation, abrasive particles are transported into the gap between the wheel and specimen one by one in order to simplify the calculation. This should not change the trend of wear behavior but only the quantitative wear value.

2.3.2 Simulation of multi-phase materials

For a homogeneous material such as a pure metal or single phase alloy, its mechanical properties are uniform i.e. the interaction between lattice sites can be described by only one type of bond with identical force coefficient. However, a multi-phase material, such as a metal matrix composite, consists of at least two

components, matrix and reinforcement, which have quite different mechanical properties. The interaction between matrix lattice sites, and that between reinforcing lattice sites are obviously different. These interactions can be related to two bond force coefficients k_m,k_c, as shown in Figure 2-8. The challenge is to determine the interfacial bonding coefficient k_{mc} for a bond connecting a metal site to a ceramic site.

It is highly provable that the reinforcing ceramic has little ability to deform plastically; the force coefficient k_c mainly describes the force during elastic deformation. However, for the matrix metal, the bond between the matrix lattice sites can experience elastic and plastic deformation. This can be expressed using two force coefficients k_{me} and k_{mp}. When interfacial bonding is considered, the difference in mechanical behavior makes the deformation of a bond between reinforcing and matrix lattice sites complicated. The metal-ceramic bond may be treated in the pure mechanical way as follows.

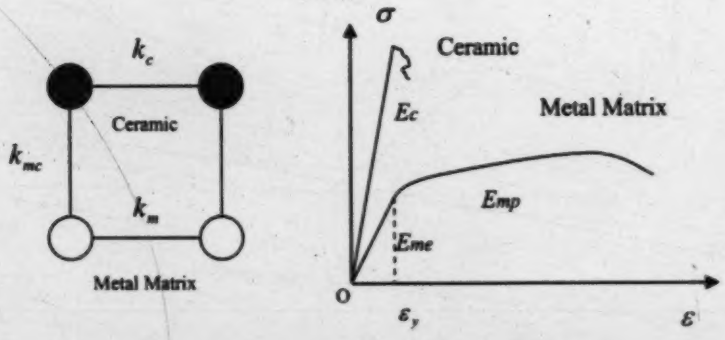

Figure 2-8 Schematic illustration of two types of bonds in a composite containing components with different mechanical properties.

Situation 1: elastic deformation occurs

$$\Delta l = \Delta l_m + \Delta l_c$$

$$\because f_{(c,m)} = k_c \Delta l_c = E_c \frac{l_0}{2} \Delta l_c = f_{(m,c)} = k_{me} \Delta l_m = E_{me} \frac{l_0}{2} \Delta l_m$$

$$\therefore \Delta l_m = \frac{E_c}{E_{me}} \Delta l_c$$

$$\therefore \Delta l = \Delta l_c + \Delta l_m = \Delta l_c + \frac{E_c}{E_{me}} \Delta l_c$$

$$\therefore \Delta l_c = \frac{\Delta l}{1 + \frac{E_c}{E_{me}}}, \qquad \Delta l_m = \frac{\Delta l}{1 + \frac{E_{me}}{E_c}} \tag{2-17}$$

$$\therefore f_{(c,m)} = E_c \frac{l_0}{2} \Delta l_c = \frac{l_0}{2} E_c \frac{\Delta l}{1 + \frac{E_c}{E_{me}}} = \frac{E_{me} E_c}{2(E_{me} + E_c)} l_0 \Delta l$$

$$\therefore k_{mc} = \frac{E_c E_{me}}{2(E_{me} + E_c)} l_0 \tag{2-18}$$

Situation 2: deformation involving both elastic and plastic components

$$\Delta l_p = \Delta l_m - \Delta l_y$$

$$\Delta l = \Delta l_m + \Delta l_c$$

$$\because f_{(m,c)} = E_{me} \frac{l_0}{2} \Delta l_y + E_{mp} \frac{l_0}{2} \Delta l_p = E_c \frac{l_0}{2} \Delta l_c$$

$$\therefore E_{me} \Delta l_y + E_{mp} (\Delta l - \Delta l_c - \Delta l_y) = E_c \Delta l_c$$

$$\Delta l_c = \frac{E_{mp} \Delta l + (E_{me} - E_{mp}) \Delta l_y}{(E_{mp} + E_c)} = \frac{\Delta l - (1 - \frac{E_{me}}{E_{mp}}) \Delta l_y}{(1 + \frac{E_c}{E_{mp}})}$$

$$\Delta l_m = \Delta l - \Delta l_c = \Delta l - \frac{\Delta l - (1 - \frac{E_{me}}{E_{mp}}) \Delta l_y}{(1 + \frac{E_c}{E_{mp}})} = \frac{E_c \Delta l - (E_{me} - E_{mp}) \Delta l_y}{E_{mp} + E_c}$$

$$= \Delta l_c \frac{E_c}{E_{mp}} + (1 - \frac{E_{me}}{E_{mp}}) \Delta l_y$$

$$\therefore f_{(c,m)} = E_c \frac{l_0}{2} \Delta l_c = \frac{l_0}{2} E_c \frac{\Delta l - (1 - \frac{E_{me}}{E_{mp}}) \Delta l_y}{(1 + \frac{E_c}{E_{mp}})} = f_{(m,c)} \qquad (2\text{-}19)$$

the parameters used in the above derivation are listed below:

l_0 the unit length of a bond in stress-free state

Δl the total deformation on a bond

Δl_m the deformation of the matrix portion on a bond

Δl_y the maximum elastic deformation in the matrix portion of deformation Δl_m on a bond

Δl_p the plastic deformation in the matrix portion of deformation Δl_m on a bond

Δl_c the deformation of the ceramic reinforcement portion on a bond

E_{me} the Young's modulus (in elastic region) of the matrix

E_{mp} the average modulus for plastic deformation of the matrix

E_c the Young's modulus (in elastic region) of the ceramic reinforcement

k_c the force coefficient of the ceramic-ceramic bond

k_{mc} the force coefficient of the matrix-ceramic bond (interfacial bond)

$f_{(m,c)}$ the force on a reinforcement site from a matrix site

$f_{(c,m)}$ the force on a matrix site from a reinforcement site

Although this approach can simply describe the interfacial bond deformation using equation (2-18) when only elastic deformation takes place, situation 2 is a little more complicated and no simple equation is available for the force coefficient of a metal-ceramic bond. As a matter of fact, the bond between a metal site and a ceramic one is largely dependent on the chemical interaction between the two

different materials. Therefore in this model, an interfacial bond is introduced to describe the interfacial strength between a metal site and a ceramic one.

As shown in Figure 2-9, two interfacial bonds are used in the modeling: a weak bond and a strong bond. The weak bond has strength lower than the yield strength of the matrix, while the strong bond has strength higher than the yield strength when compared under the same strain condition. This means the strong bond provides a higher force binding two lattice sites together. In other words, if the strength of the bond is higher, the resistance to deformation will be correspondently higher. In realistic situations, the ability to withstand strains in interfacial areas is limited and these areas are often the locations where cracks initiate [106]. That is why interfaces usually do not allow much plastic deformation to occur. The fracture strain of interfacial bond, in this simulation, is assumed to be larger than the yield strain of a metallic material in order to prevent interfacial fracture. In this way, the interfacial bond is simplified to possess elastic properties only. The interfacial bond strength can be modified in order to investigate the influence of the interface between the matrix and the reinforcement on wear of composite materials.

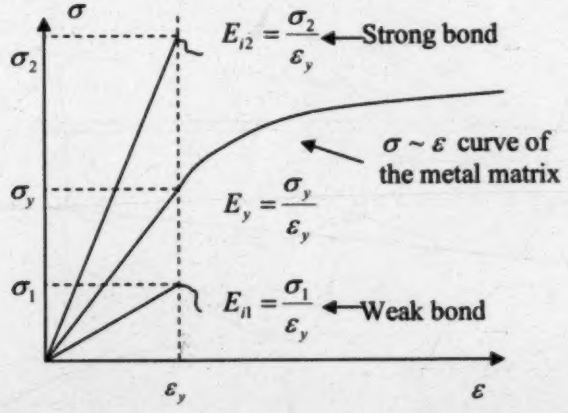

Figure 2-9 Two presumptive interfacial strengths and a $\sigma \sim \varepsilon$ curve of the matrix.

Wear results from breaking of bonds. During a simulated wear process, the force and trajectory of each lattice site are calculated in the manner described in

previous sections. When the length of a bond between two adjacent sites is larger than a critical value corresponding to the fracture strain of each material or the interfacial bond strength between two sites of different types is exceeded, the bond fails. Abrasion loss results when all bonds connecting a site or a cluster of sites to its adjacent sites are broken. The number of total loss of sites was treated as the abrasion loss of a target material. With this method, a dynamic process of abrasion could be simulated.

2.4 Time interval Δt

The accuracy of the simulation is significantly influenced by an important factor, the time step Δt. If Δt is very large, the lattice site could move to a position far away from the original position according to the relation of $\Delta l = \vec{V} \times \Delta t$. Consequently, the deformation on the bond could exceed the critical value corresponding to fracture strain, resulting in a very high wear rate which does not correspond to the real situation. One could verify whether a proper Δt is selected by plotting the wear loss of the material as a function of the simulation time step Δt, while keeping all other parameters in the simulation constant. As shown in Figure 2-10, abrasive wear loss increases rapidly when Δt is larger than 7.0×10^{-7} s. This means that when the time interval is smaller than this value, the wear loss of the material is relatively stable and the selected Δt is appropriate. If Δt is too large, a large Δl will be generated and subsequently result in a large false force on the bond causing it to break suddenly and generate high but incorrect wear loss. On the other hand, the desired time interval should be close to the critical value in order to save computing time. In the present simulation, Δt is set to be 5.0×10^{-7} s.

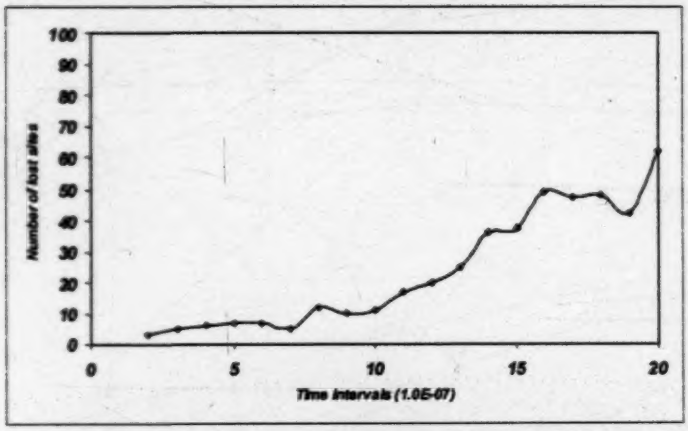

Figure 2-10 The influence of time interval Δt on abrasive wear loss

The time interval of the simulation is related to the unit initial length of the bond l_0, the external force F exerted on the target material and some other parameters. Usually, when l_0 decreases and F increases, the time interval should be shortened in order to provide sufficient accuracy. For different systems, the parameters should be examined first using the above procedure to make sure that the time interval for the simulation is reasonable. At present, in our simulation, l_0 is set to 1.0×10^{-4} m, F =100N. The target material is descritized and mapped onto a lattice containing 120×50 sites.

2.5 Advantages of MSDM and further development

The MSDN has many advantages as listed below:

1. The model is built on Newton's Law of Motion which can be generally applied to any system. Some models mentioned in the section of Introduction are based on assumptions or empirical rules [100-103] which, therefore, only suit particular situations.

2. The model allows predicting the influence of the microstructure on the wear of material with simple input of mechanical properties of different material components. The effect of interfacial bonding strength on wear of composites can also be investigated [107].

3. The model bridges microscale and macroscale studies of the wear process for both homogeneous and heterogeneous materials without surface geometry limitation [108].

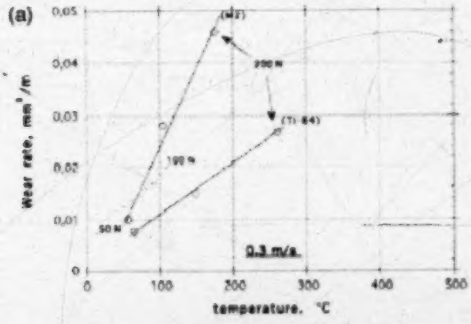

Figure 2-11 Wear rate as a function of surface temperature during sliding for Ti-6Al-4V alloy [110].

As mentioned before, MSDN has been successfully applied to study the effects of size and volume fraction of reinforcing particles on erosive wear [107]. Some external influences such as loading conditions of erosion or abrasion, impact particle size, shape and velocity were also studied. Reasonable predictions were made by the method, which were consistent with experimental observations [84, 88, 95-97]. This model can also be used to investigate frictional heating during sliding wear [109], which could significantly influence the mechanical properties of a material at the contact surface by increasing its temperature [110]. Figure 2-11 illustrates the effect of surface temperature on wear rate of Ti-6Al-4V alloy, which implies that frictional heating could have increased the wear loss. This model makes it possible to investigate the wear process and frictional heat issue at the same time.

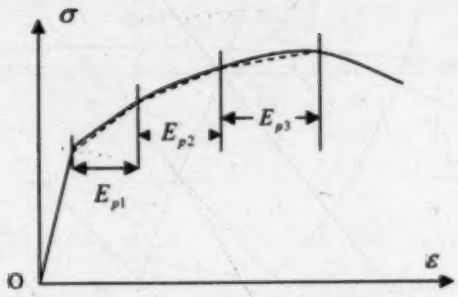

Figure 2-12 Modification of plastic modulus used in the simulation.

The model is also flexible and easily modified. For instance, the plastic modulus used in this simulation, is estimated from the slope of the line between the yield strength σ_y and the tensile strength σ_T. The real modulus is in fact a curve. The difference between the real modulus and simulation modulus can be reduced by simulating the curve with a number of lines having different slopes as shown in Figure 2-12. Currently, the approximate value of plastic modulus is considered to be acceptable to save computing time.

3 Simulation of Microstructural Effects on Abrasive Wear of Composites Part I: Basic Parameters

3.1 Simulation procedures

From the introduction, it is known that metal matrix composites are widely used to resist abrasive wear in heavy industries [22] as shown in Figure 1-3. In order to improve a material's performance, the mechanism responsible for abrasive wear should be well understood. The complex relationship between a composite material's microstructural features (e.g. hard particle size, distribution, volume fraction and sometimes interfacial bonding strength) and wear resistance requires systematic investigation, which can be carried out by well-designed computer simulation. In this chapter, the Micro-Scale Dynamic Model (MSDM) is employed to investigate the abrasive wear mechanism associated with different microstructural features of composites.

As described in Chapter 2, MSDM offers two-dimension simulation by mapping a target composite material onto a discrete lattice with basic mechanical properties. In this study, nickel alloy and tungsten carbide were selected as the matrix material and the reinforcing phase, respectively. This composite system is widely used as a hardfacing overlay to resist abrasive and erosive wear in oilsands, mining, and mineral processing industries. Silicon carbide particles were chosen as the abrasive. The mechanical properties of the three materials are given in Table 3-1. All the materials, i.e. matrix, reinforcing particles and abrasive sand are mapped using small lattice sites as illustrated in Figure 2-1. Each lattice site represents a unit volume with fixed mass. The site-site bond length under stress-free condition is $1.0\times\ 10^{-4}\ m$. The whole composite system contains 120×50 lattice sites. The simulation time step Δt is set to be $5.0\times10^{-7}s$. In order to simplify the simulation, the reinforcement used in the simulation has a rectangular shape. Other shapes of reinforcement will be investigated in Chapter 5. The reinforcing particles are randomly distributed in the matrix. Interfacial bonds between reinforcement and

matrix are assumed to have elastic behavior only. Detailed calculations of the interaction between the lattice sites have been described in a previous chapter. In order to simplify the calculation, the abrasive sand particles are assumed to scratch the target surface one by one. This would not change the trend of materials' wear behavior but only the quantitative wear value.

Table 3-1 Mechanical properties of materials involved in the simulation study

Material	Modulus E_c (Gpa)	Yield Strength σ_y (Mpa)	Tensile Strength σ_{UTS} (Mpa)	Fracture Strain ε_f (%)
Nickel (Ni)	207	59	317	30
Tungsten Carbide (WC)	690	6800	6800	1
Silicon Carbide (SiC)	430	862	862	0.2

In the following sections, simulation is focused on the effects of basic parameters i.e. volume fractions, reinforcement sizes, interfacial bonding strengths of a composite. Each simulation is conducted by altering only one of the above parameters each time and keeping the others unchanged. In addition to the microstructural features of the wear material, abrasive particle size, which is one of the most important external effects, is studied to investigate changes in wear loss with respect to the ratio of the abrasive particle size to the reinforcement size.

3.2 Results and discussion

3.2.1 Effects of reinforcement volume fraction on abrasive wear

Reinforcement volume fraction is one of the important parameters which determine the overall mechanical properties e.g. hardness, strength and toughness of composites. The resistance of a composite material to abrasive wear is largely

influenced by the volume fraction of the reinforcement [22, 38, 39, 45-47]. In this simulation, each reinforcing particle consists of 7×5 lattice sites and an abrasive particle is a square containing 14×14 lattice sites. The volume fraction of reinforcement is the only variable while the other microstructural factors and abrasion condition (i.e. abrasive sand flow rate, size, shape and angularity of the abrasive) are kept the same. Figure 3-1 illustrates the wear loss against the volume fraction of reinforcement. Figure 3-2 shows cross-sectional morphologies of three composites with different volume fractions of the reinforcement. As shown, the volume loss of the WC-Ni composite decreases initially with increasing volume fraction of reinforcement. However, after reaching a critical volume fraction, a continuous increase in the volume fraction of reinforcement results in higher wear losses. The existence of a critical volume fraction of reinforcement has been observed in many experimental studies [22, 38, 41and 111]. For different composite materials, the critical volume fraction may vary [22, 41]. It should be pointed out that the critical volume fraction is influenced by other factors such as the interfacial bond strength. Previous studies under erosion conditions [96] have demonstrated that the critical volume fraction became higher with an increase in the interfacial bond strength.

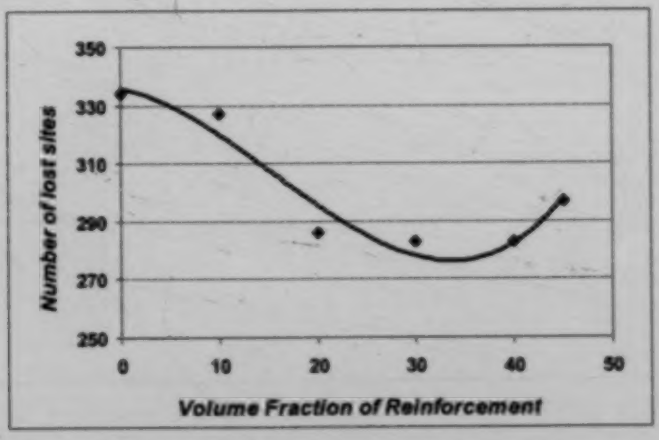

Figure 3-1 Wear loss vs. the volume fraction of reinforcement.

(a) 10% reinforcement

(b) 30% reinforcement

(c) 40% reinforcement

Figure 3-2 Cross-sectional morphologies of four composites with different volume fractions of reinforcement after abrasion by six abrasive particles.

The observed variation in the wear loss with respect to the volume fraction of reinforcement is understandable. It is known that the hard reinforcement mainly withstands the wearing force, while the matrix binds the reinforcement, accommodates deformation and absorbs impact energy, thus reducing the probability of reinforcement fracture. A proper combination of hardness and ductility/toughness should result in higher resistance to wear. Thus, there must be an optimal volume fraction of reinforcement, which provides the most suitable balance between hardness and ductility. When the volume fraction of reinforcement exceeds the critical value, the material becomes brittle and easier to be fractured, leading to a decrease in the wear resistance [22, 96]. However, if the volume fraction of reinforcement is smaller than the critical value, there are not enough hard particles in the matrix to withstand the wearing force. As a result, wear resistance would be low. It should be noted the other factors such as interfacial bonding conditions and size ratio of the sand particle to reinforcement particle may influence the critical volume fraction. These factors will be discussed in following sections.

3.2.2 Effects of interfacial bond strength on abrasive wear

Since composite materials always consist of at least two different components, adhesion between them is important because good interfacial bonding could result in relatively high wear resistance [40, 112-113]. Das et al [40] found that strong interfacial bonding in hard particle reinforced aluminum composites decreased the chance of debonding at their interfaces. Even in a high load condition, the dislodgement and loss of the ceramics, which could result in high wear loss, was rare [40] if the bond was strong. While in the study of Hwang et al [112], it was demonstrated that weak bonding facilitated crack initiation at interfacial areas due to a large hardness difference between various constituents. The propagation of cracks under further loading could lead to delamination of the matrix and result in high volume loss of composites. In addition, a study on binderless carbide [113]

demonstrated significant improvement of wear resistance by enhancing the bond strength even for ceramic/ceramic composites.

Computational studies are conducted to investigate the influences of bonding condition on abrasive wear. In these simulations, the composites are set to have the same matrix and reinforcement phase but different bond strengths. The abrasion conditions are set the same. As shown in section 2.3.2, the bond strengths are determined by the interfacial bond moduli, i.e. the ratio of the ultimate tensile strength to the fracture strain. For comparison, the fracture strain of the interfacial bond is assumed to be 1%, and the ultimate tensile strengths of two interfacial bonds are σ_1 =40MPa and σ_2 =400Mpa, respectively, in order to model weak bonding and strong bonding conditions. The yielding strength and ultimate tensile strength of matrix are σ_y = 59Mpa and σ_{UTS} =317Mpa, respectively, which are between the values of the strong bond and weak bond as illustrated in Figure 3-3(a). Two typical cross-sectional morphologies of composites with different interfacial bonding strengths after wear are illustrated in Figure 3-3 (b). It is obvious that the strong bond example leads to better wear performance with fewer lattice sites worn away. For this composite, the major fracture regions are within the matrix phase since it is relatively weak. However, for the composite with the lower bonding strength, the whole system, including ceramic and matrix lattice sites, is worn away. This is because the matrix around the interface region can be easily torn away if the interfacial bonding is not strong enough and consequently this leads to cracking of the ceramic which has lost its protectant, ductile matrix. Such a damage process can be viewed in the simulation, which shows consistency with the experimental observation referred to at the beginning of this section.

As shown in some previous studies [22, 41], a critical volume fraction of reinforcement can be found in most composite systems, above which the wear resistance will be decreased due to the increase in interfacial area. Considering the effect of the interfacial bonding strength on wear behavior, series of simulation were conducted to study how the critical volume fraction is affected by the interfacial bonding condition.

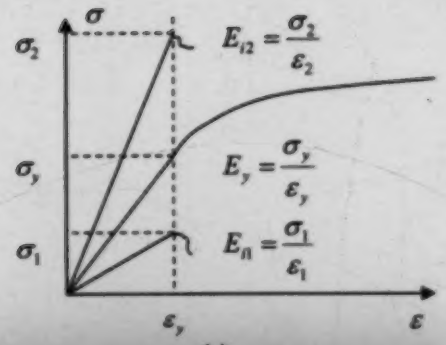

(a)

Weak interfacial bonding condition

Strong interfacial bonding condition

(b)

Figure 3-3 (a)Two presumptive interfacial moduli and elastic modulus of the matrix. (b)Cross-sectional morphologies of composites with the two different interfacial bond strength after abraded by five sand particles.

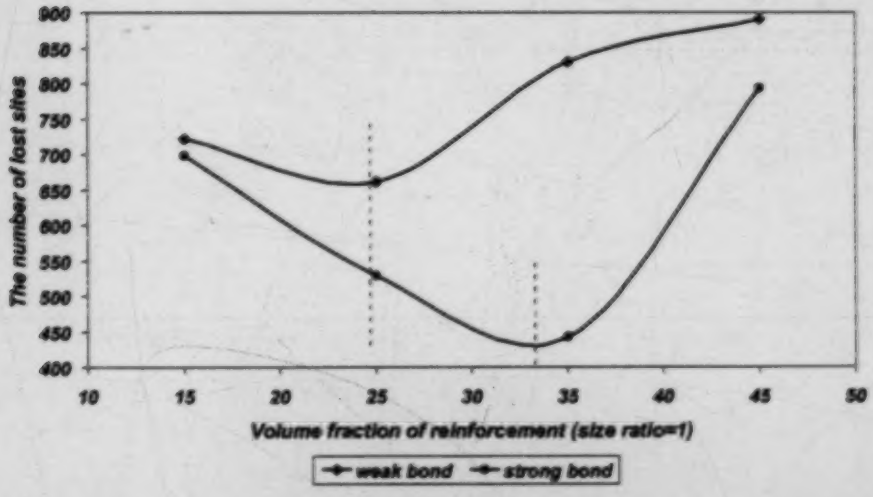

Figure 3-4 The critical volume fraction of reinforcement changes as the interfacial bond strength changes.

As illustrated in Figure 3-4, with a decrease in interfacial bond strength, the critical volume fraction of reinforcement shifts to a lower value (to the left). In the above case, the optimal content of reinforcement with the weak bond is about 24vol% while that for the strong bond is around 33vol%.

In addition, one may find that even with the optimal volume fraction of reinforcement, the degree of improvement can vary. When the interfacial bond is weak, the wear loss of composites with optimal content of reinforcement only decreases slightly (e.g. the number of lost sites decreases from 725 to 675). However with a better bonding condition, adding more reinforcement particles into the matrix can dramatically improve composites' wear resistance (e.g. the number of lost sites decreases from 700 to 440). In the context of industrial application, the above finding may be expressed as follows: when adhesion between ceramic and matrix material is not strong, the optimal volume fraction corresponding to the highest abrasive wear resistance is low and the improvement of the wear resistance is not pronounced. However, by improving the cohesion between ceramic and matrix, the composite system could accommodate more reinforcement phase with higher critical volume fraction and result in higher wear resistance. The resulting improvement of

wear resistance is significant. After exceeding the critical volume fraction, adding more reinforcement will decrease the wear resistance due to the decreased toughness of the composite.

The interfacial bond is assumed to be strong in other simulation studies detailed in this thesis unless it is stated that the bond is weak.

3.2.3 Effects of reinforcement size on abrasive wear

The size of reinforcement particles influences the wear behavior of a composite [22, 39, 45-50]. In present simulation, composite materials reinforced by WC particles (35vol %) with different sizes are investigated under the same abrasion condition. The simulation demonstrates that abrasion is reduced when the reinforcement has a larger reinforcement particle size (Figure 3-5(a)). Cross-sectional morphologies of four typical worn surfaces are shown in Figure 3-5(c). The simulation result is consistent with experimental observations [38, 45, 47, and 49]. As an example, Figure 3-2(b) presents experimentally determined abrasion loss of WC-Co coatings, in which one may see that larger carbide particles resulted in higher wear resistance.

The effect of reinforcement size on wear has been extensively discussed. As suggested [45, 47], larger reinforcing particles could be more effective in supporting and protecting the matrix. The corresponding total interfacial area is smaller, which may help to reduce the probability of interfacial failure between the matrix and the reinforcement. A composite reinforced by larger particles may also require higher load to develop cracks and delaminate a substrate layer [46]. For a composite reinforced by homogeneously dispersed small reinforcement grains, the fine particles could be ploughed out more easily. These might then act as extra abrasive particles to enhance abrasive attack [45]. In addition, small reinforcement particles have relatively larger total interfacial area, which could lead to higher probability of interfacial failure. The present simulation results are consistent with the above arguments.

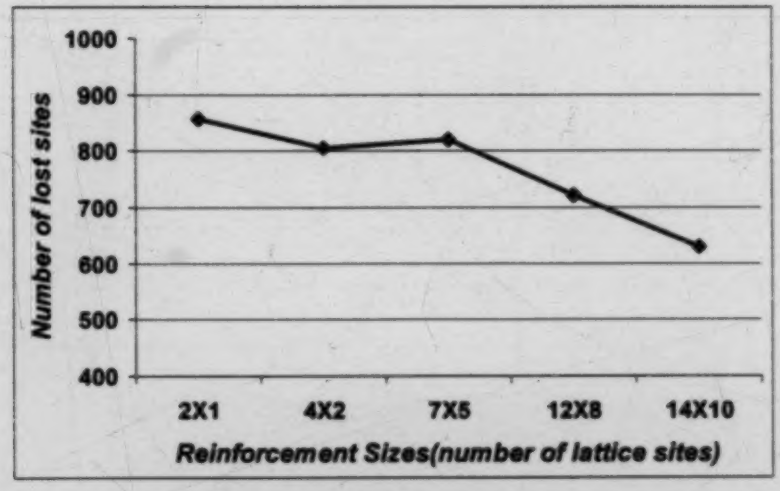

(a)

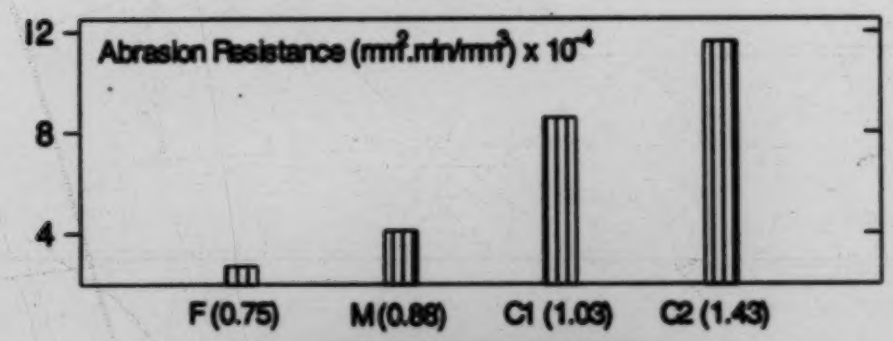

(b)

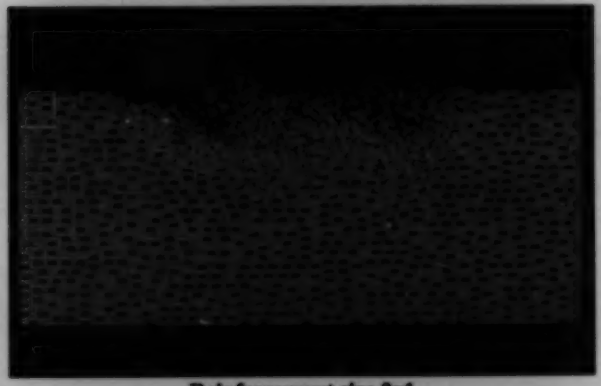

Reinforcement size 2x1

Reinforcement size 4x2

Reinforcement size 7x5

Reinforcement size 14x10

(c)

Figure 3-5 (a) The effect of the reinforcement size on wear loss; (b) Experimental observation reported by S. Usmani et al. [49]; (c) Cross-sectional morphologies of four worn composites reinforced by hard particles with different sizes.

It must be pointed out that the conclusion drawn here could be true only when the abrasive particles are bigger than the reinforcement particles. If the abrasive particles are smaller than or close to the size of reinforcement particles, it will be relatively easier for them to access and wear the soft matrix, thus leading to different wear losses. Such a situation has also been investigated in this study, and will be detailed in the next section.

3.2.4 Effects of the ratio of abrasive particle size to reinforcement size on abrasive wear

The wear loss of a composite material is largely influenced not only by microstructure and the mechanical properties of its constituents, but also by the prevailing wear conditions [22, 38, 52-57]. The abrasive particle size plays an important role in the extent of wear damage incurred. In particular, the ratio of the abrasive particle size to the reinforcement size could have a more important influence on the wear mechanism than the absolute size of either the abrasive or reinforcement. The simulation results presented in Section 3.2.3 were obtained under the condition that the abrasive particles are larger than the reinforcement particles. In this section, the effect of different abrasive particle sizes on the wear of a composite is analyzed, based on the computer simulation study. Figure 3-6(a) illustrates simulated wear loss of the material as a function of the ratio of the abrasive particle size to that of the reinforcement. The wear loss becomes higher with increasing size ratio initially and then becomes stable when it reached a certain level. Such a trend is consistent with experimental observations [59] (Figure 3-7(a)). Cross-sectional morphologies of surfaces abraded by abrasives with two different size ratios are shown in Figure 3-6(b). In addition, it is found that when the size ratio decreases, attacks on the matrix become more obvious while damage to the reinforcement particle becomes less pronounced.

The observed phenomenon may be explained as follows. During abrasion, the local wearing contact stress could be very high, e.g., in the vicinity of angular edges and corners of an abrasive particle. When a large abrasive particle is under pressure from the rubber wheel, the total force exerted on the particle is larger than that on a small particle. Consequently, the local wearing contact stress for the large abrasive particle could be higher than that for a smaller abrasive particle, thus causing more abrasion damage. Axen and Zum Gahr [57] suggested that when an abrasive sand particle size was smaller than a critical value, the wear loss mainly resulted from the loss of matrix; while when it exceeded the critical value, the wear loss could be more related to microcracking and spallation of the reinforcement that is influenced by the interfacial bonding strength more than the abrasive size. In addition, as the abrasive particle size increased, direct contact between the abrasive and the reinforcement was enhanced, and the abrasive particles could become blunt or fractured if they were softer and/or more brittle than reinforcing phase. These factors could be responsible for the existence of the critical size ratio, above which the wear loss became stable.

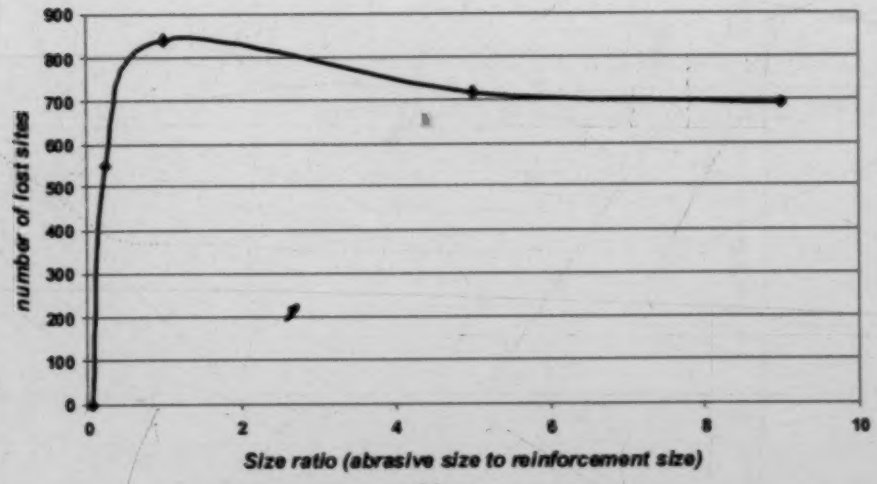

(a)

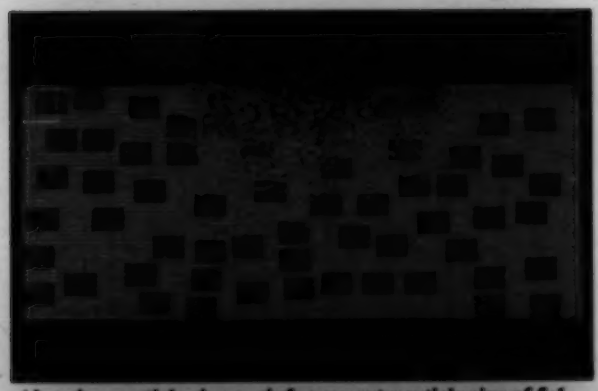

Abrasive particle size : reinforcement particle size of 5:1

Abrasive particle size : reinforcement particle size of 1:1

Abrasive particle size : reinforcement particle size of 1:4

(b)

Figure 3-6 (a)The effect of the ratio of the abrasive particle size to the reinforcement particle size on abrasive wear of a composite; (b) Cross-sectional morphologies of the material abraded by abrasive particles of different sizes.

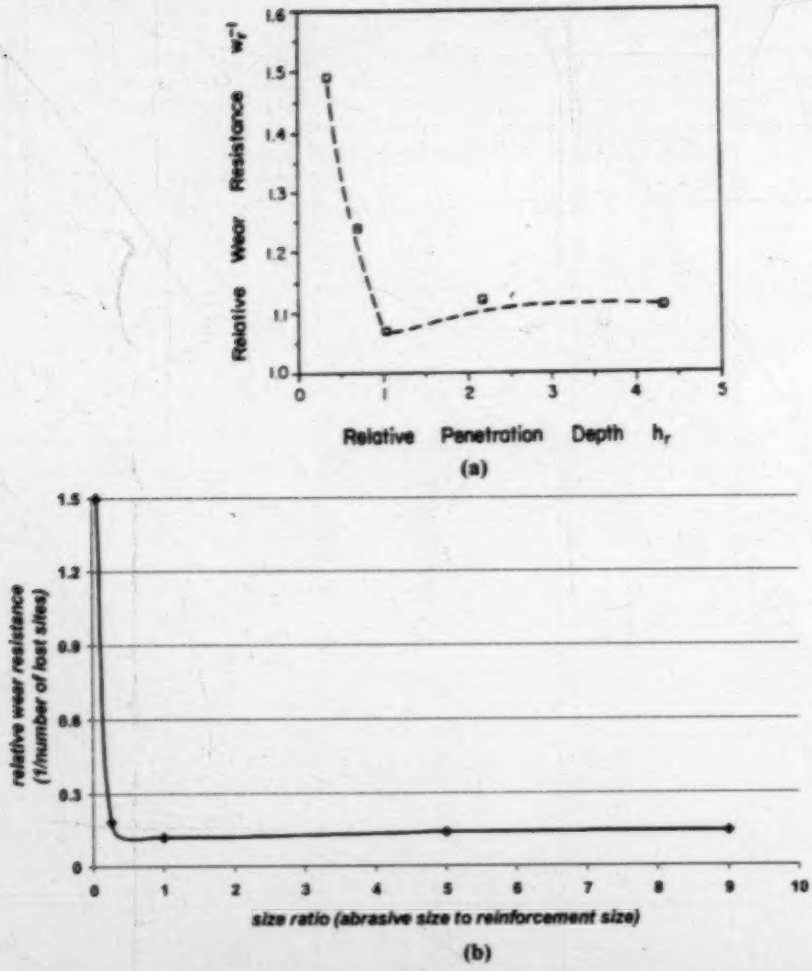

Figure 3-7 (a) Experimentally determined relative wear resistance vs. the abrasive penetration depth [59]. (b) The relative wear resistance vs. size ratio from the present simulation.

In general, abrasion damage is inversely proportional to a target material's hardness which affects the penetration of the abrasive particles into the target surface. A small penetration depth may result in less subsurface deformation and thus less abrasive wear [41]. For composites, the penetration depth obviously depends not only on the material's macro-hardness but also on other factors such as the abrasive particle size, the reinforcement size and the mean spacing between reinforcement

particles. Wang and Rack [59] have suggested an equation to estimate the penetration depth:

$$h_r = (\frac{2}{\pi K'})^{1/2} (\frac{\sigma}{H})^{1/4} (\frac{D}{d}), \qquad (3\text{-}1)$$

where D is the average diameter of the abrasive particles; d is the diameter of the reinforcement; σ, H and K' are the applied stress on the nominal contact area, hardness of the material and a geometric constant, respectively. When the material and loading condition are the same i.e. σ and H are constant, the relative penetration depth is proportional to the ratio of the abrasive particle size (D) to that of the reinforcement (d). Thus, the wear resistance should decrease with increasing size ratio. This is supported by experimental observations (e.g., see Figure 3-7 (a) [59]). When the penetration depth ($\propto D/d$) is larger than a critical value, the wear resistance becomes relatively stable. This is consistent with the computational simulation (see Figure 3-6 (a)). The existence of such a critical value cannot be explained only using equation (8). It is certainly influenced by more factors such as the spacing between reinforcement particles. However, such a trend of wear loss with respect to the size ratio can be clearly investigated using the computer modeling technique that takes account of all the above mentioned factors automatically.

3.3 Conclusion

The MSDM technique has been employed successfully to simulate the abrasive wear of composites.

Emphasis has been placed on the effects of several important microstructural parameters, i.e. volume fraction of reinforcement phase, interfacial bond strength, reinforcing particle size, and size of abrasive sand particles (by way of size ratio).

The simulation results are consistent with experimental observations, and demonstrate the efficiency and capability of computational modeling for the study of abrasive were of composites.

In addition to validating of the application of MSDM technique for abrasion modeling, the following information on abrasive wear of composite was obtained:

1 There is an optimal volume fraction of reinforcing phase that corresponds to the maximum abrasive wear resistance.

2 The interfacial bond strength can significantly influence the optimal volume fraction of reinforcement. Enhancing cohesion between ceramic and metal constituents in a composite could accommodate more reinforcing particles before the optimal value is reached and allow considerable improvement in wear resistance.

3 Wear resistance is enhanced when the size of the reinforcing phase is increased in condition when the abrasive particle is coarser than the reinforcement.

4 The simulation on the size ratio of abrasive sand particle to reinforcing particle indicates the existence of a critical ratio, above which the wear rate of the composite becomes stable. Below this critical value, increasing the size ratio results in accelerated wear damage.

4 Simulation of Microstructural Effects on Abrasive Wear of Composites Part II: Combined Effects of Basic Parameters

4.1 Introduction

Reinforcement size and volume fraction, the cohesion between matrix and reinforcing phase, and the size ratio of sand particle to reinforcement, are major factors determining the mechanical properties and wear behavior of composite materials. Strength, hardness and toughness are also important to the resistance of a composite to abrasive wear. As shown in Chapter 3, the MSDM technique was successfully employed to investigate the effects of microstructural factors and properties of both the matrix and reinforcement on wear of composite materials. Simulation results that are consistent with reported experimental observations prove that the MSDM technique is capable of simulating abrasive wear under different conditions, investigating the microstructural influence on wear and the mechanisms involved.

However, wear is a complicated surface damage process, involving a number of factors that simultaneously affect the behavior of a material. The interaction between various microstructural parameters could result in several wear mechanisms operating at the same time, making it difficult to carry out experimental investigation on abrasive wear. In addition, the wear behavior of materials under combined influences of various microstructural parameters differs from that under the individual influence of each parameter. In this chapter, the MSDM model is used to simulate the combined influences of reinforcement size, volume fraction, size ratio and interfacial bond strength on wear of composites. The simulation will help to understand the wear behavior of composites under various conditions.

The following sections will cover:

- Studies on the effects of reinforcement size distribution on abrasive wear of composites.

- An investigation of the combined effects of size ratio and volume fraction.
- Simultaneous effects of size ratio and size distribution on wear.
- Relationship between the size ratio and interfacial bond.
- Combined effects of size ratio, volume fractions and interfacial bond strength on abrasive wear of composites.

4.2 Results and discussion

4.2.1 Effects of reinforcement size distribution on abrasive wear

As indicated in Chapter 3, the volume fraction and size of reinforcing particles have strong influences on the wear resistance of composites. When the size of the reinforcement is kept the same, an increase in its volume fraction can result in higher wear resistance. In addition to an enhanced resistance to external load, this benefit accrues because the spacing between the reinforcement phases is also decreased. Therefore, the constraint effect [114] of the particles on plastic deformation becomes more pronounced. Such strengthening effect of the reinforcement results in a lower wear loss of composites. On the other hand, an increase in reinforcement size can also result in higher resistance to external load as demonstrated in previous studies [45, 47]. However, the spacing between large reinforcements widens, leading to higher wear loss when the abrasive particles are smaller than the mean free path between the reinforcing phases. In many industrial situations, size and volume fraction of reinforcement always influence the wear resistance of a composite simultaneously. In this section, the effect of size distribution of reinforcement on wear of a composite is studied.

Starting with a relatively simple situation, a composite with two different sizes of reinforcement are studied. In this case, one size of reinforcing particle contains 7× 5 unit sites. This type of reinforcement mainly supports the external loads and its

volume fraction is constant (15 vol.%). The other size of reinforcement is the fine reinforcement containing 1 unit site only and its volume fraction will be changed (0~20 vol.%) to give a different spacing between reinforcements. Keeping the simulation condition the same except for the volume fraction of fine reinforcement, we can investigate the effect of the spacing on abrasive wear of composite.

For a more complicated case, three different sizes of reinforcement have been used. Seven distributions of three different sizes of particulates are studied so that the optimal size distribution corresponding to the highest wear resistance for a specific combination of size and volume fraction of the reinforcement can be determined.

Figure 4-1 illustrates the trend of the wear loss of composites as a function of the volume fraction of fine particulate under the condition of size ratio=5. It shows that as the volume fraction of fine reinforcement increases, the wear loss of the composite decreases initially. When the volume fraction of fine reinforcement is increased further, the wear loss becomes larger. This observation of critical volume fraction is consistent with the results from 3.2.1 in which only large reinforcement particles (with 7×5 lattice sites) are used.

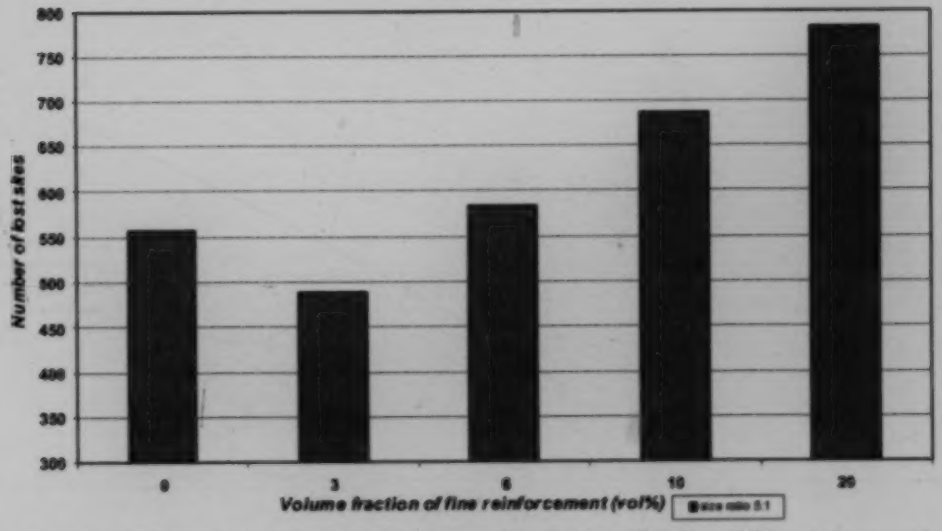

Figure 4-1 The wear loss of composite as a function of volume fraction of fine reinforcement when size ratio is 5:1 .

Experimental studies of the effect of the reinforcement size distribution on abrasive wear are rather limited and there have been almost very little theoretical investigation on the issue. In literature, reported studies only show that if small reinforcing particles are more homogeneously dispersed, the wear resistance of a composite is improved [38, 115-117]. The exception is the study of Rack et al [118], in which a statistical model is proposed to investigate the wear rate of composites reinforced by single-sized particulates and multi-sized particulates, respectively. However, experimental studies of combinations of different sizes of particulates are very limited due to experimental difficulties. Varying the size and volume fraction of the reinforcement change the spacing between reinforcing particles differently i.e. increasing the volume fraction decreases the spacing while increasing the size will increase the spacing. An identified correct spacing associated with a certain volume fraction and size of reinforcement could effectively increase wear resistance. It is logically expected that the correct combination of large and small reinforcement particles should result in higher wear resistance than a composite containing single-sized reinforcement.

Table 4-1 Size distributions of WC reinforcement used in the simulation

Size / Vol.%	Large size (7x5)	Middle size (4x2)	Small size (1x1)
0+0+35	0	0	35
0+35+0	0	35	0
35+0+0	35	0	0
8+8+19	8	8	19
8+19+8	8	19	8
19+8+8	19	8	8
12+11+12	12	11	12

In order to establish the optimal combination of different reinforcement particle sizes, the effect of size distribution on wear is simulated. In the simulation, a size distribution describes a set of volume fractions of reinforcements having various sizes (i.e. large, medium and small). In this work, the wear performance of seven

composites having different size distributions of reinforcement listed in Table 4-1 with a total volume fraction of 35% are investigated. The abrasion condition is kept the same so that the wear performance of the composites is only affected by the size distribution of the reinforcement. Figure 4-2(a) illustrates wear losses of the seven composites, and Figure 4-2(b) shows four representative cross-sectional morphologies of worn composites having different size distributions of reinforcement. It is demonstrated that the wear loss decreases when the volume fraction of large reinforcement particles increases. It is also observed that the combination of 19% large, 8% medium and 8% small particles displays the lowest wear loss. Although the performance of this composite is closely comparable to the one which is reinforced only by large particles, the benefit of using a combination of differently-sized particles can be seen there. In this simulation, only seven composite systems have been investigated. It is possible that a highest wear resistance combination could be identified if a larger numbers of size distributions are tested.

From the simulation, one may conclude that a composite may benefit more from a combination of small and large reinforcement than from single-sized reinforcements. An explanation is that the larger particles mainly withstand the wearing force, while the small dispersed particles strengthen the matrix by hindering the plastic deformation of the matrix so that it is more difficult for the abrasive particles to abrade the relatively softer matrix. In addition, the fine dispersed reinforcement reduces the access to a softer binder by reducing the mean free path between reinforcement particles. Since the mechanical properties of the matrix can be adjusted by adding small dispersed particles, when the total volume fraction of reinforcement is fixed, an optimal balance between the overall hardness and ductility could be achieved, thus resulting in superior tribological properties.

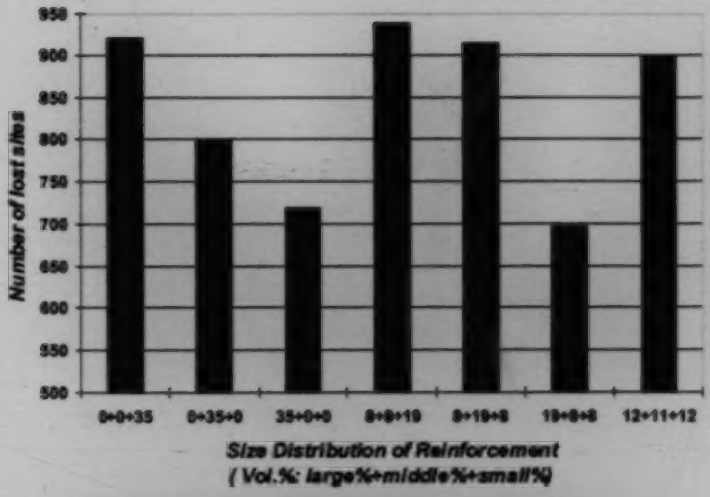

(a)

35% large+0% middle+0% small

0% large+0% middle+35% small

8% large+8% middle+19% small

19% large+8% middle+8% small

(b)

Figure 4-2 The effect of the reinforcement size distribution on wear. (a) Wear loss vs. the size distribution of reinforcement; (b) Cross-sectional view of four worn surfaces with different size distributions of reinforcement.

4.2.2 Combined effects of reinforcement size ratio and size distribution on abrasive wear

The relation between wear and microstructure is complicated. The size distribution of the reinforcement changes the microstructure of a composite by changing the spacing between the reinforcements. When the total volume fraction of the reinforcing particle is fixed, the spacing between reinforcing particles is determined by the number of reinforcing particulates [4], which varies with the size of reinforcement. The number of small particulates is greater than that of large

particulates at given mass. Therefore the spacing between the small particles is decreased which could reduce the access to softer matrix and then lower the wear loss. On the other hand, small reinforcements are not as effective as large particles in resisting the external load. Small reinforcement also results in larger total interfacial area. One may take advantage of the benefit of small reinforcement and minimize its negative effect through an optimal combination of small and large reinforcement particles, leading to the highest wear resistance. Obviously the size ratio of the abrasive particle to that of the reinforcement is another factor influencing the penetration depth of abrasive as shown in 3.2.4. Different size ratios could result in dissimilar interactions between abrasives and the reinforcement, thus leading to varying wear losses.

Simulations have been conducted to investigate the wear performances of composites having three size distributions of reinforcement. They are abraded by abrasive particles with three different sizes, respectively. It is convenient to set the size ratio as the abrasive particle size to the size of the largest reinforcement particle in the distribution since three sizes of reinforcements were used in the simulation.

Results of the simulation are given in Table 4-2. Figure 4-3 (a) illustrates wear losses for the three composites abraded by abrasive particles of three sizes with their size ratios equal to 1:4, 1:1, and 5:1, respectively. Figure 4-3 (b) shows typical morphologies of the composite after abrasion. The following information is obtained from the simulation:

(1) When the size ratio is small (1:4) (i.e. the abrasive particles are smaller than the largest reinforcement particles but larger than the smallest reinforcement), increasing the amount of dispersed small reinforcement particles in the matrix results in a higher resistance to abrasion.

(2) When the size ratio is large (5:1) (i.e. the abrasive particles are coarser than the largest reinforcement particles), the greater the volume fraction of large reinforcement particles in the matrix, the higher is the abrasion resistance of the composite.

Table 4-2 The simulation wear loss results of different size distributions and size ratios

Ratio \ Distribution	Large(7×5)%+Middle(4×2)%+Small(1×1)% 8+8+19	Large(7×5)%+Middle(4×2)%+Small(1×1)% 12+11+12	Large(7×5)%+Middle(4×2)%+Small(1×1)% 35+0+0
1:4	404	526	548
1:1	787	861	841
5:1	938	898	718

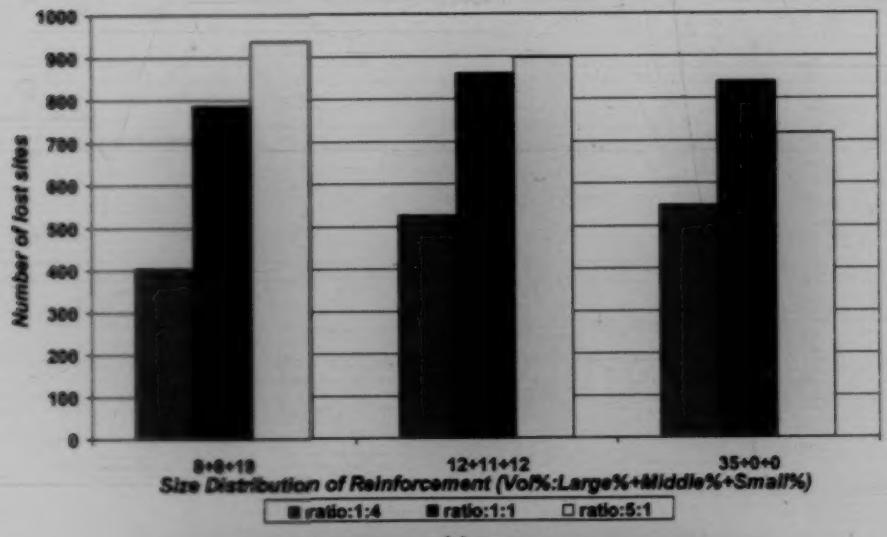

(a)

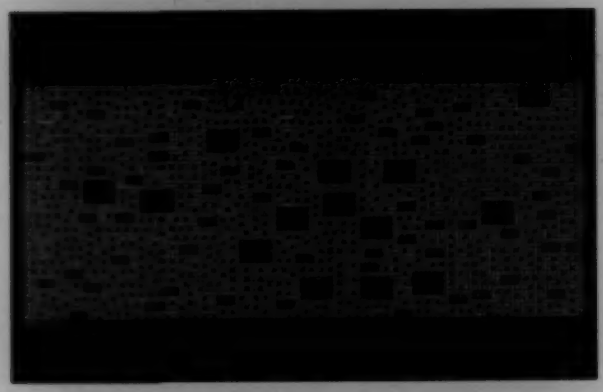

8% large (7×5) + 8% middle (4×2) +19% small (1×1), abraded by small sand particles

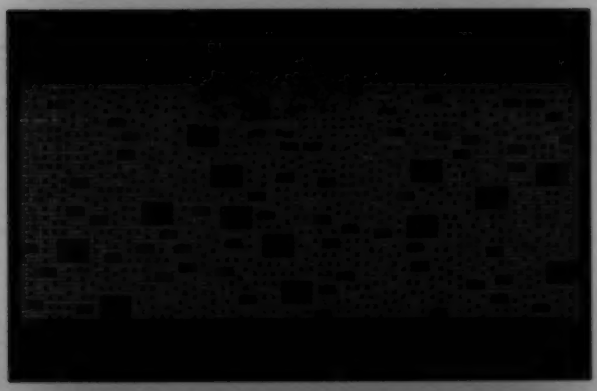

8% large (7×5) + 8% middle (4×2) +19% small (1×1), abraded by medium sand particles

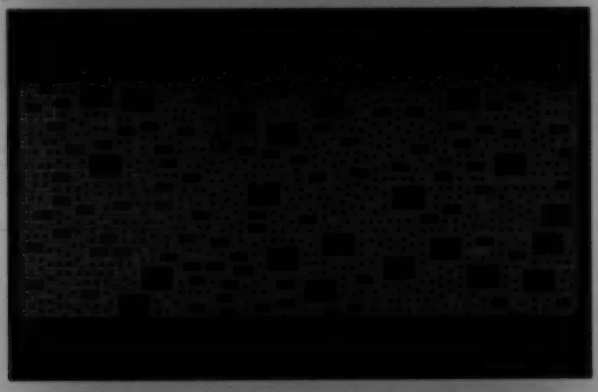

12% large (7×5) + 11% middle (4×2) +12% small (1×1), abraded by small sand particles

12% large (7×5) + 11% middle (4×2) +12% small (1×1), abraded by medium sand particles

(b)

Figure 4-3 (a) Effects of the reinforcement size distribution and the ratio of abrasive size to the reinforcement size on wear loss, (b) typical morphologies of composite materials with various size distributions after abrasion by sand of different sizes.

The above observations are understandable. For case (1), when the abrasive particles are small, the abrasives have more chance to penetrate into the soft matrix and abrade the matrix. If fine reinforcement particles, in addition to the large reinforcement, are dispersed in the matrix, the penetration of the abrasive particles would be effectively blocked by the fine reinforcements and the ploughing or cutting could be reduced, thus diminishing the wear loss. For case (2), when the abrasive particles are larger than the reinforcement particles, the blocking effect of fine reinforcements is lower, since the stress concentration caused by larger abrasives is higher. Larger reinforcement particles are superior in withstanding the wearing stress and blunting the abrasives. An increased amount of larger reinforcement particles would therefore lead to a higher resistance to abrasion. However it should be indicated that if the total amount of the reinforcement changes, the spacing between reinforcing particles would be altered consequently, which may lead to different results.

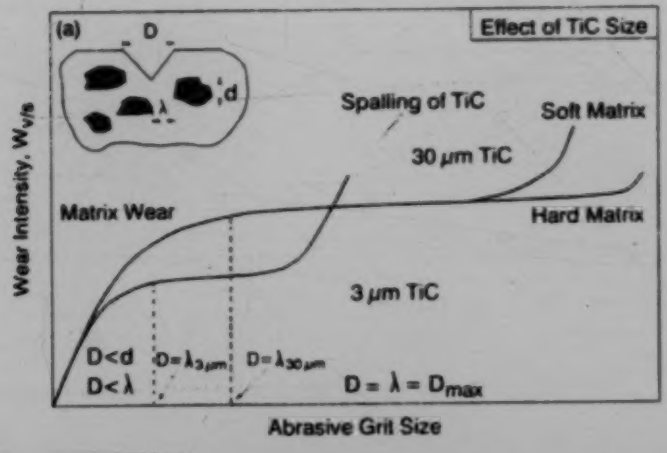

Figure 4-4 Schematic illustration of the wear intensity as a function of abrasive size and the spacing between reinforcement particles. D-groove size, d-reinforcement size, λ - mean free path, $\lambda_{3\mu m}$ -mean free path of the composite reinforced by TiC with size of 3μm, $\lambda_{30\mu m}$ -mean free path of the composite reinforced by TiC with size of 30μm [57].

From the simulation study, one may see that wear resistance is affected not only by the size ratio but also by the spacing between reinforcement particles. This has been demonstrated previously [57] (see Figure 4-5). However, when the reinforcement particles have a certain size distribution, the situation becomes much more complicated because the blocking effect of small and larger reinforcement particles is different and the spacing between reinforcement particles is also changed. It is difficult to describe such relationships using previous theory [57] or analytical equations. However, such a wear prediction could be made easily by computer modeling that takes all the factors into account.

4.2.3 Combined effects of size ratio and volume fraction on abrasive wear

As demonstrated in 3.2.1 and 4.2.1, in most cases, there exists a critical volume fraction of the reinforcement at which the composite displays the highest resistance to abrasive wear. By studying the size effect of abrasive particles (i.e. size ratio) on wear, we have seen that a material may display different resistances. It is reasonable to suppose that the size ratio can also influence the value of the critical volume fraction of reinforcement. In this section, two composite systems are studied. One has two different sizes of reinforcement (large and small). The large particle has 7×5 lattice sites and the latter contains only one site. The second composite contains only one size of reinforcement (i.e. 7×5 lattice sites). Under the three different size ratio conditions, one can examine how the critical volume fraction of the reinforcing particles varies with the size ratio. We may also find some relationship between the spacing of the reinforcements and the size ratio.

Figure 4-5 shows the wear loss as a function of the volume fraction of fine reinforcement in the first composite system. Figure 4-6 shows typical morphologies of the composites after being abraded by particles having different sizes. As shown, a critical volume fraction is observed for all three conditions involving different sizes of abrasive grits. However, the value of critical volume fraction varies.

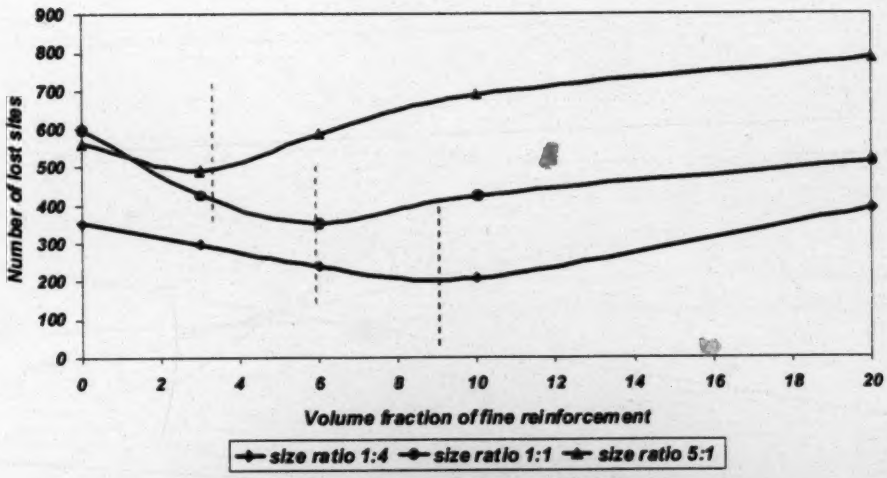

Figure 4-5 Wear loss of composites with different volume fraction of fine particulates abraded by three sizes of abrasive grit.

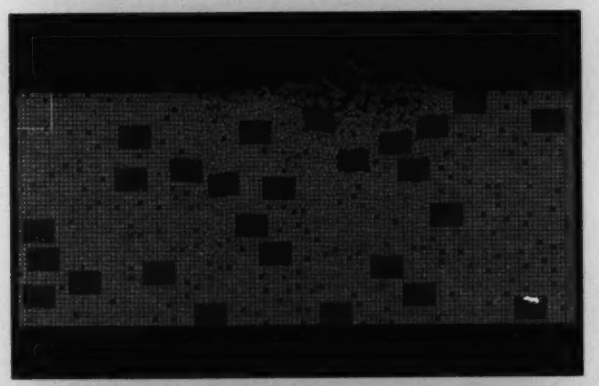

3 vol% of fine reinforcement abraded by small sand particles (size ratio=1:4)

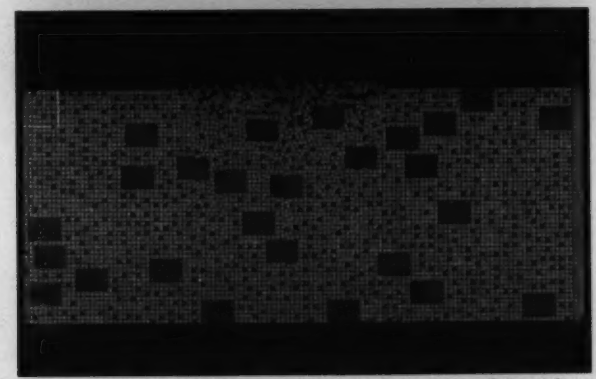

10 vol% of fine reinforcement abraded by small sand particles (size ratio=1:4)

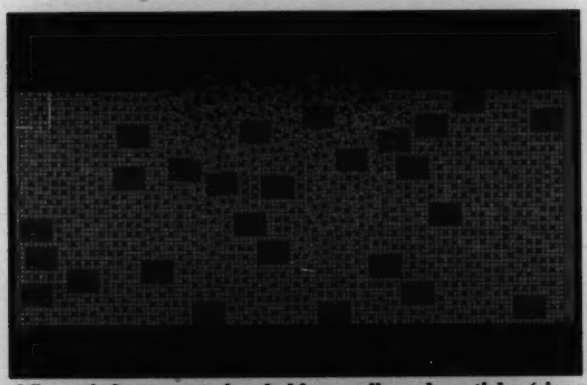

20 vol% of fine reinforcement abraded by small sand particles (size ratio=1:4)

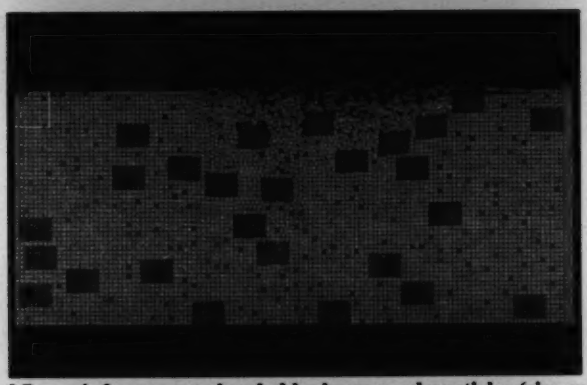

3 vol% of fine reinforcement abraded by large sand particles (size ratio= 5:1)

10 vol% of fine reinforcement abraded by large sand particles (size ratio=5:1)

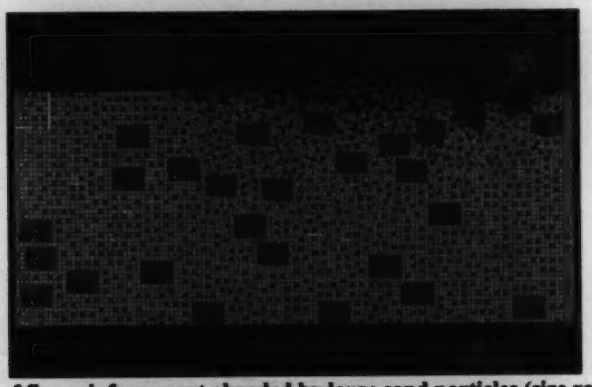

20 vol% of fine reinforcement abraded by large sand particles (size ratio=5:1)

Figure 4-6 Typical morphologies for composites containing by different volume fractions of fine reinforcements under small and large abrasive particles.

As the size of abrasive particle decreases, the critical volume fraction of the fine reinforcement shifts to a higher level. The predicted phenomena can be explained as follows.

When the abrasives are coarse, the external force transferred by them is large. Under such a condition, if the reinforcements are small and homogeneously dispersed, their contribution is mainly to increase the hardness of the matrix. However, such increases in hardness are limited and not effective in blocking the penetration of the large abrasive. The spacing between fine reinforcements is very small and it does not play an important role in blocking the penetration of the abrading sand. In consequence, the critical volume fraction of fine particulates is maintained at a lower level.

On the other hand, if the abrasives are small, the load carried by each abrasive particle is small and the penetration depth of the abrasive is small. This results in lower wear losses in general, as compared with that caused by large abrasive particles. However when the spacing is larger than the abrasive size, the wear loss increases due to the enhanced damage of matrix. When the spacing and abrasive particle size is comparable, the wear loss becomes stable because the abrasive particles can be trapped in the gaps between reinforcements or be blunted by the reinforcements. Adding more fine reinforcements decreases the spacing between

them. These fine particulates could block the penetration of the small abrasives and decrease the wear loss. As can be imagined, if the abrasive size is small, only a matrix containing larger amount of reinforcements could reduce the penetration of the abrasives and lead to higher wear resistance. This explains the shifting of the critical volume fraction to a higher level when the abrasives are small. However, excessive fine particles make the composite brittle and would increase the wear loss. These results are consistent with experimental investigations of N. Axen et al [57].

The above discussion is focused on the critical volume fraction of fine reinforcement in the composites. In order to generalize the study, composites with only a large size of reinforcing particles have also been examined. Figure 4-7 shows simulation results for a composite enhanced only by large reinforcing particulates (containing 7× 5 lattice sites) and abraded by three sizes of abrasive sands. The volume fraction of reinforcement particulates is the only variable in the simulation.

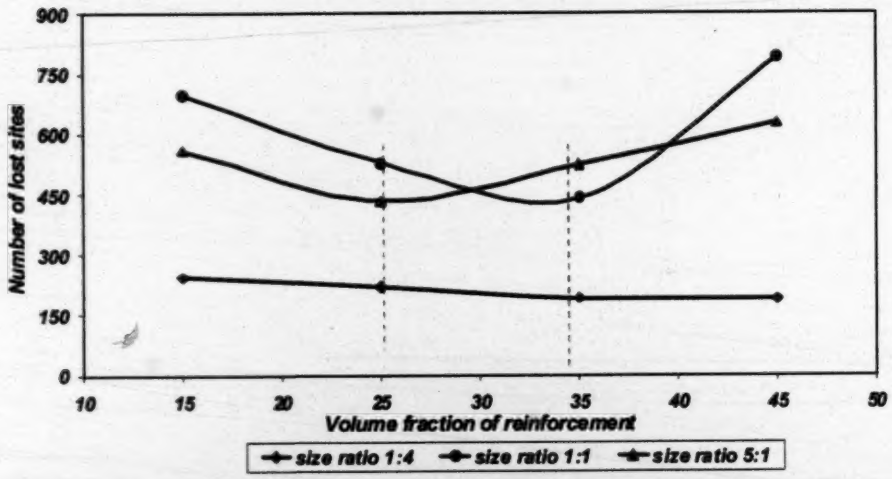

Figure 4-7 Wear loss as a function of volume fraction of reinforcement for three size ratio conditions. The critical volume fraction is shifted to a higher level when the size ratio decreases.

As shown in Figure 4-7, when abraded by fine sand particles (i.e. size ratio=1:4), it seems that the critical volume fraction exceeds the simulation range. When the abrasive sand particles are larger (i.e. size ratio=5:1), there exists an obvious critical volume fraction. Similar to the trend observed earlier, the critical

volume fraction corresponding to the small size ratio is higher than that in a large size ratio condition. Although the values of the critical volume fraction are different when the reinforcement sizes are dissimilar, the trend of increasing the critical volume fraction as the size ratio decreases is observed in all cases. So a general conclusion can be drawn that as the size ratio decreases, the critical volume fraction shifts to a higher level.

4.2.4 Combined effects of size ratio, volume fraction and interfacial bond strength on abrasive wear

As indicated in Chapter 1, many studies have shown that volume fraction and size ratio of abrasive particle to reinforcement significantly influence the wear behavior of composites. From literature on materials manufacture and processing [40, 50, 112, 113], it is noticeable that manufacturing or processing methods for composites can result in different bond strengths at the interface between the reinforcement and matrix, which affects their overall wear resistance. Under working conditions, the volume fraction, size ratio and interfacial bond strength largely simultaneously determine the tribological behavior of the composite. The synergism of all the factors makes the experimental investigation difficult and complicated; however, such synergism could be easily investigated by computer simulation. In this section, three size ratios are used by changing the size of the abrasives. Two different interfacial bond strengths are taken into account (i.e. a weak bond with its modulus lower than the Young's modulus of the matrix bond and a strong bond having its modulus higher than that of the matrix bond). Figure 4-8 illustrates changes in the wear loss of the composites under study, with the interfacial bond strength at a total volume fraction of reinforcement of 35%. Figure 4-9 shows typical morphologies of composites with weak and strong interfacial bonds, respectively.

From these figures, it can be seen that wear losses of composites with a strong interfacial bond are lower than those with a weaker interfacial bond for all three size ratios. It can be generalized that strong cohesion is desired to lower the abrasive

wear loss of composites. The phenomenon of a high interfacial bond strength improving wear resistance has been observed both experimentally [49, 112-113] and by simulation [96]. The effect of interfacial bonding is more pronounced when the size ratio is relatively large (i.e. large abrasive particle size and small reinforcement size). To consider this phenomenon, the interaction between the reinforcement and the abrasive should be reviewed.

When the size ratio is large (i.e. large abrasive particle size and small reinforcement size), the abrasives transfer higher wearing force [53, 57] on to the target surface. This can dramatically increase the wear loss. The small reinforcement particles results proportionally in more total interfacial areas [50]. If the interfacial bond is weak, more interfacial cracks are easier to initiate and propagate at the interface [49, 112]. The reinforcement can be easily detached as wear debris by cracking at the interface and delamination of the matrix, thereby significantly increasing wear loss. However, if the interfacial bond is strong, the removal of reinforcement by cracking is reduced. Also small reinforcement decreases the spacing between them, increasing the composite hardness [41]. Both lead to a lower wear loss. This explains the large difference that occurs in wear loss in weak bonding and strong bonding conditions.

When the size ratio is small (i.e. small abrasive particles and large reinforcements), the large reinforcements usually behave as hard protuberances on the composite surface resisting the external wearing force [57]. In addition, large reinforcements usually require higher stress to fracture [46] and remain in the composite system longer before cracking and being removed as wear debris [45, 47]. Although small abrasives have more chances to attack the interface between the matrix and the reinforcement, they can only affect very local areas with limited ability to fracture or extract relatively large reinforcement particles. Moreover large reinforcements result in less interfacial area, thus reducing the influence of interfacial bonding. These are reasons why under small size ratio condition, the difference in the wear loss for weak bond and strong bond is not as pronounced as that under a large size ratio condition.

However, when size ratio equals one, the strong and weak interfacial bond strengths result in the smallest difference in wear loss. Previous experiment [59] has demonstrated that at size ratio of one, the wear resistance of a composite was at the lowest level due to relative easy removal of reinforcements by penetration of the abrasive particles while still under external force (unlike finer abrasive particles). In such situation, the interfacial bond may play less critical role in resisting abrasive wear.

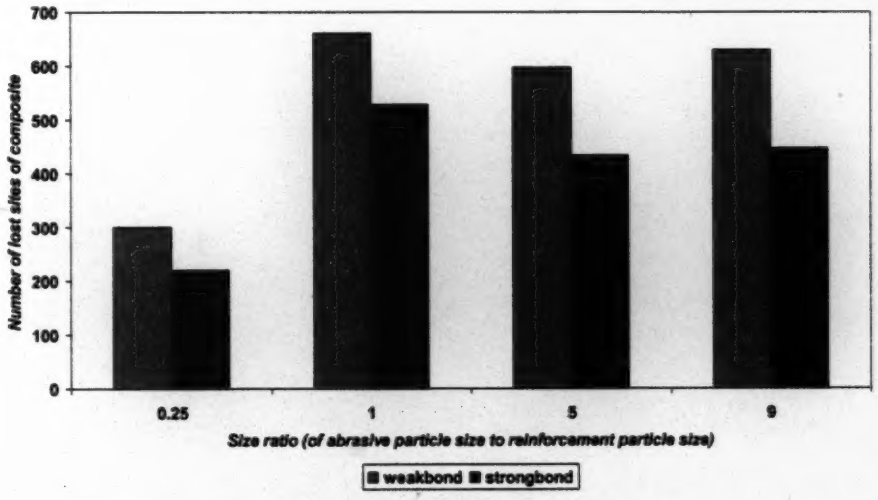

Figure 4-8 Wear losses of composites with weak bond and strong bond, respectively, under three size ratio conditions.

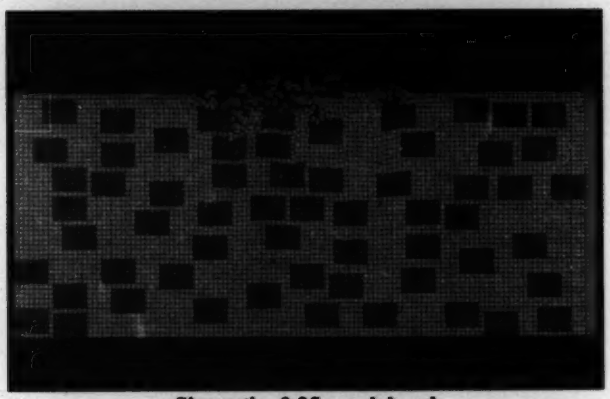

Size ratio=0.25, weak bond

Size ratio=0.25, strong bond

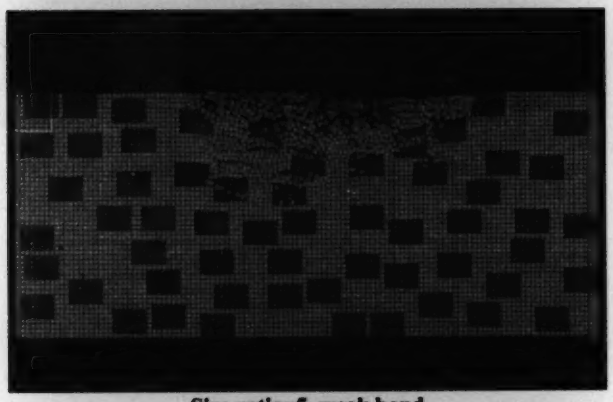

Size ratio=5, weak bond

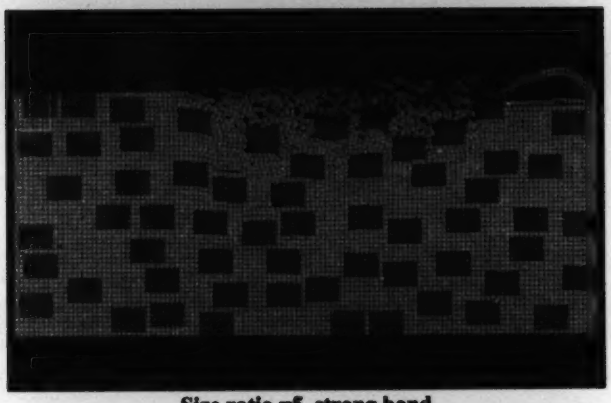

Size ratio =5, strong bond

Figure 4-9 Typical morphologies of composites abraded by two different sizes of abrasive sand particles, under weak and strong bond conditions.

Changes in wear loss as a function of volume fraction with the combined effect of interfacial bond strength and size ratio are investigated. As demonstrated in Figure 4-10, the volume faction curves show different trends for the two interfacial bonding conditions.

When the bond strength is strong, the wear loss curves as a function of three different size ratios initially decrease. After reaching a critical value (corresponding to the lowest wear loss), the wear losses increase for size ratio= 1:1 and 5:1. For ratio=1:4, the critical volume exceeds simulation range so that a continuous decrease in wear loss is observed. The shifting of the critical volume fraction of the reinforcement to a higher level as the size ratio decreases has been explained in section 4.2.3.

When the bond strength low, the curves exhibit greater wear losses for size ratio 1:4 and 5:1 as the volume fraction increases. This phenomenon has been observed experimental and by simulation for erosion of composites [107]. This is reasonable since the interfacial areas are the weakest areas of the composites, and could be damaged first followed by the removal of the ductile matrix. After losing protection from the matrix, the reinforcements will be easily attacked by the abrasive, which can cause fracture of the large ceramic or pulling-out of the small reinforcement. This could explain the continuous increase in the wear loss of the composite in the case of the weak bond. It was suggested [59] that when the size ratio was close to 1:1, the damage to composites was at maximum level. This explains why a size ratio of 1:1 results in highest wear loss among the three size ratios. The initial slight decrease in wear loss for size ratio 1:1 could be related to the spacing between the reinforcements. With volume fraction of reinforcement at 25%, the spacing between reinforcement may be the most comparable with the size of the abrasive particles. These particles are easy to indent into the spacing, decreasing their motion [59]. As a result, the wear loss is reduced to some extent, as shown in Figure 4-4 of section 4.2.2. While for other size ratio conditions, the spacing resulted from different volume fractions may be either too large or too small than the size of abrasive particles. Therefore the abrasive particle can move freely to damage the

composite. This explains why only size ratio 1:1 displays slightly decrease in wear loss initially.

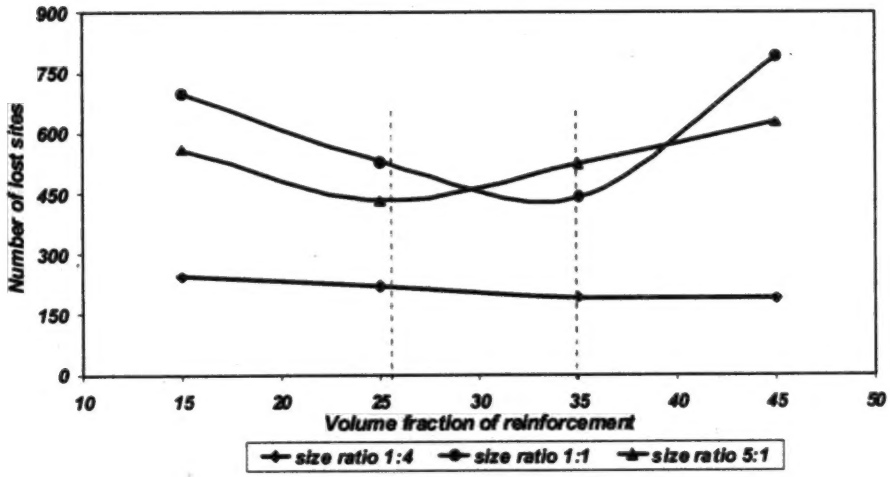

(a)

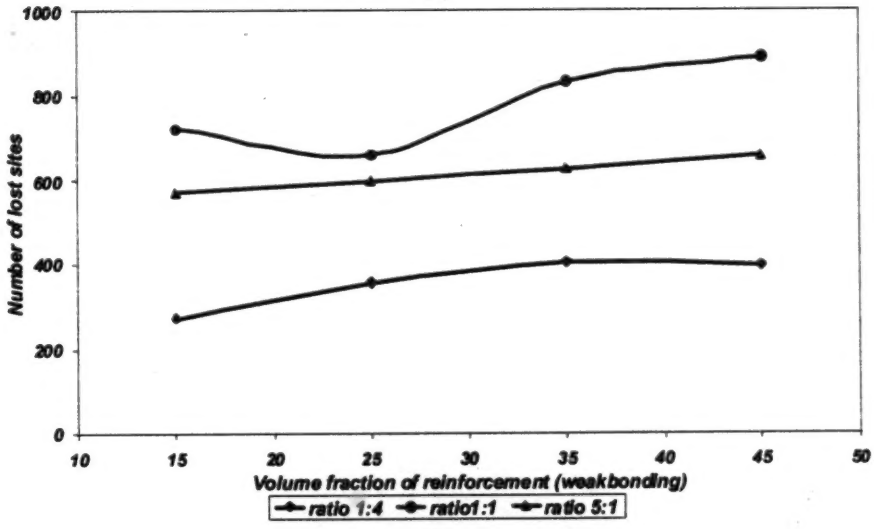

(b)

Figure 4-10 Wear losses as a function of volume fraction of reinforcement for three size ratio. Two bond strengths are considered. (a) strong bond. (b) weak bond. The critical volume fraction for each condition is different. Instead of resulting in a critical volume fraction, the weak bond likely results in continuous increase in wear loss as the volume fraction increases.

4.3 Conclusion

The combined effects of size ratio, volume fraction and interfacial bonding strength on the wear of composite materials have been investigated. Due to the synergism of these factors, relevant experimental studies are rather limited. However, the simulation has been proven to be an effective approach for such studies. The following conclusions are drawn from MSDM simulations presented in this chapter.

1. An optimum combination of large and small reinforcement particles can be more effective in improving the wear resistance of composites than single-size reinforcement.
2. For abrasion by particles of different sizes, the value of this optimal combination of large and small reinforcement varies. If the abrasives are coarser than the largest reinforcement (i.e. the size ratio is large), the wear resistance increases with increasing the amount of the large size reinforcement. However, if the abrasive is smaller than the largest reinforcement (but coarser than the smallest reinforcement), the wear resistance can be substantially improved by adding more dispersed fine reinforcement particles.
3. For different size ratios, the optimal volume fraction, which corresponds to the lowest wear loss, varies. When the size ratio decreases, the optimal volume fraction of reinforcement shifts to a higher level. This means that a large amount of reinforcement can be added to improve the wear resistance of the composite when the abrasive particles are small.
4. Strong interfacial cohesion is necessary for high wear resistance. With high interfacial bond strength, the wear resistance of the composite increases first and then decreases with respect to the volume fraction of the reinforcement. There is an optimal volume fraction of reinforcement. However, when the interfacial bond strength is low, the wear resistance decreases when the volume fraction of reinforcement increases. No optimal volume fraction is observed under a low interfacial bond condition for size ratios 1:4 and 5:1.

5 Shape Effects of the Reinforcement and the Wear Particle on the Abrasive Wear of Composite Materials

5.1 Introduction

Wear is a complicated surface damage process involving deformation and fracture of the surface layer of the target material. For a composite, wear could be caused by damage of the matrix, by interfacial failure or by fracture of the reinforcement. A few years ago, effects of phase geometry on the overall deformation of the metal matrix composites were investigated [114]. It was noticed that the shape of the reinforcement strongly affected their wear performance [22]. Many studies addressing the relationship between the shape of reinforcement and the strain distribution in composites have been carried out [114, 119-125]. Most of the work has been done with the help of Finite Element Methods [114, 119-122, 124] incorporating some assumptions. However, FE simulations are mainly focused on the stress/strain distribution but not on the direct relation between the reinforcement shape and the wear loss. One task of the current work is to investigate how the reinforcement particle shape directly affects the wear behavior of a composite.

On the other hand, the shape of abrasive particles determines their ability to abrade, thus significantly influencing the wear behavior of a composite. It has been shown that an increase in particle angularity can dramatically increase the rate of abrasion [62] because angular abrasives increase microcutting [63]. However, a precise description of the effect of abrasive angularity on wear is not easy. In the 1980s, Swanson and Christman [62, 121] proposed quantitative methods to describe the size and shape effect of abrasive particles on wear. In the late 1990s, Hamblin et al [63] studied the angularity of the abrasives by means of a quantitative description of the boundary of the abrasives. These approaches were developed to simulate realistic situations of abrasion. However, they are very complicated and difficult to be applied in industry.

In this chapter, a few simple fundamental shapes, including diamond, square and sphere (in two-dimensions), are investigated. These shapes have different angularities and result in different degrees of damage to composites. In order to exclude size effect in this study, the reinforcement and the abrasive size were kept the same and only their shapes were changed. The effect of reinforcement shape on abrasive wear is studied first using three different shapes. Then, the angularity of abrasive particles and its effect on abrasive wear loss are investigated. Finally, strain distributions are determined and correlated to the shapes of both the reinforcement and the abrasive. When the effect of abrasive shapes on strain distribution is investigated, a homogeneous material is used as the target material. In order to obtain the strain distribution for different shapes of reinforcement, only one reinforcement particle is embedded into the matrix.

5.2 Results and discussion

5.2.1 Effects of reinforcement shape on abrasive wear of composite

In this section, the wear losses of composites with different shapes of reinforcement are studied using the MSDM technique. Three shapes of reinforcement are used in the two-dimensional simulation, i.e. sphere, square and diamond (square shape with rotation of 45°). Each composite contains only one shape of reinforcement particle. The different shapes of reinforcement are all of the same size (containing approximately the same number of lattice sites). The other parameters, including properties of the matrix materials, the interfacial bonding strength and the abrasion condition (sand flow rate, abrasive particle shape and size) are maintained the same for all three simulations.

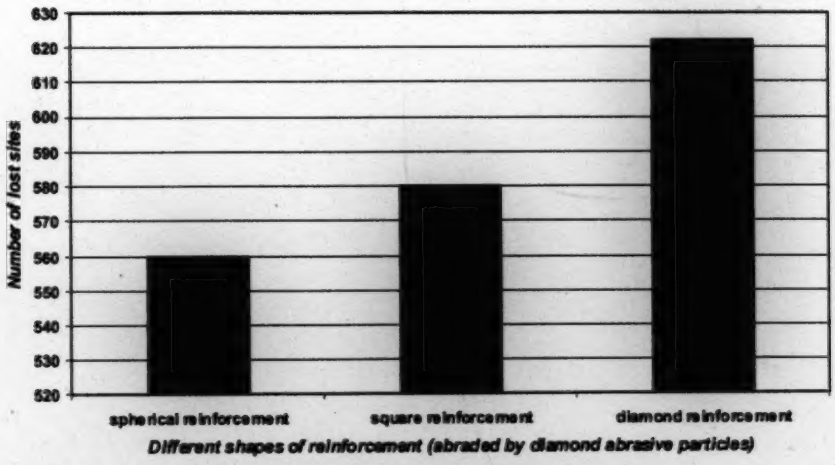

Figure 5-1 Effects of different reinforcement shapes on abrasive wear of composites under identical abrasion conditions.

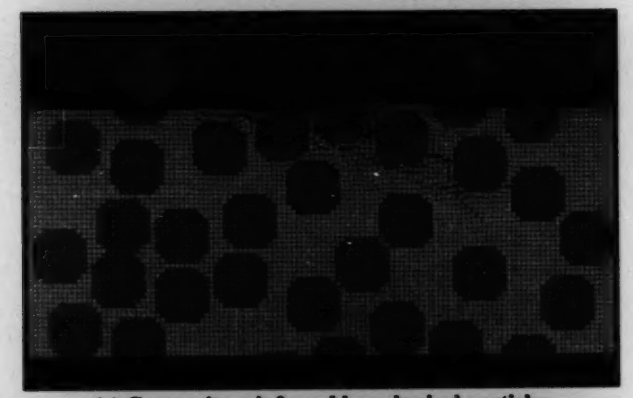

(a) Composite reinforced by spherical particles

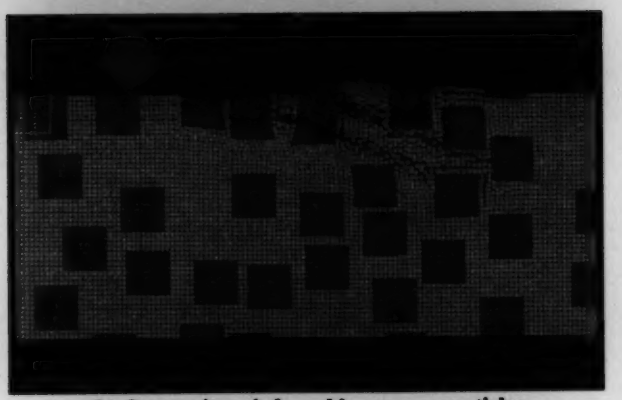

(b) Composite reinforced by square particles

(c) Composite reinforced by diamond particles

Figure 5-2 The morphologies of three composites with different shapes of reinforcements abraded by diamond abrasive particles.

Figure 5-1 illustrates the effect of different reinforcement shapes on abrasive wear of composites under identical abrasion conditions. Figure 5-2 presents morphologies of the composites after being abraded by abrasive particles. From Figure 5-1 one can see that the composite with spherical reinforcing particles shows the lowest wear loss while the material with the diamond reinforcing particles has the highest wear loss. Although the square reinforcement has the same angularity as the diamond reinforcement, the simulation results indicate that the orientation of the reinforcement results in different degrees of wear damage to the composites. In the paper of C. R. Chen et al. [120], it was stated that the composite reinforced by angular particles tended to fail more through particle fracture, while the spherical particles tended to fail through void nucleation, growth and coalescence in the matrix region near the particles [126]. Figure 5-2 (b) and (c) illustrate the fracture of the reinforcement particle while in Figure 5-2 (a) the cracks around the round particles can be seen. Many researchers agreed that spherical reinforcement could result in lower strain in the matrix [114, 119-121] and this helped to develop better resistance to external load. With regard to the orientation of the reinforcement in the present study, it is believed that the diamond shape of reinforcement leads to larger strain concentration in the surrounding matrix and thus facilitates the abrasive particles to dig into the matrix. As shown [114], during tensile testing, intense plastic

deformation occurred along a direction of about 45° to the loading axis. The orientation of the diamond reinforcement particle makes it easier for abrasives to interact with the softer matrix in the direction of 45°, resulting in high strain in the matrix. After reaching the fracture strain of the matrix, it is fractured and torn away as shown in Figure 5-2(c). This matrix debris, however, could also remove the reinforcement leading to severe damage and high wear loss to the composite.

5.2.2 Effects of abrasive particle shape on abrasive wear of composites

In this section, wear losses of composites abraded by abrasive particles of different shapes are studied using the MSDM technique. Three shapes are used in the 2D simulation, i.e. sphere, square and diamond (square shape with rotation of 45°). In order to exclude the size effect, the abrasives of different shapes have the same size (containing approximately the same number of lattice sites). Again, other parameters, including the properties of the matrix materials, the properties of the reinforcement (only one shape of the reinforcement particle is used in all three simulations), the interfacial bonding strength and the sand flow rate are kept the same.

Figure 5-3 illustrates that when abrasive particles of three different shapes abrade the composites reinforced by the same amount of identical square reinforcement, the diamond particle, which is the most angular, results in the highest wear loss; the spherical and square particles abrade the material at similar levels. Figure 5-4 illustrates morphologies of composite abraded by abrasive particles of different shapes. One can see that the diamond abrasives (Figure 5-4 (c)) can easily access and damage the metal material, generate cracks in the matrix and fracture the reinforcing phase. Compared with the diamond abrasive particles, the spherical particles show lower abrasivity. No large cracks are observed in the matrix; however, direct interaction between the abrasive and the reinforcement results in fracture of the reinforcement. This is understandable since in the simulation the abrasive

particles are assumed to be rigid. When impacted by such strong abrasive particles, the reinforcements are readily damaged.

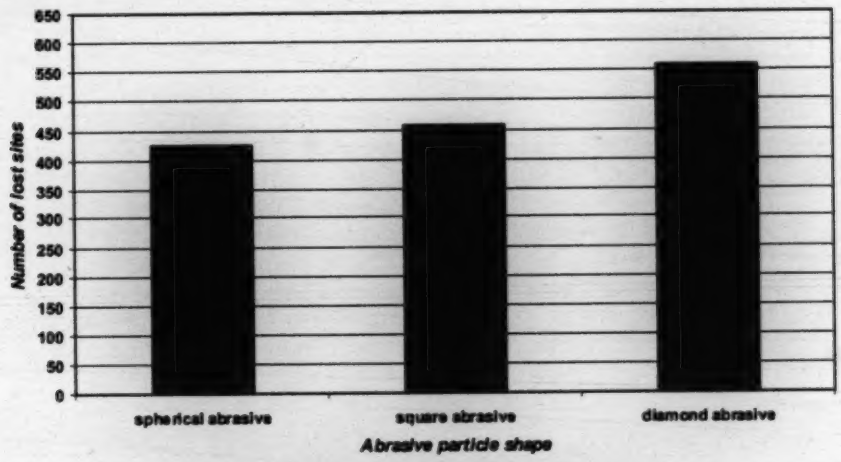

Figure 5-3 Effects of different abrasive particle shapes on abrasive wear of composites under identical abrasion conditions.

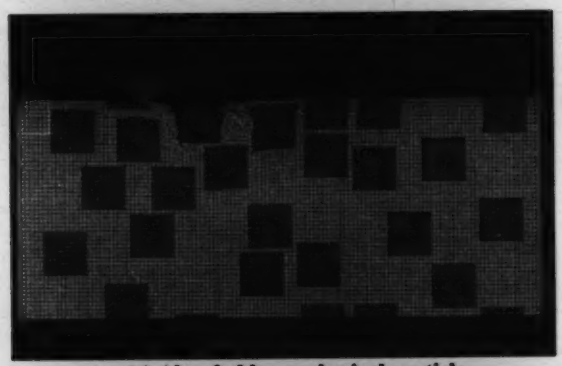

(a) Abraded by a spherical particle

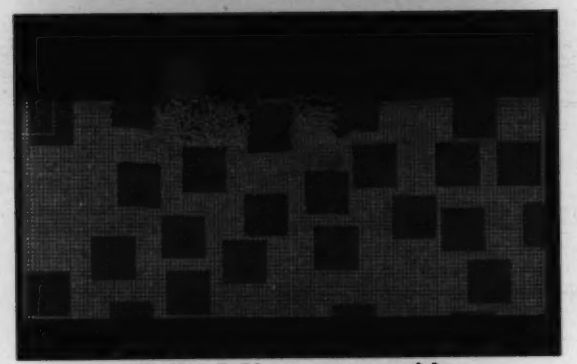

(b) Abraded by a square particle

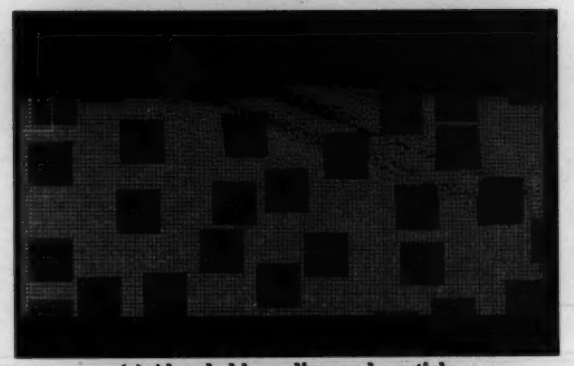

(c) Abraded by a diamond particle

Figure 5-4 Morphologies of three composites abraded by particles of different shapes.

After analyzing the morphologies of the composites after abrasion, it can be seen that the sharp abrasive particles can result in more damage to the matrix than the round abrasives. The degree of damage to the material also depends on the orientation of the angular abrasive. Although it seems that the square and diamond abrasive particle have the same size and sharpness, their abrasion abilities are different due to different orientations with respect to the target surface. After rotating 45°, the contact between the square abrasive sand and the target material changes from an area contact (see Figure 5-5 (a)) to a point one (see Figure 5-5 (b)) resulting in much higher stress on the target surface. This situation was discussed in previous work [127] where it was indicated that a very sharp and angular abrasive particle could initiate fracture of reinforcement in a composite and facilitate further crack extension. In conclusion, a sharp and angular abrasive particle could result in high stresses in both matrix and reinforcement and consequently cause high wear losses.

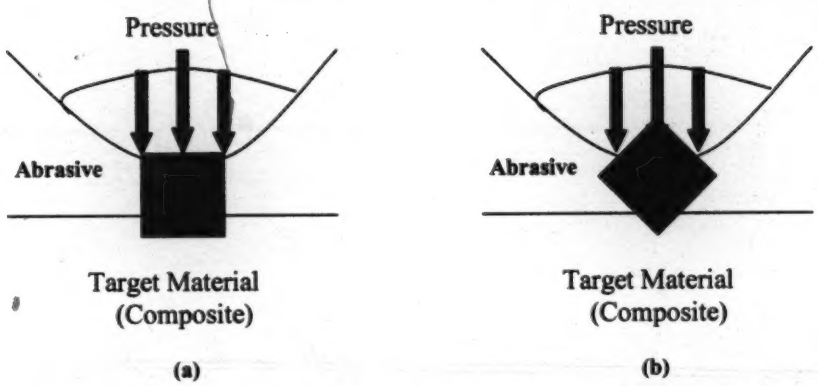

Figure 5-5 The contact between a abrasive particle and the target surface changes from an area contact to a point contact (a) an area contact (b) a point contact after the square abrasive is rotated by 45°.

5.2.3 The combined shape effects on abrasive wear loss

In the previous two sections, we have examined the shape effect of both the reinforcement and the abrasive particles separately. It has been demonstrated that when abraded by diamond abrasive particles, the spherical reinforcement offers the highest wear resistance among the three shapes. For a composite reinforced by a square reinforcement, the shape of the most aggressive abrasive particle is diamond. In this section, wear processes involving all the three shapes of reinforcement and three abrasive shapes are examined, in order to evaluate the combined shape effect of reinforcement and abrasive particles on wear.

In this simulation, three reinforcement shapes are considered. Each composite sample contains reinforcement of only one shape and abraded by particles having the three shapes, respectively.

Figure 5-6 shows simulated wear loss as a function of reinforcement and abrasive particle shapes. It may be concluded that the diamond reinforcement leads to the lowest resistance to abrasion regardless of the shape of the abrasives. It is followed by the square and the most resistant spherical reinforcements. The abrasive

particles with a diamond shape always causes the greatest damage, followed by the square and then the spherical abrasives.

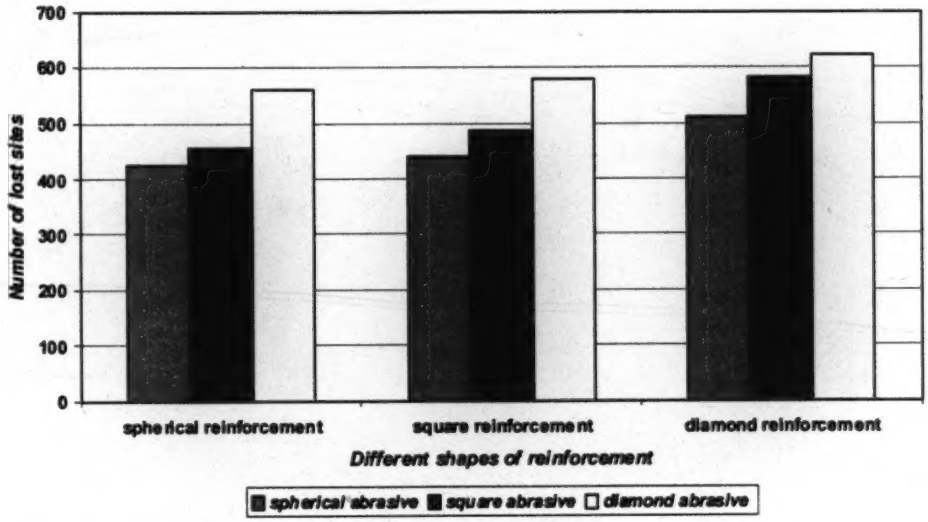

Figure 5-6 Effects of reinforcement shape and abrasive shape on wear.

The shape of reinforcement also has strong effect on wear loss. Theoretical studies on metal-ceramic composites have been conducted extensively in past years. Some have demonstrated the relationship between the reinforcement shape and the constraint imposed by the reinforcement to the ductile matrix [114, 121]. It was shown that the reinforcement prevented the propagation of plastic deformation in the matrix and thus increased resistance to the external load. However, the angular reinforcement increased the stress concentration and raised the strain level in the matrix around the reinforcement as shown Figure 5-7 [120]. This explained why the composite reinforced by angular particles have high wear loss. In addition, the reason for the high damage propensity of angular particles could also be related to the high stress concentration from a point contact, as stated in section 5.2.2.

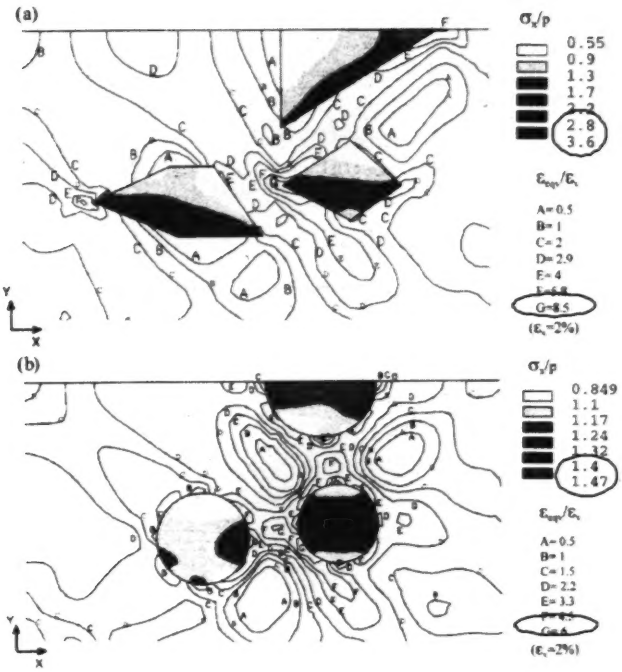

Figure 5-7 The stress σ_x in particles and the equivalent strain ε_{eqv} in matrix when the displacement load $u_x = \varepsilon_x L_x$ ($\varepsilon_x = 2\%$) is applied at the right edge $x = L$ of each condition, where the plane strain condition is applied (P: the x-direction overall stress of each situation). (a) the stress and strain distribution around the angular particles; (b) the stress and strain distribution around spherical particles [120].

5.2.4 Strain analysis for reinforcement and abrasive particles having different shapes

In order to better understand the reinforcement and abrasive shape effect on abrasive wear, strain distributions corresponding to different shapes of reinforcement and abrasive particles during sliding and indentation are investigated using MSDM. The target materials are constrained at the bottom, left and right side. The top surface is subject to the wearing force and can be worn away. The abrasive particles wear the target material in a direction parallel to its top surface at an initial velocity (V_h), which is determined by the rubber wheel speed. When the abrasives travel to the central area of the target material, an elliptical load from the rubber wheel is

exerted on the abrasive sand. This external force results in a vertical movement of the abrasive particle which indents the target surface. The resultant velocity of the abrasive particle is (V_t) as shown in Figure 5-8. Since the velocity of the abrasive is influenced by the resistance from the target surface, its magnitude and the direction is thus a function of time and interaction between the abrasive particle and the target surface. In such a way, the wear force is transferred to the target material, and the interaction between the abrasive and the composite can be simulated. However, when investigating shape effects on wear, it is recognized that the loading condition is very complicated (compression and shearing can be exerted on the surface at the same time). In order to simplify the simulation process, only vertical force is taken into account, and the initial horizontal velocity of the abrasive particle is kept constant for each simulation. The strain of the system referred to is the volumetric strain $e = \varepsilon_1 + \varepsilon_2 = \Delta V / V$ in the 2D modeling. For 3D modeling, the volumetric strain should be expressed as $e = \varepsilon_1 + \varepsilon_2 + \varepsilon_3 = \Delta V / V$. Here $\varepsilon_1, \varepsilon_2, \varepsilon_3$ are the principle strain components. Detailed calculation can be found in 2.2.5.

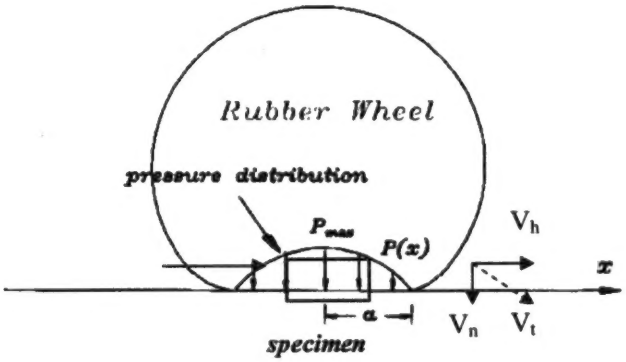

Figure 5-8 During the ASTM G 65rubber wheel test, the velocity of the sand particle has two components, the vertical velocity V_n and the horizontal velocity V_h .The total velocity V_t is a function of time and the interaction between the abrasive particle and the target surface.

5.2.4.1 Abrasive shape and strain

In order to examine the abrasive shape effect on strain, a homogeneous target material is used in the simulation thereby the influence from all other factors are excluded. Abrasive particles with different shapes slide on the target surface from left to right. The initial sliding velocity is determined by the rotation speed of the rubber wheel. As mentioned earlier, the interaction between the abrasive particle and the target surface changes the velocity of the abrasive during abrasion, but this is corrected automatically by the computer model. Table 5-1 lists the maximum tensile and compressive strains occurred in the homogeneous material when abraded by different shapes of abrasive particles. Figure 5-9 illustrates strain distributions caused by abrasive particles having three shapes after sliding.

As shown, the areas of the volumetric strain are quite different. The diamond abrasive results in relatively narrow but deep strained area. The strain resulted from square abrasive is more extended but the vertical zone is shallower than that of the diamond shape. The spherical particle produces the shallowest vertical zone but extends over the widest area. The above results can be explained by considering the load transferred by the particles. The diamond shape can result in the highest stress concentration. As marked on Figure 5-9, the diamond shape results in highest values of both tensile and compressive strains on the surface. The high tensile strain indicates that the diamond abrasive can tear the material away more easily. While the high value of compression strain corresponds its capability to penetrate the material. This makes the abrasive particle move in the vertical direction penetrating deeply beneath the surface.

Table 5-1 The maximum tensile and compressive strains in a homogeneous material caused by different shapes of abrasive particles

Shape of abrasive particles	$\varepsilon_{max} > 0$ (tensile strain)	$\varepsilon_{max} < 0$ (compressive strain)
Diamond shape	1.59×10^{-1}	-1.96×10^{-1}
Square shape	1.34×10^{-1}	-1.76×10^{-1}
Spherical shape	1.10×10^{-1}	-1.73×10^{-1}

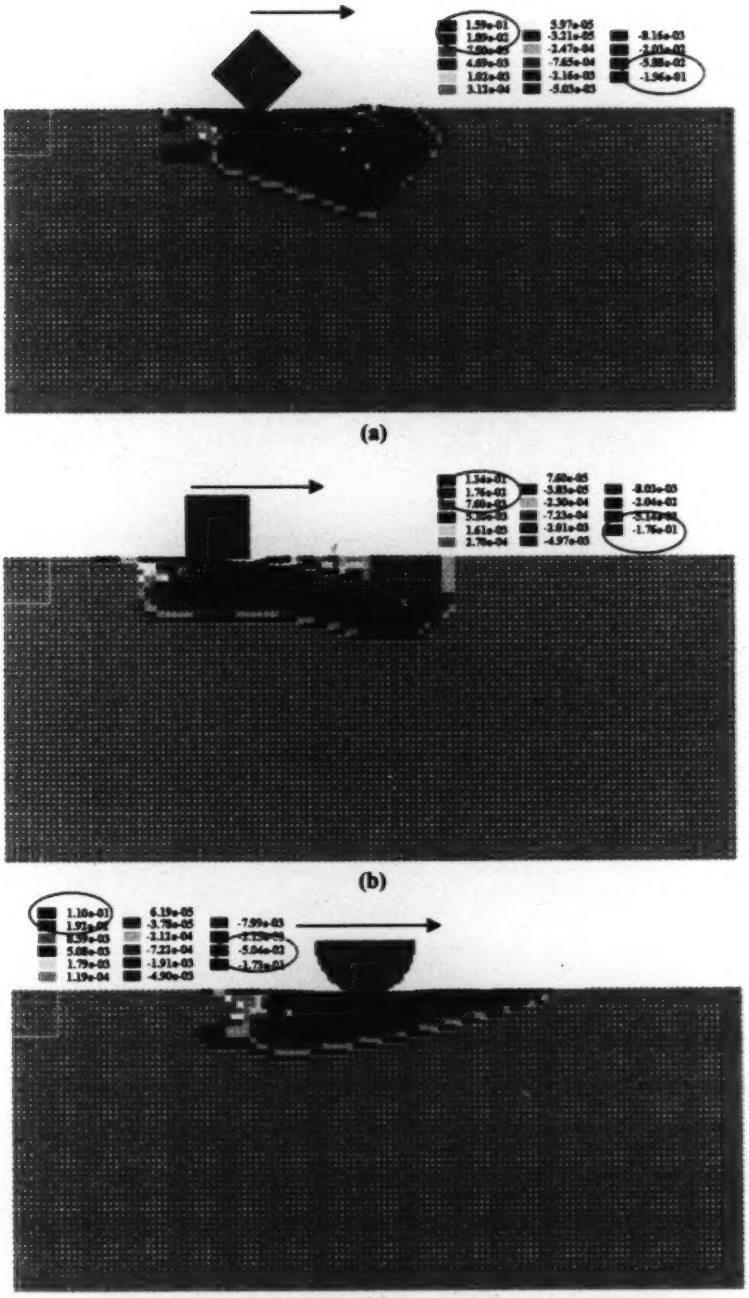

Figure 5-9 Strain distributions in a target material abraded by abrasive particles having different shapes, respectively: (a) diamond abrasive; (b) square abrasive; (c) half-sphere abrasive particles. The shown is the second abrasive particle sliding over the area which has been abraded by the first particle.

As indicated by the dark red color in Figure 5-9, high tensile strain (with value of 1.59×10^{-1}) appears intensively in wide areas when material is abraded by the diamond abrasive, while for materials abraded by abrasives with other shapes, the tensile strained areas are limited both in horizontal and vertical directions. The highest tensile strain values resulted from square and spherical abrasives are 1.34×10^{-1} and 1.10×10^{-1}, respectively. Since most materials fail easily under tensile stress, the value of tensile strain reasonably reflects the degree of wear damage resulted from different abrasive shapes. As demonstrated in Section 5.2.2, the diamond shape of abrasive resulted in highest wear loss while the square and spherical abrasives damaged the materials at similar levels. The highest compressive strain values resulted from diamond, square and spherical abrasive are 1.96×10^{-1}, 1.76×10^{-1} and 1.73×10^{-1}, respectively. These values are consistent with the discussion in 5.2.2, which indicated that for the square and spherical shape of abrasive particulate, the pressure exerted on the surface was lower than that resulted from diamond shape due to larger contact areas. The abrasive can travel longer in the horizontal direction and results in a wider but shallower strained region. In conclusion, the simulations on wear loss and strain distribution resulted from different shapes of abrasive particles are consistent with each other.

The simulation clearly demonstrates that an angular abrasive particle will damage the material more intensively than a less angular abrasive particle due to high values both in compression and tensile strain. Compared with the results from FEM analysis (Figure 5-10) given in [128], one may find that the compressive strain is directly beneath the contact region while the tensile strain exists at the left side of the figure. The result from MSDM is consistent with FEM analysis. Shown in the color of orange, the tensile strained areas in MSDM also appear in the left side of the material and the large compressive strain region can been observed under the surface of the material. However the resolution of MSDM is lower than the FEM result and could be improved if a finer lattice grid is used.

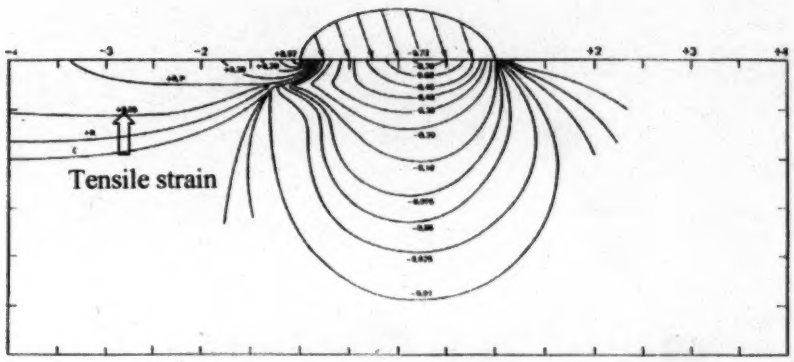

Figure 5-10 Contours of maximum principal stress caused by a combination of elliptical distribution of tangential and normal force [128].

5.2.4.2 Reinforcement shape and strain

The MSDM approach can also correctly describe the strain state in a contact region during an indentation process, as justified by the comparison between the MSDM result and the FEM analysis [129].

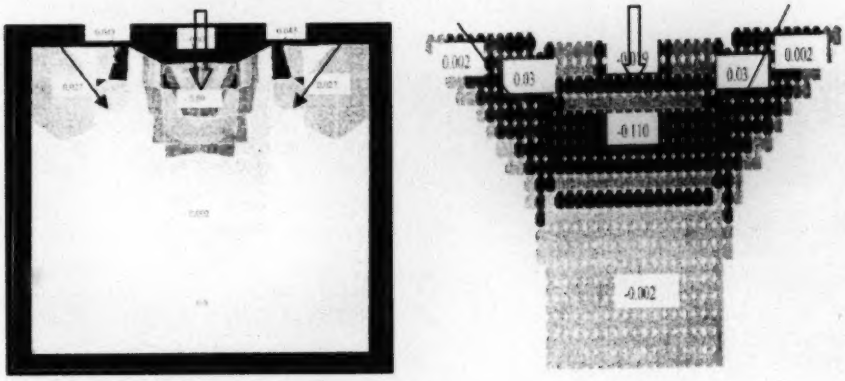

(a) **(b)**

Figure 5-11 Strain distributions from different approaches (a) from a commercial FEM package (ANSYS); (b) from the MSDM technique in previous study[129].

Figure 5-11 (a) illustrates the strain distribution of a homogeneous material during an indentation process obtained by the FEM approach. Figure 5-11 (b)

demonstrates the corresponding volumetric strain distribution using MSDM. One may see that although the resolution of MSDM is not as high as FEM simulation, they have similar distributions of compressive and tensile strains. The arrows show that the tensile strain bands exist on left and right hand sides in 45° direction while the block arrow shows the compressive strain distribution occurs right beneath the contact region. The strain distribution resulted from MSDM is consistent with that from FEM.

In the simulation, the effect of the reinforcement shape on the strain distribution in the matrix during an indentation process was investigated. Each composite contained only one reinforcement particle. Three shapes i.e. diamond, square and sphere were studied. A spherical abrasive was pressed onto the surface of the composite and resulted in a strain distribution in the contact region. Table 5-2 demonstrates the maximum tensile and compressive strains in the matrix around the reinforcements at different time steps. Figure 5-12 demonstrates the variation in strain distribution for the composites containing three shapes of reinforcements at different time steps during indentation processes. In order to determine the volumetric strain using the equation of $e = \Delta V / V = \varepsilon_x + \varepsilon_y$, which is only suitable for small deformation, the indentation depth was limited to a small scale. For all strain distributions, the compressive strain region is just under the contact region while the tensile strain mainly exists in direction of 45° with respect to the horizontal surface.

Table 5-2 The maximum tensile and compressive strains caused by dissimilar shapes of reinforcements at different time steps

	$\varepsilon_{max} > 0$ (tensile strain)			$\varepsilon_{max} < 0$ (compressive strain)		
	t=8000	t=15000	t=20000	t=8000	t=15000	t=20000
Diamond reinforcement	1.12×10^{-3}	2.39×10^{-3}	3.44×10^{-3}	-1.57×10^{-2}	-1.79×10^{-2}	-1.72×10^{-2}
Square reinforcement	8.62×10^{-4}	2.03×10^{-3}	2.23×10^{-3}	-1.70×10^{-2}	-1.54×10^{-2}	-1.40×10^{-2}
Spherical reinforcement	9.20×10^{-4}	1.03×10^{-3}	1.20×10^{-3}	-1.73×10^{-2}	-1.47×10^{-2}	-1.34×10^{-2}

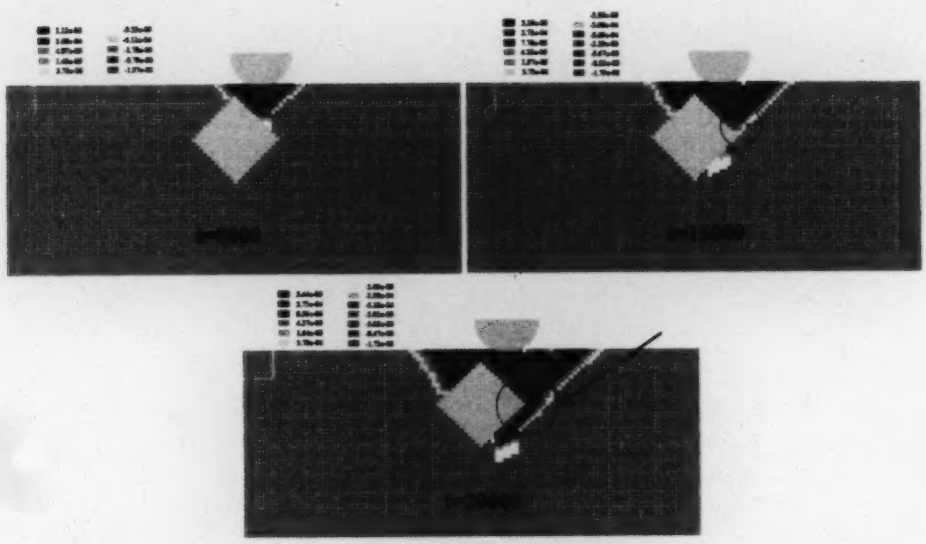

(a)

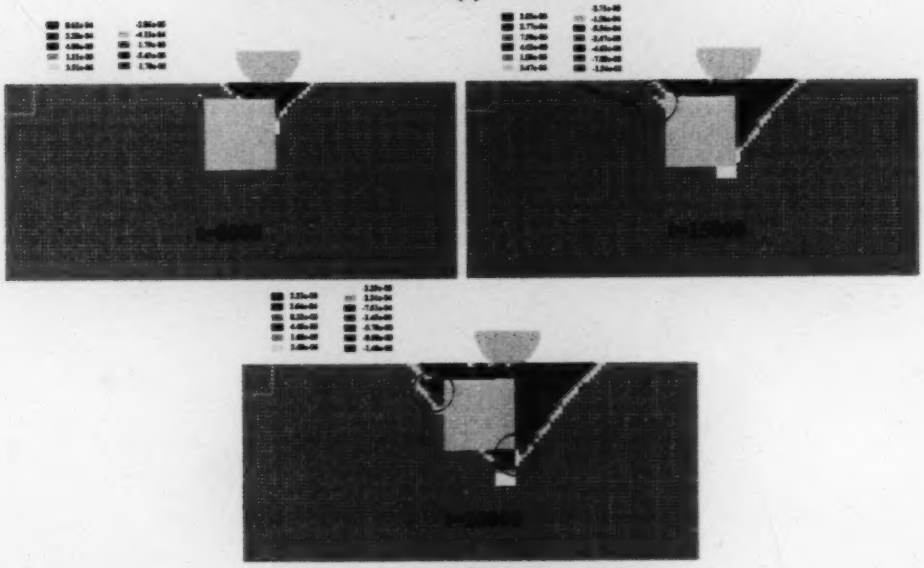

(b)

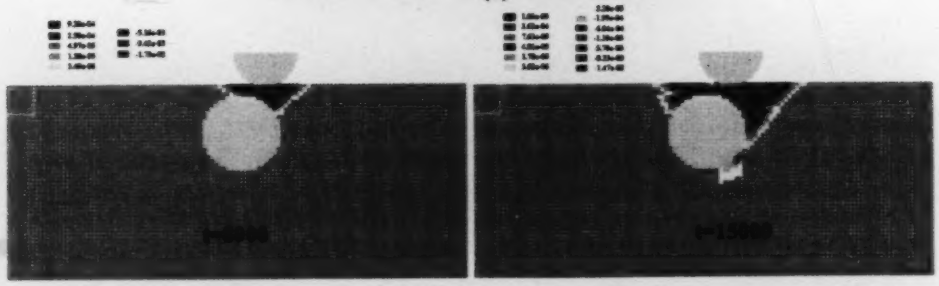

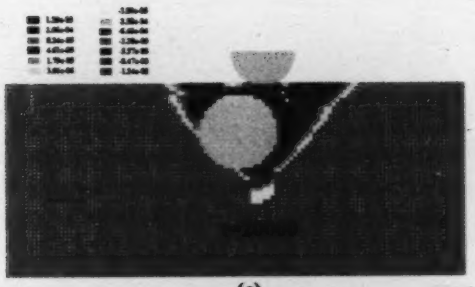

(c)

Figure 5-12 Strain distributions of composites with different reinforcement particle shapes under compression by a half-sphere abrasive particle at different simulation time steps (a) diamond reinforcement, (b) square reinforcement, (c) sphere reinforcement.

Due to the difference in reinforcement shape, the strain values for three reinforcement shapes are dissimilar. At time step t=8000, the tensile strain in the matrix resulted from diamond reinforcement has the highest value, followed by the spherical and square reinforcement. However, the compressive strain resulted from spherical shape shows the highest value, followed by square and diamond shape. It demonstrates that at the beginning of the indentation process, the diamond shape of reinforcement results in the highest tensile but lowest compressive strain, while the spherical reinforcement caused higher tensile and compressive strains than that caused by square reinforcement.

As the simulation goes on, the reinforcement shapes influence the strain evolution differently. At t=15000, the tensile strain resulted from diamond reinforcement increases significantly (from 1.12×10^{-3} to 2.39×10^{-3}). The degree of the increase in tensile strain resulted from square shape (from 8.62×10^{-4} to 2.23×10^{-3}) is almost as high as that from diamond shape; the corresponding increase in spherical shape is the lowest (from 9.20×10^{-4} to 1.20×10^{-3}). As the tensile strain increases, the compressive strain resulted from diamond reinforcement increases as well, which corresponds to its strain concentration caused by angular corners. For square and spherical shapes of reinforcements, the compressive strains decrease. The beneficial effect of spherical shape can be seen since the strain

concentration level (both for tensile and compressive strain) is lower than that of the square reinforcement.

At t=20000, one can see that the diamond shape results in the highest value of tensile strain in the matrix. The square reinforcement also results in increased tensile strain; however, the highest value of the tensile strain (2.23×10^{-3}) caused by square shape is lower than that of the diamond shape (3.44×10^{-3}). One may also find that the tensile strain occurs more likely around the corner of a sharp shape as marked by oval marker. This may facilitate the strain concentration around the sharp corners and result in crack initiation and propagation. When the spherical reinforcement is studied, its tensile strained area has lower value (1.20×10^{-3} compared with the results for other two shapes). There is no sharp corner region where tensile strain can intensely develop. The compressive strain decreases for all three reinforcement shapes. However, it is also found that the decrease in compressive strains resulted from three shapes is not pronounced during investigated period. This is because the external force is exerted on the system constantly during indentation. The strain concentration for diamond reinforcement is the most pronounced, followed by the square reinforcement and the spherical one results in the lowest strain concentration.

From the simulation, one may conclude that during an indentation process, the tensile strain value in matrix increases dramatically in the case of diamond shape. For both diamond and square shapes, high tensile strain is likely to occur around the sharp corners, which can be responsible for cracking initiated in the vicinity of interface. As the tensile strain develops, the compressive strain in the matrix slightly decreases to similar levels for square and spherical shapes, while the compressive strain of the diamond shape increases slightly. The considerable increase in tensile and compressive strains of diamond shape probably causes high stress concentration and results in great wear loss as it has been seen in 5.2.1.

The strain distributions resulted from different reinforcement shapes have been investigated by many researchers [119-123] in various deformation processes. For instance, it is demonstrated that when tensile loading is applied to the system, the

spherical particles will cause less stress/strain concentration in the matrix than other shapes [120]. MSDM simulation study is consistent with the research report.

It should be noticed that the resolution of the strain distribution from MSDM is not high when comparing with FEM simulation. If a finer lattice grid is used, higher resolution could be obtained but longer simulation time is required.

5.3 Conclusion

In this chapter, the shape effects of the reinforcement and the abrasive particles have been studied using MSDM approach.

Simulation results show that the angular abrasive particle will result in higher wear loss. The orientation of angular abrasive particle also leads to significant change in stress at contact surface. Diamond reinforcement does not benefit the wear resistance since it causes the stress concentration around the sharp corners. Sphere reinforcement demonstrates the highest resistance to abrasive wear.

Strain distribution analysis further supports above findings. An angular abrasive particle can abrade the material more deeply than other shapes. The sharp abrasive introduces high compressive strain which reflects its capability to penetrate the material. Since a sharp reinforcement results in strain concentration, especially increasing the tensile strain in the matrix around the sharp corners, it would facilitate the crack initiation and propagation around the sharp corners. The cracks will cause debonding at the interface and delamination of the materials, which is responsible for higher wear loss of the composite reinforced by diamond particles. This is consistent with other simulation results from other methods such as FEM.

6 Overall Conclusions and Future Work

6.1 Summary of the results in different chapters

In this research, the Micro-Scale Dynamic Model, which is based on Newton's Law of Motion, has been applied to study the microstructural effects on abrasive wear of composites. Detailed background and description of the model are given in Chapters 1 and 2.

Chapter 3 focuses on the microstructural effect on wear, including the volume fraction of reinforcement, interfacial bond strength, reinforcing particle size, and size of abrasive particles. It has been demonstrated that the simulation results are consistent with experimental observation and theoretical prediction. This confirms the efficiency and capability of computational study using MSDM technique to predict abrasive wear. The following information on the abrasive wear of composites is obtained from Chapter 3:

1 There is an optimal volume fraction of reinforcing phase that provides the highest abrasive wear resistance. Below the critical value, increasing the content of reinforcement to the optimal level could increase the wear resistance. This effect is reversed when the content of the reinforcing phase exceeds the critical value.

2 Interfacial bond strength could significantly influence the optimal volume fraction of reinforcement. Enhancing the cohesion between the reinforcement and the matrix in a composite could accommodate more reinforcing particles before reaching an optimal value thus allowing a considerable improvement in wear resistance.

3 When the abrasive is larger than the reinforcement, the coarser the reinforcing particles, the better the wear resistance.

4 The simulation on the size ratio of abrasive particle to the reinforcing particle indicates the existence of a critical ratio, above which the wear rate of the composite becomes stable. Below this critical value, increases the size ratio accelerates the wear rate.

In Chapter 4, the application of MSDM is extended to more complicated situations. The combined effects of size ratio, volume fraction and interfacial bonding strength are investigated. The following information is obtained:

1 An optimum combination of large and small reinforcements could be more effective in improving the wear resistance of composites than using single size reinforcement particles.

2 When abraded by abrasive particles of different sizes, the value of this most effective combination of large and small reinforcement varies. If the abrasives are larger than the coarsest reinforcement, the wear resistance improves with increases in the amount of the large size reinforcement. However, if the abrasive is finer than the largest reinforcement (but coarser than smallest reinforcement), the wear resistance can be substantially improved by adding more dispersed fine reinforcement particles.

3 At different size ratios, the optimal volume fraction of reinforcement which corresponds to the lowest wear loss changes. When the size ratio decreases, the optimal volume fraction of reinforcement shifts to a higher level. This means a large amount of reinforcement is required to improve the wear resistance of composite when the abrasive sand particle is small.

4 Strong interfacial cohesion is always desired to obtain higher wear resistance. With high interfacial bond strength, the optimal volume fraction of reinforcement increases. However, when the interfacial bond strength is sufficiently low, the wear resistance of composites simply decreases when the volume fraction of reinforcement increases and no optimal volume fraction is observed.

In Chapter 5, the effects on abrasive wear of composite of both the shapes of reinforcement and abrasive particle are studied. The simulation results show that the diamond abrasive particles will result in higher wear loss than abrasive particle of square and spherical shapes due to large stresses at contact surface. Sharp reinforcements do not benefit the wear resistance significantly, since their sharp corners will result in a higher strain concentration. The strain distribution analysis

further proves the above findings. The sharp abrasive can abrade the material more deeply than other shapes due to high compressive stress. The sharp reinforcement results in tensile strain concentration around the sharp corners, which facilitates crack initiation and propagation at interface and finally results in higher wear loss.

6.2 Future work

1. Effect of abrasion heat

In this model, the frictional heating generated during wear process is not taken into account, since the temperature rise during rubber-wheel abrasion test is not large. However, in industrial abrasion processes, temperature rise could be large, which may influence the mechanical properties of the material, and thus result in higher wear loss under real abrasion condition than that under the simulation condition. The work on frictional heating could be done, which may lead to more accurate prediction. The frictional heating can be incorporate in MSDM as demonstrated in other paper [109].

2. Effect of multiple abrasive particle abrasion

In reality, abrasives of different shapes and sizes can interact with a target material simultaneously. In the present simulations, abrasive particles have the same size and shape and are sent to abrade a target material one by one. This may not influence the wear trend of different materials, but affect the accuracy of the simulation. By including abrasive having different shapes and sizes, could simulate real industrial abrasion processes with quantitative output. Simulating abrasive wear under attack by an abrasive flow containing multi-size and multi-shape abrasives should be taken into account in future modeling.

3. Effect of the time interval and initial length of bonds

In the present work, the time interval Δt was selected in a reasonable range which is determined by running trial simulations at different time intervals. It is not

convenient to always conduct such a computer test to determine the time interval in different situations. The time interval should be related to many factors, such as the original length of bonds, the external loading condition, etc. In future, when such investigations are conducted and the possible analytical relations between Δt and these factors can be established, the model could be more convenient to apply.

4. Improvement of the stress/strain calculation of MSDM

As shown in Chapter 5, the strain calculation of MSDM has low resolution. However, it does provide some useful information on the strain distribution. In future, the resolution of stress/strain distribution will be improved and it would offer competitive results as FEMs. As a matter of fact, the resolution can be improved by using a smaller lattice grid. However, using smaller grids would increase the computing time. Using super computer would be a solution to this limitation.

References

1. D. Dowson, *History of Tribology*. 1979, New York: Longman. xvii, 677.
2. ASTM International American Society for Testing and Materials, *Standards International*, in *Metal Corrosion, Erosion and Wear*. 1993, ASTM: Philadelphia, Pa.
3. M. J. Neale and M. G. Gee, *Guide to Wear Problems and Testing for Industry*. 2001, Norwich, N.Y.: William Andrew Pub. vii, 150.
4. K-H Zum Gahr, *Microstructure and Wear of Materials*. Tribology series. 10. 1987, New York: Elsevier. ix, 560.
5. Ernest Rabinowicz, *Friction and Wear of Materials*. 2nd ed. 1995, New York: Wiley, 315.
6. NRC Canada, *Associate Community on Tribology,*. 1986(report no.26556,).
7. ASM International. Handbook Committee., *ASM Handbook*. Vol. 18. 1992, Materials Park, OH: ASM International. 184-190, 801-811.
8. B. Bhushan and B. K. Gupta, *Handbook of Tribology : Materials, Coatings, and Surface Treatments*. 1991, New York: McGraw-Hill. (various pages).
9. Ian M. Hutchings, *Tribology : Friction and Wear of Engineering Materials*. 1992, Boca Raton: CRC Press.
10. A. R. Lansdown and A. L. Price, *Materials to Resist Wear : A Guide to Their Selection and Use*. 1st ed. The Pergamon materials engineering practice series. 1986, New York: Pergamon Press. ix, 128.
11. T. F. Norman, in *Abrasive Wear of Materials-Handbook of Mechanical Wear*, L. Colwell C. Lipsom, Editor. 1991, University of Michigan Press. p. 277-314.
12. David A. Rigney, American Society for Metals. Materials Science Division. and Metallurgical Society of Aime., *Fundamentals of Friction and Wear of Materials : Papers Presented at the 1980 ASM Materials Science Seminar, 4-5 October 1980, Pittsburgh, Pennsylvania*. 1981, Metals Park, Ohio: American Society for Metals. 470.
13. M. J. Murray, P. J. Mutton and J. D. Watson, *Abrasive Wear Mechanisms in Steels*. Journal of Lubrication Technology-Transactions of the Asme, 1982. **104**(1): p. 9-16.
14. H. J. Yu and S. D. Bhole, *Development of a Prototype Abrasive Wear Tester for Tillage Tool Materials*. Tribology International, 1990. **23**(5): p. 309-316.
15. K. Hokkirigawa and K. Kato, *An Experimental and Theoretical Investigation of Plowing, Cutting and Wedge Formation During Abrasive Wear*. Tribology International, 1988. **21**(1): p. 51-57.
16. N. P. Suh, *Delamination Theory of Wear*. Wear, 1973. **25**(1): p. 111-124.
17. H. Hertz, *Über die Berührung fester elasitscher Körper*. J. reine und angewandte Mathermatik, 1892. **92**: p. 156-171.
18. Arthur G. Metcalfe, *Interfaces in Metal Matrix Composites*. Composite materials, 1. 1974: Academic Press.
19. J. R. Vinson and R. L. Sierakowski, *The Behavior of Structures Composed of Composite Materials*. Mechanics of structural systems ; 5. 1986, Boston, Hingham, MA, USA: Kluwer Academic Publishers. xi, 323.

20. B. Cantor, *Metal and Ceramic Composites*. 2004: Institute of Physics Publishing.
21. Deborah D. L. Chung, *Composite Materials: Functional Materials for Modern Technologies*. 2003, New York: Spinger.
22. A. P. Sannino and H. J. Rack, *Dry Sliding Wear of Discontinuously Reinforced Aluminum Composites - Review and Discussion.* Wear, 1995. **189**(1-2): p. 1-19.
23. A. K. Ghosh, *Solid-State Processing*, in *Fundamentals of Metal Matrix Composites*, A. Mortensen S. Suresh, A. Needleman, Editor. 1993, Butterworth-Heinemann: Boston. p. ix, 342.
24. J. Hooker and P. Doorbar, *Metal Matrix Composites for Aeroengines*, in *Metal and Ceramic Composites*, B. Cantor, Editor. 2004, Institute of Physics Publishing. p. 3-18.
25. T. W. Clyne and P. J. Withers, *An Introduction to Metal Matrix Composites*. Cambridge solid state science series. 1993: New York NY USA : Cambridge University Press. xvi, 509.
26. K. H. J. Buschow, *The Encyclopedia of Materials Science and Technology*. 2001, New York: Elsevier.
27. V. J. Michanud, *Liquid-State Processing*, in *Fundamentals of Metal Matrix Composites*, A. Mortensen S. Suresh, A. Needleman, Editor. 1993, Butterworth-Heinemann: Boston.
28. R.C. Cochran and C. N. Roy, *U. S. Patent No 3,547,180*. December 15, 1970.
29. R. Asthana, S. Das, T. K. Dan and P. K. Rohatgi, *Solidification of Aluminum-Silicon Alloy in the Presence of Graphite Particles.* Journal of Materials Science Letters, 1986. **5**(11): p. 1083-1086.
30. D. Lewis, *In Situ Reinforcement of Metal Matrix Composites*, in *Metal Matrix Composites: Processing and Interfaces.*, R. K. Everett, Arsenualt, R. J., Editor. 1991, Academic Press Inc.: New York. p. 121-150.
31. H. J. Rack, *Powder Techniques in Processing of Metal Matrix Composites*, in *Metal Matrix Composites: Processing and Interfaces*, R. K. Everett, Arsenualt, R. J., Editor. 1991, Academic Press Inc.: New York. p. 85-99.
32. R. K. Everett, *Diffusion Bonding*, in *Metal Matrix Composites: Processing and Interfaces*, R. J. Arsenualt R. K. Everett, Editor. 1991, Academic Press Inc.: New York. p. 17-41.
33. J. C. M. Li, *Microstructure and Properties of Materials*. 1996, River Edge, NJ: World Scientific.
34. R. J. Arsenault, *Tensile and Compressive Properties of Metal Matrix Composites*, in *Metal Matrix Composites: Mechanism and Properties*, R. K. Everett, Arsenault, R. J., Editor. 1991, Academic Press Inc.: New York. p. 133-187.
35. M. Kobayashi, K. Funami, S. Suzuki and C. Ouchi, *Manufacturing Process and Mechanical Properties of Fine TiB Dispersed Ti-6Al-4V Alloy Composites Obtained by Reaction Sintering.* Materials Science and Engineering a-Structural Materials Properties Microstructure and Processing, 1998. **243**(1-2): p. 279-284.

36. D. L. Mcdanels, *Analysis of Stress-Strain, Fracture, and Ductility Behavior of Aluminum Matrix Composites Containing Discontinuous Silicon-Carbide Reinforcement.* Metallurgical Transactions a-Physical Metallurgy and Materials Science, 1985. **16**(6): p. 1105-1115.
37. L. H. Qian, T. Kobayashi, H. Toda, et al., *Fracture Toughness of a 6061Al Matrix Composite Reinforced with Fine SiC Particles.* Materials Transactions, 2002. **43**(11): p. 2838-2842.
38. R. L. Deuis, C. Subramanian and J. M. Yellup, *Abrasive Wear of Aluminum Composites - A Review.* Wear, 1996. **201**(1-2): p. 132-144.
39. H. Oh, S. Lee, J. Y. Jung and S. Ahn, *Correlation of Microstructure with the Wear Resistance and Fracture Toughness of Duo-Cast Materials Composed of High-Chromium White Cast Iron and Low-Chromium Steel.* Metallurgical and Materials Transactions a-Physical Metallurgy and Materials Science, 2001. **32**(3): p. 515-524.
40. S. Das, D. P. Mondal and G. Dixit, *Correlation of Abrasive Wear with Microstructure and Mechanical Properties of Pressure Die-Cast Aluminum Hard-Particle Composite.* Metallurgical and Materials Transactions a-Physical Metallurgy and Materials Science, 2001. **32**(3): p. 633-642.
41. K. H. Zum Gahr, *How Microstructure Affects Abrasive Wear-Resistance.* Metal Progress, 1979. **116**(4): p. 46-52.
42. K. H. Zum Gahr, *Influence of Internal Notches on Abrasive Wear.* Zeitschrift Fur Metallkunde, 1978. **69**(5): p. 312-319.
43. I. M. Hutchings, *Wear by Particulates.* Chemical Engineering Science, 1987. **42**(4): p. 869-878.
44. I. M. Hutching, *Advanced Materials and Processes.* 1991, Cambridge: University of Cambridge. 56.
45. O. Yilmaz and S. Buytoz, *Abrasive Wear of Al_2O_3-Reinforced Aluminium-Based MMCs.* Composites Science and Technology, 2001. **61**(16): p. 2381-2392.
46. Z. F. Zhang, L. C. Zhang and Y. W. Mai, *Wear of Ceramic Particle-Reinforced Metal Matrix Composites .1. Wear Mechanisms.* Journal of Materials Science, 1995. **30**(8): p. 1961-1966.
47. S. Chung and B. H. Hwang, *A Microstructural Study of the Wear Behavior of Sic_P Al Composites.* Tribology International, 1994. **27**(5): p. 307-314.
48. H. Ahlatci, E. Candan and H. Cimenoglu, *Effect of the Particle Size on the Mechanical Properties of 60 vol. % SiCp Reinforced Al Matrix Composites.* Zeitschrift Fur Metallkunde, 2002. **93**(4): p. 330-333.
49. S. Usmani, S. Sampath, D. L. Houck and D. Lee, *Effect of Carbide Grain Size on the Sliding and Abrasive Wear Behavior of Thermally Sprayed WC-Co Coatings.* Tribology Transactions, 1997. **40**(3): p. 470-478.
50. E. Candan, H. Ahlatci and H. Cimenoglu, *Abrasive Wear Behaviour of Al-SiC Composites Produced by Pressure Infiltration Technique.* Wear, 2001. **247**(2): p. 133-138.

51. O. Yilmaz and H. Turhan, *Effect of Size and Volume Fraction of Particulates on the Sliding Wear Resistance of CuSn Composites.* Wear, 2001. **249**(10-11): p. 901-913.
52. T. A. Stolarski, E. Jisheng, D. T. Gawne and S. Panesar, *The Effect of Load and Abrasive Particle-Size on the Material Removal Rate of Silicon-Nitride Artifacts.* Ceramics International, 1995. **21**(5): p. 355-366.
53. D. P. Mondal, S. Das, A. K. Jha and A. H. Yegneswaran, *Abrasive Wear of Al Alloy-Al_2O_3 Particle Composite: A Study on the Combined Effect of Load and Size of Abrasive.* Wear, 1998. **223**(1-2): p. 131-138.
54. D. Forrest, K. Matsuoka, M. K. Tse and E. Rabinowicz, *Accelerated Wear Testing Using the Grit Size Effect.* Wear, 1993. **162**: p. 126-131.
55. Larsenba.J, *Influence of Grit Size on Groove Formation during Sliding Abrasion.* Wear, 1968. **11**(3): p. 213-223.
56. E. Rabinowicz, *Effect of Abrasive Particle Size on Wear.* Wear, 1965. **8**: p. 381-390.
57. N. Axen and K. H. Zumgahr, *Abrasive Wear of TiC-Steel Composite Clad Layers on Tool Steel.* Wear, 1992. **157**(1): p. 189-201.
58. K. S. Al-Rubaie, H. N. Yoshimura and J. D. B. De Mello, *Two-Body Abrasive Wear of Al-SiC Composites.* Wear, 1999. **235**: p. 444-454.
59. A. Wang and H. J. Rack, *Abrasive Wear of Silicon-Carbide Particulate-Reinforced and Whisker-Reinforced 7091 Aluminum Matrix Composites.* Wear, 1991. **146**(2): p. 337-348.
60. K. Hokkirigawa, K. Kato and Z. Z. Li, *The Effect of Hardness on the Transition of the Abrasive Wear Mechanism of Steels.* Wear, 1988. **123**(2): p. 241-251.
61. M. A. Moore and P. A. Swanson, *The Effect of Particle Shape on Abrasive Wear: A Comparison of Theory and Experiment*, in *Wear of Materials 1983*, K. C. Ludema, American Society of Mechanical Engineers. and American Society for Testing and Materials., Editors. 1983, American Society of Mechanical Engineers: New York, N.Y. p. xiv, 656.
62. P. A. Swanson and A. F. Vetter, *The Measurement of Abrasive Particle-Shape and Its Effect on Wear.* Asle Transactions, 1985. **28**(2): p. 225-230.
63. M. G. Hamblin and G. W. Stachowiak, *Description of Abrasive Particle Shape and Its Relation to Two-Body Abrasive Wear.* Tribology Transactions, 1996. **39**(4): p. 803-810.
64. J. Zhang and A. T. Alpas, *Wear Regimes and Transitions in Al_2O_3 Particulate-Reinforced Aluminum-Alloys.* Materials Science and Engineering a-Structural Materials Properties Microstructure and Processing, 1993. **161**(2): p. 273-284.
65. Dierk Raabe, *Computational Materials Science, the Simulation of Materials Microstructure and Properties*. 1998: Wiley-Vch.
66. B. J. Alder and T. E. Wainwright, *Studies in Molecular Dynamics .1. General Method.* Journal of Chemical Physics, 1959. **31**(2): p. 459-466.
67. L. A. Girifalco and V. G. Weizer, *Application of the Morse Potential Function to Cubic Metals.* Physical Review, 1959. **114**(3): p. 687-690.
68. R. T Fenner, *Finite Element Methods for Engineers*. 1975.

69. Paul E. Allaire, *Basics of the Finite Element Method--Solid Mechanics, Heat Transfer and Fluid Mechanics*. 1985, Dubuque, Iowa: Wm. C. Brown Publishers.
70. S. Sao, *The Finite Element Method in Engineering*. 1989: Pergamon press.
71. K. Komvopoulos and D. H. Choi, *Elastic Finite Element Analysis of Multiasperity Contacts*. Journal of Tribology-Transactions of the Asme, 1992. **114**(4): p. 823-831.
72. P. E. Mchugh, R. J. Asaro and C. F. Shih, *Computational Modeling of Metal Matrix Composite Materials .1. Isothermal Deformation Patterns in Ideal Microstructures*. Acta Metallurgica Et Materialia, 1993. **41**(5): p. 1461-1476.
73. P. E. Mchugh, R. J. Asaro and C. F. Shih, *Computational Modeling of Metal Matrix Composite Materials .2. Isothermal Stress-Strain Behavior*. Acta Metallurgica Et Materialia, 1993. **41**(5): p. 1477-1488.
74. J. Gunnars and A. Alahelisten, *Thermal Stresses in Diamond Coatings and Their Influence on Coating Wear and Failure*. Surface & Coatings Technology, 1996. **80**(3): p. 303-312.
75. C. J. Mundy, S. Balasubramanian and M. L. Klein, *Hydrodynamic Boundary Conditions for Confined Fluids via a Nonequilibrium Molecular Dynamics Simulation*. Journal of Chemical Physics, 1996. **105**(8): p. 3211-3214.
76. M. R. Sorensen, K. W. Jacobsen and P. Stoltze, *Simulations of Atomic scale Sliding Friction*. Physical Review B, 1996. **53**(4): p. 2101-2113.
77. J. Svoboda and P. Lukas, *Modelling of Kinetics of Directional Coarsening in Ni-Superalloys*. Acta Materialia, 1996. **44**(6): p. 2557-2565.
78. X. F. Tian and B. Bhushan, *A Numerical Three-Dimensional Model for the Contact of Rough Surfaces by Variational Principle*. Journal of Tribology-Transactions of the Asme, 1996. **118**(1): p. 33-42.
79. P. Gumbsch, S. J. Zhou and B. L. Holian, *Molecular Dynamics Investigation of Dynamic Crack Stability*. Physical Review B, 1997. **55**(6): p. 3445-3455.
80. R. W. Smith, *A kinetic Monte Carlo Simulation of Fiber Texture Formation during Thin-Film Deposition*. Journal of Applied Physics, 1997. **81**(3): p. 1196-1203.
81. H. Berns, A. Melander, D. Weichert, et al., *A New Material for Cold Forging Tools*. Computational Materials Science, 1998. **11**(3): p. 166-180.
82. Hiroshi Eda, *Computer Simulations in Abrasive Grinding Process*. International Journal of the Japan Society of Precision Engineering, 1998. **32**(4): p. 233-239.
83. J. Shimizu, H. Eda, M. Yoritsune and E. Ohmura, *Molecular Dynamics Simulation of Friction on the Atomic Scale*. Nanotechnology, 1998. **9**(2): p. 118-123.
84. D. Y. Li, K. Elalem, M. J. Anderson and S. Chiovelli, *A Microscale Dynamical Model for Wear Simulation*. Wear, 1999. **229**: p. 380-386.
85. S. Moaveni, *Finite Element Analysis--Theory and Application with ANSYS*. 1999, New Jersey: Prentice Hall.

86. M. O. Robbins and M. H. Muser, *Computer Simulations for Friction, Lubrication and Wear*, in *Handbook of Modern Tribology*, B. Bhushan, Editor. 2000, CRC press.
87. X. Y. Fu, M. L. Falk and D. A. Rigney, *Sliding Behavior of Metallic Glass - Part II. Computer Simulations.* Wear, 2001. **250**: p. 420-430.
88. D.Y. Li K. Elalem, M.J. Anderson, S. Chiovelli, *Modeling Abrasive Wear of Homogeneous and Heterogeneous Materials*, in *Hydraulic Failure Analysis: Fluids, Components and System effects*, D. K. Wills G. E. Totten, D. Feldmann, Editor. 2001, American Society for Testing and Materials, ASTM: West conshoocken. p. 1339.
89. S. S. Cho and S. Park, *Molecular Dynamics Simulation of Adhesion Processes.* KSME International Journal, 2002. **16**(11): p. 1440-1447.
90. D. Hortig and D. Schmoeckel, *Analysis of Local Loads on the Draw Die Profile with Regard to Wear Using the FEM and Experimental Investigations.* Journal of Materials Processing Technology, 2001. **115**(1): p. 153-158.
91. K. Shimizu, T. Noguchi, H. Seitoh, et al., *FEM Analysis of Erosive Wear.* Wear, 2001. **250**: p. 779-784.
92. M. H. Muser, *Atomistic Simulations of Solid Friction*, in *Bridging the Time Scale: Molecular Simulations for the Next Decade*, M P. Nielaba, Mareschal and G. Ciccotti, Editor. 2002, Springer: New York.
93. A. Posmyk, *Influence of Material Properties on the Wear of Composite Coatings.* Wear, 2003. **254**(5-6): p. 399-407.
94. W. C. D. Cheong and L. C. Zhang, *Monocrystalline Silicon Subjected to Multi-Asperity Sliding: Nano-Wear Mechanisms, Subsurface Damage and Effect of Asperity Interaction.* International Journal of Materials & Product Technology, 2003. **18**(4-6): p. 398-407.
95. Q. Chen and D. Y. Li, *Computer Simulation of Solid Particle Erosion.* Wear, 2003. **254**(3-4): p. 203-210.
96. Q. Chen and D. Y. Li, *Computer Simulation of Solid-Particle Erosion of Composite Materials.* Wear, 2003. **255**: p. 78-84.
97. Q. Chen and D. Y. Li, *Computer Simulation of Erosion-Corrosion of a Non-passive Alloy Using a Micro-Scale Dynamic Model.* Materials Science and Engineering a-Structural Materials Properties Microstructure and Processing, 2004. **369**(1-2): p. 284-293.
98. M. Mirghany and Z. M. Jin, *Prediction of Scratch Resistance of Cobalt Chromium Alloy Bearing Surface, Articulating Against Ultra-High Molecular Weight Polyethylene, due to Third-Body Wear Particles.* Proceedings of the Institution of Mechanical Engineers Part H-Journal of Engineering in Medicine, 2004. **218**(H1): p. 41-50.
99. W. C. Swope, H. C. Andersen, P. H. Berens and K. R. Wilson, *A Computer-Simulation Method for the Calculation of Equilibrium-Constants for the Formation of Physical Clusters of Molecules - Application to Small Water Clusters.* Journal of Chemical Physics, 1982. **76**(1): p. 637-649.
100. L. A. Fang, J. D. Xing, W. M. Liu, et al., *Computer Simulation of Two-Body Abrasion Processes.* Wear, 2001. **250**: p. 1356-1360.

101. A. A. Polycarpou and A. Soom, *Application of a 2-Dimensional Model of Continuous Sliding Friction to Stick-Slip.* Wear, 1995. **181**: p. 32-41.
102. S. Spuzic, M. Zec, K. Abhary, et al., *Fractional Design of Experiments Applied to a Wear Simulation.* Wear, 1997. **212**(1): p. 131-139.
103. T. A. Blanchet and W. G. Sawyer, *Differential Application of Wear Models to Fractional Thin Films.* Wear, 2001. **250**: p. 1003-1008.
104. J. Hu and D. Y. Li, *Computational Investigation of Microstructural Effects on Abrasive Wear of Composites.* Wear, 2005, in press.
105. T. M. Atanackovic and A.Guran, *Theory of Elasticity for Scientist and Engineers*. 2000, Boston: Birkhauser.
106. W. J. Fleming and J. M. Temis, *Numerical Simulation of Cyclic Plasticity and Damage of an Aluminum Metal Matrix Composite with Particulate SiC Inclusions.* International Journal of Fatigue, 2002. **24**(10): p. 1079-1088.
107. Q. Chen, *Computer Simulation of Solid-Particle Erosion and Related Phenomena Using a Micro-Scale Dynamic Model*, in *Department of Chemical and Materials Engineering,*. 2003, University of Alberta,: Edmonton. p. 105.
108. Khaled T. Elalem, *Development of a Micro-Scale Dynamic Model for Wear Simulation*, in *Department of Chemical and Materials Engineering*. 2000, University of Alberta: Edmonton. p. 140.
109. Q. Chen and D. Y. Li, *A Computational Study of Frictional Heating and Energy Conversion during Sliding Processes.* Wear, 2005, in press.
110. G. Straffelini and A. Molinari, *Dry Sliding Wear of Ti-6Al-4V Alloy as Influenced by the Counterface and Sliding Conditions.* Wear, 1999. **236**(1-2): p. 328-338.
111. H. Z. Ye, *Development of New Wear-Resistant Material: TiNi-Based Composite*, in *Chemical and Materials Engineering*. 2002, University of Alberta: Edmonton.
112. B. Hwang, J. Ahn and S. Lee, *Correlation of Microstructure and Wear Resistance of Ferrous Coatings Fabricated by Atmospheric Plasma Spraying.* Metallurgical and Materials Transactions a-Physical Metallurgy and Materials Science, 2002. **33**(9): p. 2933-2945.
113. H. Engqvist, G. A. Botton, N. Axen and S. Hogmark, *Microstructure and Abrasive Wear of Binderless Carbides.* Journal of the American Ceramic Society, 2000. **83**(10): p. 2491-2496.
114. Y. L. Shen, M. Finot, A. Needleman and S. Suresh, *Effective Plastic Response of 2-Phase Composites.* Acta Metallurgica Et Materialia, 1995. **43**(4): p. 1701-1722.
115. J. Li, Y. Y. Wu, D. L. Wang and X. G. Hu, *The Microstructure and Wear Resistance Characteristics of Electroformed Nickel and Partially Stabilized Zirconia Composite Coatings.* Journal of Materials Science, 2000. **35**(7): p. 1751-1758.
116. R. K. Galgali, H. S. Ray and A. K. Chakrabarti, *Wear Characteristics of TiC Reinforced Cast Iron Composites Part 2 - Abrasive Wear.* Materials Science and Technology, 1998. **14**(11): p. 1189-1193.

117. H. M. Kim, T. S. Kim, C. Suryanarayana and B. S. Chun, *Microstructure and Wear Characteristics of Rapidly Solidified Al-Pb-Cu Alloys.* Materials Science and Engineering a-Structural Materials Properties Microstructure and Processing, 2000. **287**(1): p. 59-65.
118. A. P. Sannino and H. J. Rack, *Tribological Investigation of 2009 Al-20 vol% SiC_P/17-4 PH .2. Counterpart Performance.* Wear, 1996. **196**(1-2): p. 202-206.
119. S. Y. Qin, C. R. Chen, G. D. Zhang, et al., *The Effect of Particle Shape on Ductility of SiC_p Reinforced 6061 Al Matrix Composites.* Materials Science and Engineering a-Structural Materials Properties Microstructure and Processing, 1999. **272**(2): p. 363-370.
120. C. R. Chen, S. Y. Qin, S. X. Li and J. L. Wen, *Finite Element Analysis about Effects of Particle Morphology on Mechanical Response of Composites.* Materials Science and Engineering a-Structural Materials Properties Microstructure and Processing, 2000. **278**(1-2): p. 96-105.
121. T. Christman, A. Needleman and S. Suresh, *An Experimental and Numerical Study of Deformation in Metal Ceramic Composites.* Acta Metallurgica, 1989. **37**(11): p. 3029-3050.
122. H. Shen and C. J. Lissenden, *3D Finite Element Analysis of Particle-Reinforced Aluminum.* Materials Science and Engineering a-Structural Materials Properties Microstructure and Processing, 2002. **338**(1-2): p. 271-281.
123. S. Rangaraj and K. Kokini, *Influence of Particle Shape and Aspect Ratio on Thermally Activated Viscoplastic (Time-Dependent) Response of Ceramic (Zirconia)-Metal (NiCoCrAlY) Particulate Composites.* Materials Science and Engineering a-Structural Materials Properties Microstructure and Processing, 2004. **366**(2): p. 356-366.
124. K. D. Bouzakis, G. Koutoupas, A. Siganos, et al., *Increasing of Cutting Performance of PVD Coated Cemented Carbide Inserts in Chipboard Milling Through Improvement of the Film Adhesion, Considering the Coating Cutting Loads.* Surface & Coatings Technology, 2000. **133**: p. 548-554.
125. A. Borri-Brunetto, A. Carpinteri and S. Invernizzi, *Characterization and Mechanical Modeling of the Abrasion Properties of Sintered Tools with Embedded Hard Particles.* Wear, 2003. **254**(7-8): p. 635-644.
126. S. G. Song, N. Shi, G. T. Gray and J. A. Roberts, *Reinforcement Shape Effects on the Fracture Behavior and Ductility of Particulate-Reinforced 6061-Al Matrix Composites.* Metallurgical and Materials Transactions a-Physical Metallurgy and Materials Science, 1996. **27**(11): p. 3739-3746.
127. S. V. Prasad and T. H. Kosel, *A Study of Carbide Removal Mechanisms During Quartz Abrasion 2. Effect of Abrasive Particle-Shape.* Wear, 1984. **95**(1): p. 87-102.
128. J. O Smith and C. K. Liu, *Stress due to Tangential and Normal Loads on an Elastic Solid with Application to Some Contact Stress Problems*, ASME Transaction, **75** 1953: p. 157-165.

129. K. T. Elalem, *Development of a Micro-Scale Dynamic Model for Wear Simulation*, in *Chemical and Materials Engineering*. 2000, University of Alberta: Edmonton.